

Effects of magnesium degradation products and hypoxia on angiogenesis and osteogenesis during fracture healing

Dissertation

zur Erlangung des akademischen Grades

Doktor der Ingenieurwissenschaften

(Dr.-Ing.)

der Technischen Fakultät

der Christian-Albrechts-Universität zu Kiel

vorgelegt von

LEI XU

Kiel 2019

Erstgutachterin: Prof. Dr. Regine Willumeit-Römer

Zweitgutachter/in: Prof. Dr. Christine Selhuber-Unkel

Termin der Disputation: 26.06.2019

Eidesstattliche Erklärung

Hiermit erkläre ich, dass die beigefügte Dissertation, abgesehen von der Beratung durch die Betreuerin, nach Inhalt und Form meine eigene Arbeit ist.

Die Arbeit, ganz oder zum Teil, wurde nie schon einer anderen Stelle im Rahmen eines Prüfungsverfahrens vorgelegt und ist abgesehen, von den im Anhang angegebenen Veröffentlichungen, nicht anderweitig zur Veröffentlichung vorgelegt worden.

Außerdem ist die Arbeit unter Einhaltung der Regeln guter wissenschaftlicher Praxis der Deutschen Forschungsgemeinschaft entstanden.

Geesthacht, den

Unterschrift

Abstract

Background: Magnesium (Mg) based metals have been applied in orthopaedic and cardiovascular (as stent) applications due to (e.g.) their excellent biodegradability and tissue regeneration abilities. Endothelial cells (ECs) and mesenchymal stem cells (MSCs) represent two protagonists of angiogenesis and osteogenesis. The responding of angiogenesis and the EC-MSC communication to Mg degradation products and oxygen content are vital to vascular remodelling and later fracture regeneration. **Methods:** Firstly, human primary ECs were exposed to various concentrations of extracellular Mg degradation products (control (0.8 mM - cell culture media), 2, 4, and 8 mM) under either hypoxia (5% O₂) or normoxia (20% O₂). Furthermore, in order to understand the influences of Mg degradation and oxygen conditions on the ECs-MSCs communication, a non-contacting (or transwell system) and a contacting cell culture models were established. With these models, the various stages of fracture healing could be mimicked: angiogenesis, MSCs attraction / migration and tissue modelling. In the monoculture, cell metabolism and proliferation, as well as wound healing and tube formation assays (reflecting two different stages of angiogenesis: migration and tube formation) were studied. In coculture, cells proliferation and ratio were measured by deoxyribonucleic acid (DNA) content and flow cytometry, respectively. Additionally, MSCs migration was assessed by wound healing assay. Gene regulation in monoculture and different coculture were investigated by semi-quantitative real time polymerase chain reaction (qRT-PCR). Furthermore, several angiogenic factors, such as vascular endothelial growth factor A (VEGFA) were also quantified. **Results:** Increased proliferation and reduced metabolism of ECs were measured with Mg extracts under hypoxia but not under normoxia. Under normoxia and with Mg extracts, ECs migration exhibited a bell-shaped curve. The same pattern was observed with vascular endothelial growth factors (VEGFs) expression. Under normoxia and with Mg extracts but not hypoxia, ECs tube formation was decreased. The regulation of selected genes during angiogenesis under the influence of Mg degradation products and O₂ contents were also investigated and different expression profiles were found between the migration and tube formation stage. In coculture systems, Mg decreased the proliferation of MSCs in transwell under hypoxia while an increased ratio MSCs/ECs in direct-contact coculture was measured as well as a more obvious decreased proliferation of ECs. MSCs migration was increased by magnesium extracts only under hypoxia. Expression of selected genes like factors related to extracellular matrix, hypoxia inducible

factors and other angiogenic regulators was obviously influenced by Mg and hypoxia. In transwell, hypoxia decreased the effect of Mg on cytokines levels (e.g., migratory factors and other regulators like VEGFA). However, these cytokines as well as mineralisation were remarkably increased with Mg degradation products under heterotypic contact and hypoxia conditions. **Conclusion:** These results suggest that Mg extracts did not interfere with angiogenesis under hypoxia. Furthermore, Mg, hypoxia, and heterotypic contact were beneficial to stromal ECs and MSCs, providing a suitable niche environment and highlighting the application of Mg in regenerative medicine.

Zusammenfassung

Der Hintergrund: Biologisch abbaubare Magnesium (Mg) – basierte Legierungen wurden aufgrund ihrer hervorragenden biologischen Eigenschaften wie Abbaubarkeit und an die Geweberegeneration in der Orthopädie und Gefäßchirurgie in Form von Stents eingesetzt. Endothelzellen (ECs) und mesenchymale Stammzellen (MSCs) repräsentieren zwei Protagonisten der Angiogenese und Osteogenese. Die Reaktion der Angiogenese und die EC-MSC-Kommunikation auf eine Mg²⁺ Supplementation und einen verminderten Sauerstoffgehalt ist für die vaskuläre Remodelierung und die spätere Frakturheilung von entscheidender Bedeutung. **Die Methoden:** Humane primäre ECs wurden verschiedenen Konzentrationen extrazellulärer Mg Degradationsprodukte entweder unter Hypoxie oder Normoxie ausgesetzt. Um die EC-MSC-Kommunikation beim Abbau des Mg und unter veränderten Sauerstoffbedingungen zu verstehen, wurden ein kontaktfreies (Transwell-System) und ein Zellkulturmodell, das einen direkten Kontaktierung ermöglicht, etabliert. Somit können die verschiedenen Stadien der Frakturheilung nachgeahmt werden. Diese sind: Angiogenese, Anziehung / Migration von MSC und Gewebemodellierung. In Kokultursystemen wurden die Zellproliferation und das Zahlenverhältnis durch DNA-Gehalt bzw. Durchflusszytometrie gemessen. Darüber hinaus wurde die MSC-Migration, die durch einen Wundheilungsassay beobachtet wurde. Die Genregulation der ECs-Monokultur und verschiedener Kokulturen wurde mittels qRT-PCR untersucht. **Die Ergebnisse:** Erhöhte Proliferation und reduzierter Metabolismus der ECs wurden mit Mg-Extrakten unter Hypoxie gemessen, nicht jedoch unter Normoxie. Unter Normoxie und mit Mg-Extrakten zeigte die EC-Migration eine glockenförmige Kurve. Unter Normoxie und mit Mg-Extrakten war die Bildung von EC-Röhrchen verringert, nicht jedoch unter Hypoxie. Dasselbe Muster wurde bei der Expression vaskulärer Endothelialwachstumsfaktoren (VEGFs) beobachtet. Die Regulierung ausgewählter Gene während der Angiogenese, beeinflusst durch Mg-Abbauprodukte und O₂-Gehalte, wurde ebenfalls untersucht und es wurde ein offensichtlich unterschiedliches Expressionsprofil zwischen dem Migrations- und dem Stadium der Kapillaren Bildung gefunden. In Kokultursystemen reduzierte Mg die Proliferation von MSCs in Transwells unter Hypoxie, erhöhte jedoch das Verhältnis von HUCPV / HUVEC in direkten Kontaktkulturen und verringerte die Proliferation von ECs. Eine verringerte Proliferation von ECs war bei der direkten Kontaktkultivierung offensichtlicher. Die MSC-Migration wurde nur unter Hypoxie durch Mg-Extrakten erhöht. Die durch Mg induzierte Genregulation wurde unter hypoxischen Bedingungen

verändert, wie Faktoren, die mit extrazellulärer Matrix, Hypoxie-induzierbaren Faktoren und anderen angiogenetischen Regulatoren zusammenhängen, anzeigen. Im Transwell-System verringerte Hypoxie die Wirkung von Mg auf den Zytokinspiegel von Migrationsfaktoren und anderen Regulatoren wie VEGFA. Diese Zytokine und die Mineralisierung waren jedoch mit Mg-Abbauprodukten unter heterotypischen Kontakt- und Hypoxiebedingungen signifikant erhöht. **Das Fazit:** Diese Ergebnisse legen nahe, dass Mg-Abbauprodukte die Angiogenese unter Hypoxie nicht negativ beeinflussen. Die positiven Eigenschaften von Mg, Hypoxie und heterotypischen Kontakt auf den stromalen ECs und MSCs stellen eine geeignete Nische Umgebung dar und zeigen eine mögliche Anwendung von Mg in der regenerativen Medizin.

Contents

1	Introduction	1
2	State of the art	2
2.1	Magnesium in biology	2
2.2	Mg-based biodegradable implants	4
2.3	Bone remodelling and the ECs-MSCs interaction	8
2.1.1.	Mg and angiogenesis	10
2.1.2.	Mg in the MSC-EC interaction and MSC fate	11
2.1.3.	The model for investigating the MSC-EC interaction	12
3	Motivation and objectives.....	13
4	Materials and methods.....	14
4.1	Magnesium degradation products	14
4.1.1	Materials.....	14
4.1.2	Samples cleaning and sterilisation and Mg extract preparation	14
4.2	The isolation of human umbilical cord	15
4.2.1	Materials and ethical approval	15
4.2.2	The structure of the human umbilical cord.....	16
4.2.3	HUCPV cell isolation	16
4.2.4	HUVEC isolation	17
4.3	HUCPV and HUVEC characterisation	17
4.3.1	Immunophenotyping.....	17
4.3.2	Differentiation potential	21
4.4	Cell expansion	21
4.5	Coculture system	22
4.6	Deoxyribonucleic acid (DNA) quantification	24
4.6.1	Materials.....	24
4.6.2	Procedures.....	24
4.7	Metabolism assay	26
4.7.1	Materials.....	26
4.7.2	Metabolism.....	26
4.7.3	Rhodamine 123 assay	28
4.7.4	WST-1 assay.....	28
4.8	Real-time quantitative polymerase chain reaction (RT-qPCR).....	29
4.8.1	Materials.....	29
4.8.2	Ribonucleic acid (RNA) extraction and quality control of RNA	29
4.8.3	Complementary DNA (cDNA) synthesis	29
4.8.4	Primers and RT-qPCR	30
4.9	ALP activity	33
4.9.1	Materials.....	33
4.9.2	The principle and procedure	33
4.10	ARS staining	34
4.10.1	Materials.....	34
4.10.2	Procedures.....	34
4.11	Enzyme-linked immunosorbent assay (ELISA)	34

4.11.1	Materials.....	34
4.11.2	Procedures.....	35
4.12	Wound healing assay	36
4.12.1	Materials.....	38
4.12.2	Procedures.....	38
4.13	Tube formation assay	39
4.13.1	Materials.....	40
4.13.2	Procedures.....	40
4.14	Statistical analysis	41
5	Results	42
5.1	The isolation, validation and differentiation potential of existing HU-CPV and HUVEC ..	42
5.2	Optimisation and validation of the coculture system	45
5.3	Magnesium degradation products and hypoxia influenced the HUVEC angiogenesis stage	47
5.3.1	Proliferation of HUVECs indicated by DNA quantification	47
5.3.2	Metabolism measured <i>via</i> WST-1 assay and rhodamine 123	47
5.3.3	Migration ability was increased by Mg in normoxia	49
5.3.4	Tube formation was decreased by Mg in normoxia	51
5.3.5	Gene regulation during migration and tube formation was influenced by Mg and hypoxia	51
5.3.6	VEGFA and VEGFB levels during migration and tube formation indicated by ELISA	56
5.4	Magnesium degradation products and hypoxia influenced the intermediate stage of HU-CPV cells and HUVECs	58
5.4.1	Proliferation of HU-CPV cells and HUVECs in transwell coculture.....	58
5.4.2	Gene expression of HU-CPV cells and HUVECs in 7-day-transwell coculture	59
5.4.3	Cytokine levels in transwell coculture up to 7 days	61
5.4.4	HU-CPV cell migration and gene regulation	63
5.5	Magnesium degradation products and hypoxia influenced osteogenesis and the cytokine environment after HU-CPV/HUVEC direct-contact coculture	66
5.5.1	Proliferation in direct-contact coculture investigated by DNA content and flow cytometry	66
5.5.2	Cytokine levels of direct-contact coculture in ELISA tests	67
5.5.3	Osteogenesis investigated by ARS staining and ALP activity.....	68
6	Discussion.....	70
6.1	Magnesium and hypoxia influence the angiogenesis of HUVECs	72
6.2	Magnesium degradation products and hypoxia influence the EC-MS-C interaction	78
6.2.1	The MS-C-EC interaction in the intermediate stage is influenced by Mg and hypoxia	79
6.2.2	MS-C migration interaction with ECs is influenced by Mg and hypoxia.....	81
6.2.3	Magnesium degradation products and hypoxia influence heterotypic EC-MS-C contact	82
7	Conclusion	84
	References	85
	Acknowledgements	101

Appendix.....	102
Supplementary figures	102
Symbols and abbreviations	105
Curriculum Vitae	107
List of publications and conferences	108

1 Introduction

In the arena of public health, disability and chronic disease are worldwide problems that influence independence in community life, work absenteeism, and physical activity levels. Population ageing is expected to rapidly rise during the next decades, and older populations tend to be more disturbed by chronic diseases. Lasting cures for chronic diseases always carry high medical costs and long-term disabilities. Approximately 86% of annual health care expenditures in the USA involve chronic diseases¹. Osteoporosis (OP) causes more than 8.9 million fractures annually and results worldwide in an osteoporotic fracture every 3 seconds^{2,3}. Blood vessel formation (angiogenesis) is an important element that accompanies fracture healing (osteogenesis) and influences eventual clinical outcomes. Additionally, angiogenesis dysfunction also plays vital roles in cardiovascular disease, which is the leading cause of death worldwide⁴.

To cope with these issues, intervention is widely applied to prevent dysfunctional angiogenesis. In the field of regenerative medicine, fixation implants and tissue regeneration have been developed to support healing after bone diseases and fractures. Because of their material properties and biocompatibility, magnesium (Mg)-based materials have been developing into promising implants for bone fixation and recovery. The mechanism still requires investigation into the interactive context of bone implantation due to the complex hierarchical structure of bones.

Thus, the present study concentrates on the roles of mesenchymal stem cells (MSCs) and endothelial cells (ECs), which are two important local stromal cells involved in hypoxia during bone healing. The role of the endothelial cell, as the protagonist of blood vessel formation, in capillary formation is investigated under the influence of Mg-containing degradation products and hypoxia. Furthermore, gene regulation, metabolism and VEGF secretion, when mediated by Mg and hypoxia, are investigated. Cytokine secretion, the gene regulation of MSCs-ECs, the migration of MSCs and the eventual fate of MSCs are investigated when interacting with ECs, environmental hypoxia and Mg-containing degradation products.

2 State of the art

2.1 Magnesium in biology

Metal ions are normally obtained within the food chain across the ecosystem. Magnesium is the fourth most abundant essential element of vertebrate animals and the second most abundant intracellular cation after potassium (K). An adult human body contains a total of ~24 g of Mg, which is naturally introduced into the body *via* dietary intake⁵.

Mg is unequally circulated within organisms and tissues in the form of salts (e.g., MgCl_2 and MgSO_4). The balance between intestinal absorption and renal excretion regulates Mg^{2+} homeostasis, as indicated in Fig. 1. Almost 52.9% of the Mg *in vivo* is located in bones, and only 0.8% is found in the blood. Mg in the human body is categorised into ionised, complexed and protein-bound states, with ionised Mg having the greatest biological activity. Mg homeostasis is maintained by absorption through the gut, bone and kidney. In the gut, Mg is absorbed mainly in the small intestine by a passive and paracellular mechanism, which is driven by an electrochemical gradient and solvent drag⁶. A minor but important Mg fraction is transported *via* the transcellular transporter transient receptor potential melastatin 6 and 7 (TRPM6/7)⁷. Then, Mg ions are stored in bone mineral, with 1/3 of skeletal Mg remaining on either the cortical bone or hydroxyapatite surface, or in the hydration shell around the crystal⁸. Such bone surface Mg can act as a reservoir and exchange correspondingly with Mg loading from serum and the physiological extracellular environment^{6,9}. Eventually, excess Mg is excreted *via* the kidney and the faeces (Fig. 1).

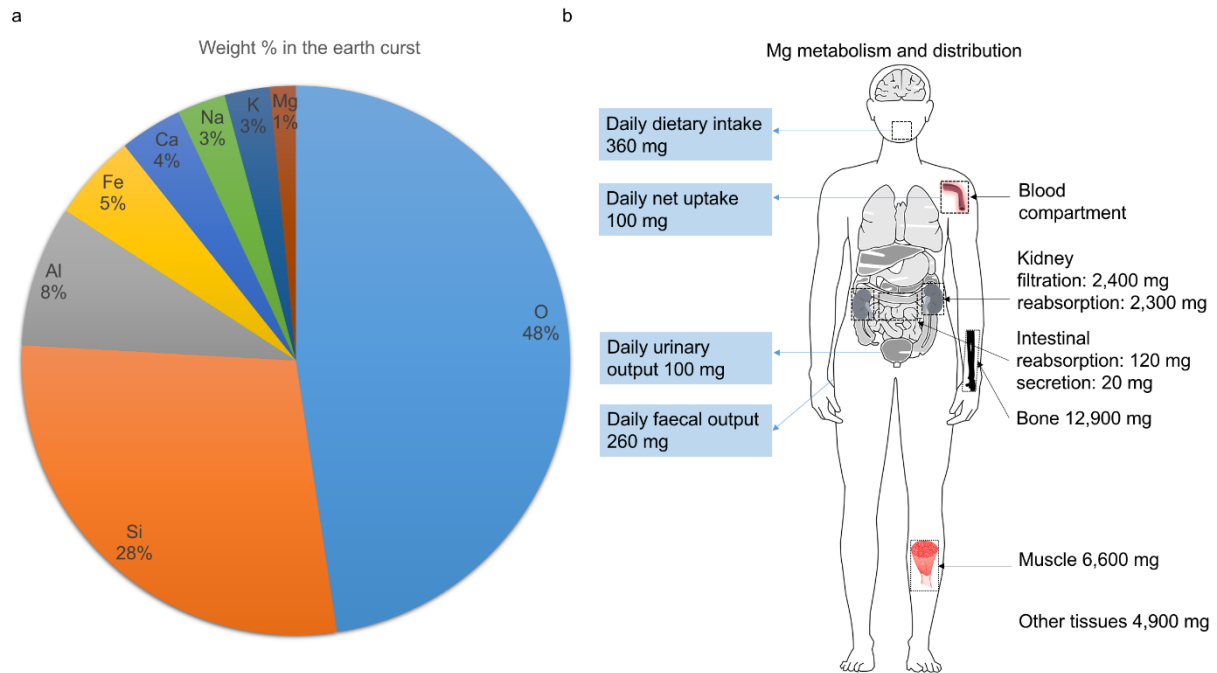


Fig. 1 Magnesium distribution and homeostasis in the body. Bones and muscles are the most important reserves of Mg, one-third of which is exchangeable between the reservoir and blood serum to maintain the extracellular homeostasis.

Extensive clinical observation and epidemiological investigation have raised awareness of the clinical association between disease and Mg status (Table 1). Even short disturbances in Mg homeostasis have induced cellular events¹⁰, and the health risk induced by Mg deficiency should be considered. Various bone symptoms are reported to correlate with Mg status in both genders and at different ages¹¹. Lower concentrations of serum magnesium lead to hypomagnesaemia, which is widely reported as an essential hospitalisation status and can result in various pathological consequences⁵, such as cardiovascular diseases¹², diabetes¹³ and osteoporosis⁹. The pathological research suggests roles for Mg in osteoporosis (OP) that involve an influence on cytokine secretion, inflammation activation, osteoclast formation and osteoblast inhibition⁹. Accordingly, Mg supplementation is implicated in the stimulation of bone regeneration by reversing inflammation cascades, such as by decreasing the cytokine profile into an anti-inflammatory one in the clinic¹⁴. Mg disorder also depends on an altered absorption of other metal ions on the cell membrane and numerous biochemical reactions. For example, Ca help with the hydrolysis of adenosine triphosphate (ATP)¹⁵. Due to similar chemical features, Mg often acts as a non-competitive antagonist to metal ions⁶. For instance, Mg and Ca absorption both occur *via* TRPM6 and TRPM7 transport in the intestine⁷. Mg can occupy voltage-dependent Na⁺-Ca²⁺ channels^{16,17} and the N-methyl-D-aspartate receptor (NMDAR) regulating the Na⁺-Ca²⁺-K⁺ pump^{16,17}. The non-competitive

antagonism by Mg is determined by its hydration shell, which cannot be easily stripped off to allow passage through the narrow channels on cell membranes⁶.

Table 1 Diseases and factors related to magnesium deficiency and supplementation

Mg treatment	Disease	Influenced molecule/parameter
Magnesium deficiency	Osteoarthritis (OA); Joint space narrowing (JSN); Osteoporosis (OP)	tumour necrosis factor α (TNF- α); substance P (SP); parathyroid hormone (PTH); 1, 25-dihydroxyvitamin D (VD3); N-methyl-D-aspartate (NMDA) receptor; interleukin-1 β (IL1 β); nuclear factor- κ B ligand (NF- κ B); C-reactive protein (CRP); bone mineral density (BMD)
	Inflammation	blood pressure; fibrinogen; plasma albumin; IL6; lysophosphatidylcholine (LPC); thiobarbituric acid reactive substances (TBARS); vitamin E; free radicals; granulocyte colony-stimulating factor receptor (G-CSF-R); chemokine (C-C motif) ligand 4 (CCL4); TNF- α ; CRP
	Metabolic syndrome	SP; calcitonin gene-related peptide; n-methyl-D-aspartate (NMDA) receptor/channel complex; sensory-motor C-fibres; nitric oxide (NO); reactive oxygen species (ROS); lipid peroxidation products; endogenous antioxidants; renin-angiotensin
	Cardiovascular pathology	IL1; IL6; TNF- α ; endothelin; SP; serum TBAR-materials; intracellular Glutathione (GSH); plasminogen activator inhibitor factor 1 (PAI-1); CRP; prostacyclin 2 (PGI2); Ca influx
Magnesium supplementation	Inflammation susceptibility	Apoptosis; oxidative stress; TNF- α ; IL6
	Anti-inflammation	IL1 β ; IL1Ra; IL6; IL7; IL8; intercellular adhesion molecule 1 (ICAM-1); NF- κ B; β -thromboglobulin (β -TG); platelet factor 4 (PF4); ATPase; HLA-DR, B7 Molecules; apolipoprotein E (ApoE); CCL2/4/5; chemokine (C-X-C motif) ligand 1 (CXCL1); neuronal injury; leukocyte migration; TNF- α

2.2 Mg-based biodegradable implants

To heal fractures, cure soft-tissue injuries and reconstruct tissue, orthopaedic applications presently use various materials such as polymers (e.g., polylactic acid or PLA), titanium and cobalt-chrome alloys, ceramics and composites (e.g., PLA/hydroxyapatite (HA) and carbon fibre composites). Such fixation devices provide stability and maintain the alignment of bone fragments (Table 2) in an external or intramedullary location¹⁸. However, such devices can induce side effects. For instance, (D, L-Lactide)

DL-PLA and HA-based materials have inadequate mechanical properties as load-bearing components¹⁹. Even some skeletal fixator materials with adequate strength can result in wide flaws because of their non-resorbability and different mechanics compared to cortical bones. For instance, some skeletal fixators have been reported to induce infection², osteopenia¹⁹, a stress-shielding effect²⁰ and an increased body sensitivity in responding to implant components such as nickel. The infection-created chronic inflammation can hinder the recovery from injury by decreasing the bone mass. Although often used as an “ideal” orthopaedic material, titanium, when worn as an “insert”, may lead to implant failure and hypersensitivity to metal debris²¹. Therefore, surgery is generally preferred after fracture healing to remove these implants.

Table 2 Fixation products for orthopaedic application

Product name	Effect	Reference
Compression plate	Increase the contact area	[18,22]
	Increase fragments stability	
	Decrease stress on the implant	
Screw	Interfragmental compression	[23,24]
	Combine with plates to prevent displacement	
	Support fragments	
Pin and wire	Fix small fragment or fracture	[25–27]
	Attach other devices	

To address the side effects from implants, effective strategies have been introduced, such as accelerating the degradation of implant, early bone grafting and the early removal of implant²⁸. Past decades have brought the emergence of biodegradable materials, such as biopolymers and biodegradable metallic substances, supplying implant materials made of zinc, iron and magnesium alloys, among others. Such materials can provide adequate mechanical stability to allow tissue regeneration while reducing inflammation, maintaining biocompatibility and avoiding secondary surgery by progressive resorption.

The orthopaedic use of magnesium-based material was first reported at the start of the 20th century²⁹. Many researchers were inspired to develop Mg as biodegradable implants for widened clinical application. In the late 1990s, reinvigorated interest in Mg-based alloys occurred in the realm of biomaterials since article numbers on this topic increased to 10-15 per week in international journals³⁰. The beneficial performance of Mg compared to other metals is presented in Table 3.

Table 3 Properties of common absorbable metals. The present table is modified by reference [31] and permitted under CC BY 4.0 license.

Metal	Yield strength (MPa)	Tensile strength (MPa)	Maximum elongation (%)	Corrosion rate (mm/year)
Iron-based: Young's modulus ~200 GPa, density ~7.8 g/cm ³				
Pure iron as annealed	150	200	40	0.1
Mg-based: Young's modulus ~45 GPa, density ~1.7 g/cm ³				
Pure Mg as extruded	30	100	7	8
Mg-1Ca as extruded	135	240	10	12.5
Mg-4Y-3RE(WE43) as extruded	180	280	10	4.3
Zinc-based: Young's modulus ~100 GPa, density ~7.1 g/cm ³				
Pure zinc as extruded	60	90	8	0.16
Zn-1Mg as extruded	170	250	10	0.12
Zn-3Cu-1Fe as extruded	210	270	20	0.13

Magnesium alloys demonstrate a good combination of heightened mechanical strength and ductility together with a reduced stress-shielding effect³². Mg-based alloys are still under development, which is limited by their unsteady mechanical properties as well as degradation induced gas production and cavities. However, some reports indicate that the released gas and cavities have no long-term toxicity to the local tissue or effect on final clinical outcomes and still enable bone healing^{33,34}. The application of Mg-based alloys has recently accelerated because of the benefits of improved corrosion resistance and mechanical properties resulting from rapidly advancing metallurgy technologies²¹. A series of preclinical studies and clinical applications of Mg-based materials regarding fracture fixation, bone flaps and cardiovascular stents has been performed across the world:

- 1) Germany was the first country to report outcomes for a bioabsorbable magnesium-based screw (MgYReZr) used to treat hallux valgus. Because of no significant difference between Mg and Ti in a post-surgery trial, the MgYReZr screw was approved and commercialised with the Conformité 11 Européenne (CE) mark in 2013³³. Additionally, MgYReZr screws were applied in wide cases for the treatment of Madelung deformity in 2015³⁵, scaphoid fracture in 2016³⁶, distal fibular fracture in 2017³⁷ and medial malleolar fractures in 2018³⁸.
- 2) The application of vascularised bone grafting with a specially designed high purity Mg screw was also reported to treat osteonecrosis of the femoral head (ONFH)³⁹; This clinical trial was first conducted in China and indicated satisfactory results for the Harris hip score (HHS) and bone flap displacement imaged radiographically. Additionally, this trial greatly accelerated the product

registration process of pure Mg-based screws in the field of ONFH reconstruction surgery³³.

- 3) Mg-Ca-Zn screws were used for distal radius fractures; maxillofacial, sagittal and split ramus osteotomy; and set back surgery and reported to repair radius fractures. This clinical research on Mg-Ca-Zn screws accelerated their approval by the Korea Food and Drug Administration (KFDA) in April 2015 as the second officially approved Mg-based orthopaedic device⁴⁰. This alloy was shown to bear more stress and to increase stability⁴¹.
- 4) Magnesium and its alloys were studied as biodegradable cardiovascular stents. For instance, mg-based scaffolds were developed as bioabsorbable scaffolds (BRS) to improve the permanent caging of the vessels, stent thrombosis (ST) and drug-eluting. Magmaris (Biotronik AG, Bülach, Switzerland) has received CE approval in Europe in June 2016, which is the first bio-corrodible metallic BRS available on the market⁴². In cardiovascular diseases, arteries can be clogged by plaque attached to their walls and made of calcium, cholesterol and fat. Angioplasty is performed to adjust the blood flow or stretch the vessel lumen by placing a mesh, tube-like scaffold to modify the vessel space. Materials for use in a cardiovascular stent require mechanical strength and no toxicity, at least when acting as a vessel scaffold in the long term, e.g., 6-12 months. To date, the gold standard for a cardiovascular stent is the 316L stainless steel model. Mg-based stents are credited for their potentially sustained mechanical support and no long-term toxicity or chronic inflammatory effect^{43,44}. Another important advantage of Mg stents is that their flexibility is enough to allow surgical revascularisation after a vessel is stretched⁴⁵. The Mg alloy Mg-2.2Nd-0.1Zn-0.4Zr was reported as promising for constructing stents when comparing to stainless steel or polymer because of its tissue compatibility and long-term (6 months) structural and mechanical integrity *in vivo*⁴³. Arginine-leucine-based poly(ester urea-urethane)s (Arg-Leu-PEUUs) were used as bio-functional coatings for the MgZnYNd stent and can significantly increase its corrosion resistance. The AE21 alloy consists of Mg, 2% aluminium and 1% rare earth metals (Ce, Pr, Nd) and meets most mechanical, biocompatibility and degradation/absorption performance requirements for use in a cardiac stent⁴⁵.

Because of their direct contact with the inner layer of vessels and the easy elution of substances from their surface by blood flow, stents are considered adaptable and efficient carriers for drugs or stimulation factors, in addition to their engineering utilisation. Key improvements will soon enhance the vascular compatibility of stents and adjust delivery efficiency *via* transforming the stent surface

or coating⁴⁶. A coated Mg stent was used as a vehicle for drug delivery to the lesion area and as an angiogenesis stimulator in coronary angioplasty, for which the material characteristics can be improved through manufacturing techniques, e.g., equal-channel angular pressing (ECAP) and extrusion processing^{46,47}.

Because of its relatively high negative electrode potential, Mg tends to degrade through dissolving Mg ions gradually into the electrolytic aqueous physiological environment^{29,48}. The *in vivo* degradation of Mg is complex and can be influenced by the type of protein⁴⁹, material surface⁵⁰ and cation composition⁵¹. The degradation products are circulated *via* blood flow, excreted through urine⁵², produce little change in blood composition and are harmless to the excretory functions of liver and kidneys⁵³. However, Mg implants have been proven to degrade and accumulate Mg near the interface between tissues and implants⁵⁴. However, such degraded Mg has positive effects, such as biocompatibility⁵⁵ and an appropriate inflammation of the surrounding bone tissues⁵⁶.

2.3 Bone remodelling and the ECs-MSCs interaction

Bone remodelling is defined as ossification or osteogenesis, continues throughout life and can be classified as intramembranous and endochondral ossification. The interplay between degraded Mg and bone remodelling is complicated because the bone fracture environment is controlled and nuanced by numerous cascades affecting the hierarchical structure, such as cellular activity, physical factors and proteins^{57,58}. All of these surrounding cellular and microenvironmental factors contribute to the formation of the stem cell niche. The cell niche controls the quiescence, self-renewal and differentiation activity of stem cells; for instance, MSC niches enable homeostasis and maintain MSC populations⁵⁹. Though the maintenance of mammalian stem cell niches is still not interpreted, the communication of cells is vital⁶⁰. For instance, niches for MSCs are located close to ECs, vessel walls⁶¹ or perivascular areas, even though MSCs have different origins⁶².

As indicated in Fig. 2, it is easy to conclude that both angiogenesis and mesenchymal stem cell (MSC) activity are involved in fracture healing.

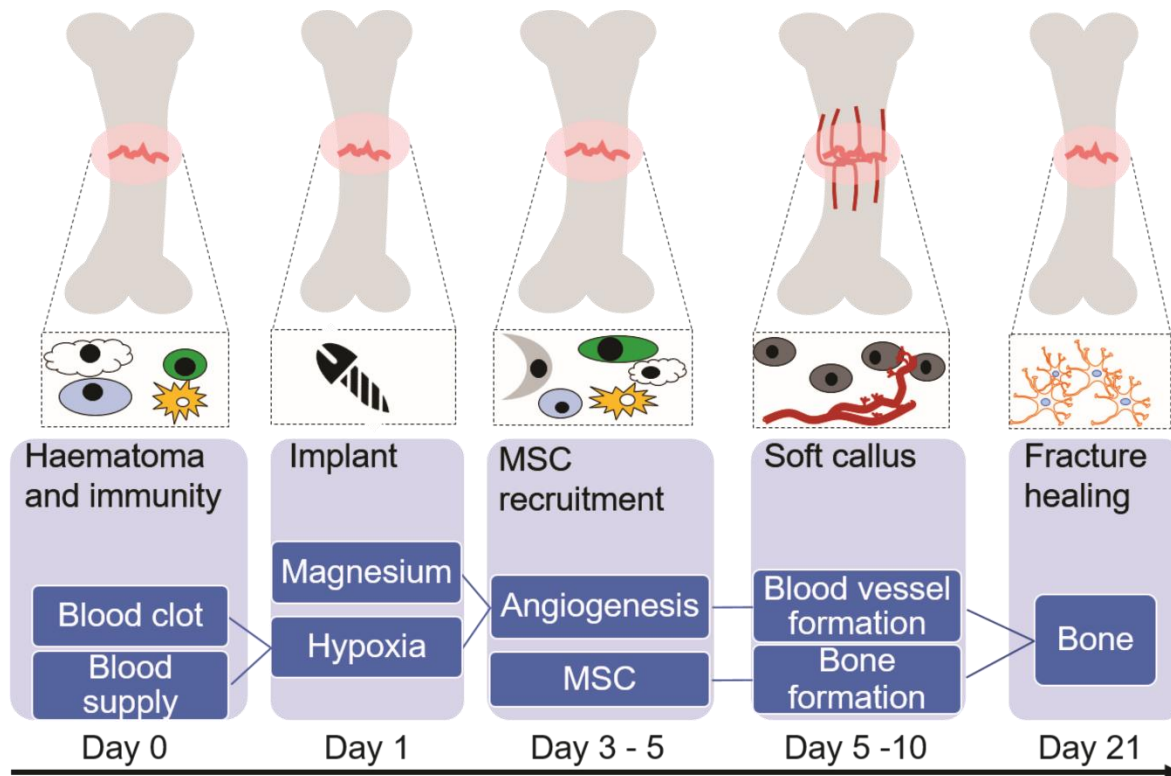


Fig. 2 The process of fracture healing.

The following events occur in fracture healing (Fig. 2):

- 1) Inflammation activity: inflammation is induced by T and B cells and macrophages.
- 2) MSCs within mesenchyme or the medullary cavity of a bone fracture initiate the intramembranous ossification *via* migration and differentiation. Once MSCs migrate into a specific area to act as osteoprogenitor cells and start to differentiate into osteoblasts⁶³, MSCs show a variety of gene expression and cytokine secretions. For instance, collagen I is vital for the later mineralisation of hydroxyapatite⁶⁴. Additionally, collagens affect the osteoid formation and cooperate with calcium salts and phosphorous to mineralise the bone tissue⁶⁵. ECs can migrate into callus and develop micro-blood vessels.
- 3) Bony callus: osteoblasts differentiated from MSCs convert cartilaginous into a bony callus.
- 4) Bone remodelling: ultimately, bony callus hardens, fracture remodelling occurs, and the shape is restored to compact bone.

Moreover, bone remodelling is influenced by a balance between the removal of old or damaged bone (resorption) and the subsequent formation of new bone (formation). Normally, the bone-resorptive

osteoclasts (OCs) and bone-forming osteoblasts (OBs) are in balance. But due to (*e.g.*) age, gender, cancer or some other immune-system-activated diseases, this process can be disturbed and lead to local or systemic bone loss or increase^{66,67}. Mg is believed to mediate OB and OC activities⁶⁸. Considering the osteoblast precursor role of MSCs, Mg could also regulate MSCs before directly influencing OBs during bone remodelling.

Hypoxia is an oxygen shortage and another important parameter in bone remodelling. Hypoxia is reported to regulate osteogenesis and angiogenesis (refer to section 2.3.1). This oxygen shortage is induced by blood clotting, but hypoxia could also be expected since Mg degradation is oxygen dependent⁶⁹. In summary, ECs and MSCs can act as protagonists for angiogenesis and osteogenesis. Because of the broad and close relationship between MSCs, ECs, and hypoxia in the stromal cell niche, the effects of Mg on bone regeneration must be investigated in a more collective, complicated system.

2.1.1. Mg and angiogenesis

Angiogenesis defines the process by which new blood vessels form and in which the EC is the protagonist. For instance, ECs provide a functional basis by maintaining the integrity of the blood vessel inner surface⁷⁰ and regulating homeostasis, vascular tone, coagulation, growth regulation and the modulation of blood flow⁵⁶. Angiogenesis is an essential procedure for replacing damaged tissue such as fractured bone. Specifically, angiogenesis defines EC detachment, migration and reorganisation. The migration stage begins with adhesion and migration, while tube formation begins with adhesion, migration, protease activity and subsequent tubulogenesis (Fig. 3)^{72,73}. In each step, ECs utilise corresponding growth factors to mediate proteinases leading to ECM degradation, integrins during adhesion and some morphogenetic molecules for cytoskeleton transformation. Mg is reported to influence angiogenesis. For instance, Mg can change the cell morphology *via* rearranging the actin cytoskeleton⁷⁴.

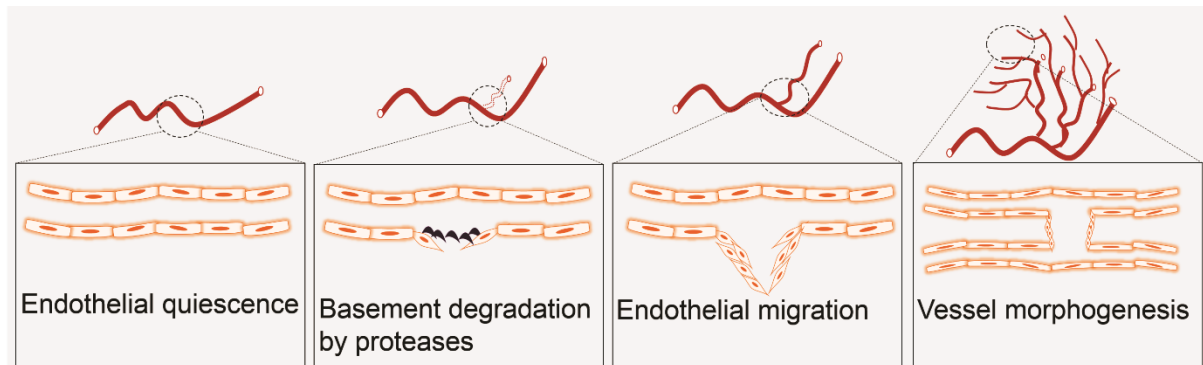


Fig. 3 Angiogenesis process.

2.1.2. Mg in the MSC-EC interaction and MSC fate

Besides angiogenesis, the MSC is another protagonist in bone regeneration. MSCs are widely distributed in bone marrow, periosteum, adipose tissue, skin and dental tissues⁷⁵. MSCs show multilineage potential, with the ability to self-replicate and differentiate into mesenchymal tissues, *e.g.*, bone, cartilage, ligament, tendon, muscle and adipose tissue⁷⁶. MSCs are stable with cell surface markers and markers of *in vitro* differentiation potential⁷⁷. MSCs can mediate chronic inflammation and angiogenesis in the microenvironment of the host tissue by secreting cytokines, anti-inflammatory factors and immune receptors⁷⁶.

Though MSCs possess ideal natural capacities, their activity may differ when MSCs are under the influence of exogenous materials, *e.g.*, biomaterials. Recent evidence indicates that the clinical outcome and future research could benefit from a concentration on improving and better understanding of cell migration, osteoblastic differentiation and the local environment. The homing and migration of MSCs are prerequisites to reach the target tissue and effectively express activity to regenerate and regulate a local fracture or normal tissue⁷⁸. The resident MSCs in the knee joint synovium are proven to undergo proliferation and chondrogenic differentiation after MSC infusion *in vivo*⁷⁹. Most cases, however, suggest that the homing of MSCs after cell seeding is insufficient^{75,80}. Research suggests that this failure is related to a low expression of homing molecules, loss of migration molecules during expansion and an increase in heterogeneity⁸⁰. After migration, a better understanding of the molecular mechanisms involved in the successive steps of MSC-osteoblastic differentiation appears to be crucial for enhancing bone regeneration^{81,82}. In the microenvironment of the cell niche, besides the chemokine factors⁸³, MSCs can also share Mg degradation products and hypoxia with ECs and eventually contribute to fracture healing⁸¹.

The present investigation of Mg effects on osteogenesis mostly focuses on MSCs or ECs alone. Mg was reported to suppress transcriptional remodelling⁸⁴ while supporting the chondrogenic differentiation⁸⁵ of bone marrow MSCs (BM-MSCs). The significance of the study may be limited mostly because the observations were not performed within the cell niche.

2.1.3. The model for investigating the MSC-EC interaction

The methodology to study the interaction *in vitro* depends on direct-contact coculture or indirect coculture to mimic the native cell niche⁸⁶. To mimic optimally the native conditions, the donor influence between cell types must be minimised. For example, the osteoblast differentiation mechanisms show significant differences between humans and mice⁸². A direct-contact coculture system is necessary for investigating the effects of cell-cell contact, which is widely reported but still debated^{87,88}.

ECs can be obtained from the human umbilical cord as human umbilical vein endothelial cells (HUVECs), which can produce relatively low contamination with smooth muscle cells and fibroblasts. HUVECs are widely used in the laboratory for studying angiogenesis function and endothelial pathology. The MSC donors can be different adult- or birth-associated tissues, such as adipose tissue (AT), bone marrow (BM), peripheral blood (PB), placenta, amnion, umbilical cord (UC) and umbilical cord blood (UCB)⁸⁷. Human UC has prominent advantages, including ready availability that avoids ethical issues such as painful body invasion accompanied by pain and infection risk⁸⁷. MSCs from UC are proven to possess faster self-renewal along with enhanced tissue repair and immunoregulation^{89,90}. Moreover, UC-MSCs, compared to adult-derived sources, possess a variety of superior embryonic and biological capacities, such as improved proliferation, life span and differentiation potential⁸⁷. MSCs can be isolated from the different UC compartments, such as Wharton's jelly (WJ)⁹¹, umbilical cord blood (UCB)⁹², vein, arteries, the UC lining and the subamnion and perivascular regions⁹⁰. MSCs are easy and risk-free to isolate from UCB, but the MSC yield is very low⁹³. Isolation from vein and arteries could bring the highest yield (~80%) but also contamination with ECs or blood cells while the perivascular area and WJ store 21% of the MSCs⁹⁴. Therefore, MSCs are isolated by culturing the vein covered with perivascular tissues. The isolated MSCs are called human umbilical cord perivascular vein (HUCPV) cells.

3 Motivation and objectives

To gain a more comprehensive understanding of Mg effects, different HUCPV-HUVEC monocultures and cocultures were applied under normoxia and hypoxia conditions. The findings can also present the value of MSCs in regenerative medicine. To acquire purified MSC and EC populations, HUCPV cells and HUVECs were isolated from human umbilical cord and validated by surface markers. The differentiation potential of isolated ECs and MSCs were investigated by induced tube formation and osteogenesis, respectively. To mimic angiogenesis, the HUVEC type was investigated by the wound healing and tube formation assays. To investigate the respective effects of paracrine and cellular heterotypic contact between MSCs and ECs in the stem cell niche, transwell and direct-contact cocultures were used to grow HUCPV cells and HUVECs. In all models, the proliferation, metabolism, gene regulation and cytokine levels were investigated.

4 Materials and methods

4.1 Magnesium degradation products

4.1.1 Materials

Table 4 Materials and equipment for Mg extraction and characterisation.

Product	Abbreviation	Supplier
99.95% Pure magnesium	Pure-Mg	Helmholtz-Zentrum Geesthacht, Germany
Minimum essential medium, Eagle-alpha modification	α -MEM	Fisher Scientific GmbH, Schwerte, Germany
Foetal bovine serum for Human mesenchymal stem cells	SC-FBS	Biological Industries, Beit-Haemek, Israel
100% n-Hexane	100% n-Hexane	Merck, Darmstadt, Germany
100% Acetone	100% Acetone	Merck, Darmstadt, Germany
100% Ethanol	100% Ethanol	Merck, Darmstadt, Germany
70% Ethanol	70% Ethanol	Merck, Darmstadt, Germany
Penicillin/Streptomycin	P/S	Fisher Scientific GmbH, Schwerte, Germany
CO ₂ incubator	Incubator	Thermo Scientific – Fisher Scientific GmbH, Langenselbold, Germany
Inductively coupled plasma mass spectrometry	ICP-MS	Agilent, Waldbron, Germany
Cryoscopic osmometer	Osmometer	Gonotec, Berlin, Germany
Sentron pH meter	pH Meter	Sentron Europe BV, VD Leek, Netherlands

4.1.2 Samples cleaning and sterilisation and Mg extract preparation

Pure-Mg (99.95%) was prepared by permanent mould gravity casting at Helmholtz-Zentrum Geesthacht (Geesthacht, Germany). T4 treated ingots were extruded into rods of 1 cm diameter. The rods were machined into a diameter of 0.9 cm. Disks were cut at a 1.5 mm thickness and then cleaned *via* 20 min sonication in 100% n-hexane, 100% acetone, 100% ethanol, sterilised in 70% ethanol, and further dried under clean-bench conditions. Mg-degradation products or extracts were produced according to EN ISO standards I. 10993-5:2009 and I. 10993-12:2012 (0.2 g of material/mL of extraction medium) for 72 h under physiological conditions (37 °C, 5% CO₂, 20% O₂, 95% relative humidity). The extraction media were α -MEM plus 15% SC-FBS and 1% P/S. Afterwards, the Mg, Ca and phosphorous (P) contents

were measured (Table 5) via ICP-MS. The Mg extract was diluted to 2, 4, and 8 mM with the same media as those used for extraction. The osmolality and pH of the diluted extract were tested by an osmometer and an ArgusX pH meter, respectively.

Table 5 Characterisation of Mg degradation products. *Values were obtained from calculations or the cell culture media composition provided by the manufacturer.

Extract	Magnesium (mM)	Calcium (mM)	Natrium (mM)	Phosphorus (mM)	Osmolality (osmol/kg)	pH
Control	0.81*	1.80*	143.43*	1.01*	0.290±0.003	7.55±0.005
1×	70.37±1.16	0.63±0.11	150.72±5.23	0.26±0.09	0.41±0.001	8.06±0.01
2 mM Mg	2.00*	0.65±0.11	150.60±5.14	0.27±0.09	0.30±0.003	7.59±0.06
4 mM Mg	4.00*	0.68±0.10	150.39±5.00	0.29±0.09	0.31±0.002	7.59±0.07
8 mM Mg	8.00*	0.75±0.10	149.97±4.70	0.34±0.08	0.31±0.003	7.67±0.03

4.2 The isolation of human umbilical cord

4.2.1 Materials and ethical approval

Ethical approval for the isolation of the cells was obtained from the Ethik-Kommission der Ärztekammer Hamburg (PV4058).

Table 6 Materials and equipment used for cell isolation.

Name	Abbreviation	Supplier
Endothelial cell growth medium	ECGM	PromoCell, Heidelberg, Germany
Endothelial cell growth supplement	ECGS kit	PromoCell, Heidelberg, Germany
Minimum essential medium, Eagle-alpha modification	α-MEM	Fisher Scientific GmbH, Schwerte, Germany
Foetal bovine serum optimised for human mesenchymal stem cells	SC-FBS	Biological Industries, Beit-Haemek, Israel
Penicillin/Streptomycin	P/S	Fisher Scientific GmbH, Schwerte, Germany
Phosphate-buffered saline	PBS	Thermo Scientific – Fisher Scientific GmbH, Langenselbold, Germany
Foetal bovine serum	FBS	Biochrom, Berlin, Germany
Nunc™ EasYFlask™ 175 cm ²	T175 flask	Fisher Scientific, Roskilde, Denmark
Collagenase (from <i>Clostridium histolyticum</i> Type IA)	Collagenase	Sigma-Aldrich, Munich, Germany
Nalgene sterile syringe filter, 0.2 µm	Syringe filter	Fisher Scientific GmbH, Schwerte, Germany

4.2.2 The structure of the human umbilical cord

The human umbilical cord contains two artery vessels and one vein vessel, which are covered with perivascular Wharton's jelly (WJ). WJ is the gelatinous substance that insulates umbilical blood vessels, intermediate WJ, cord lining WJ and maternal sheath with outer covering from the inside (Fig. 4b)^{95, 96}. The perivascular region is the closest surrounding the vessels and is part of the WJ matrix, which has been the focus area for UC-MSC isolation (Fig. 4c).

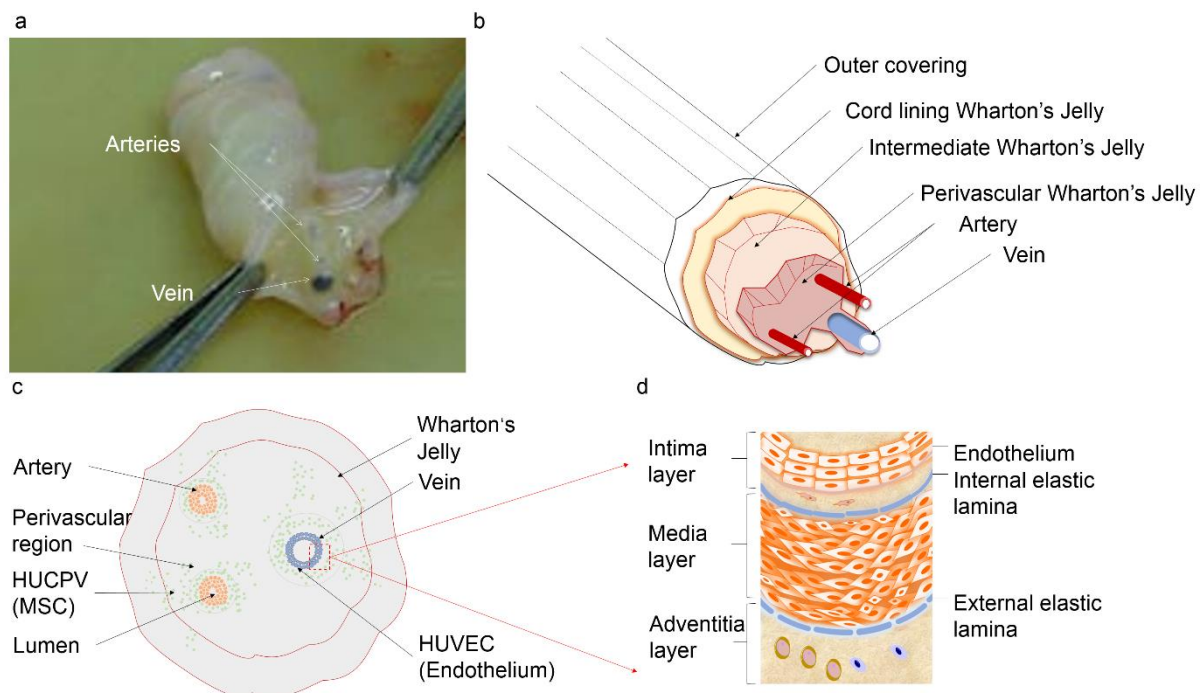


Fig. 4 Dissection of human umbilical cord (UC) shown (a) photographically, (b) as a schematic diagram, (c) UC cross-section, (d) endothelial cells and endothelium in a blood vessel. Fig. 4b is adapted from [97] and premised by Wiley Publication. Copyright© 2000-2019 by John Wiley & Sons, Inc.

4.2.3 HUCPV cell isolation

Referencing the WJ distribution shown in Fig. 4b and the cell distribution indicated in Fig. 4c, HUCPV cells were expanded by cultivating the arteries with perivascular WJ:

- 1) The blood was removed *via* washing with sterilised PBS.
- 2) The umbilical cord was dissected to acquire the arteries and vein.
- 3) Both ends of the arteries were ligated with sterilised surgical thread.
- 4) The ligated arteries were cultured in a T175 flask with α -MEM-complete medium (supplemented with 15% SC-FBS and 1% P/S).
- 5) The cell proliferation was observed to avoid more than 70% confluence (possible cell

differentiation).

4.2.4 HUVEC isolation

HUVECs can be derived from the endothelium of veins from the umbilical cord *via* digesting the tissue connection between the endothelium, internal elastic lamina and smooth muscle cells (Fig. 4d). Collagenases are usually used as a ferment dispase (proteolytic enzymes) for digesting cells. Compared to other collagenases, type I possesses the lesser protease activity and was applied as a ferment dispase to derive ECs from the vein lumen⁹⁸.

HUVECs were acquired and cultured based on the following procedures:

- 1) Blood was washed by sterilised PBS.
- 2) The umbilical cord was dissected to acquire the vein.
- 3) The inner lumen of the vein was flushed by injecting sterilised PBS.
- 4) Collagenase solution (0.2% w/v) was injected, and the solution filled the lumen of the vein.
- 5) The ends of the vein were ligated, and the vein was incubated in 37 °C-sterilised PBS for 15 min.
- 6) The vein lumen was flushed with ECGM-complete medium (ECGM supplemented with ECGS and 10% FBS).
- 7) The flushed medium was centrifuged (1,000 rpm, 10 min).
- 8) The centrifuged cell pellet was resuspended and cultured in ECGM-complete medium with 5,000 cells/cm² under physiological conditions (37 °C; 95% air and 5% CO₂, saturated with H₂O).
- 9) The cultures were examined for typical “cobblestone” morphology every 24 h, and possible contamination (such as a blood clot) was removed *via* washing with PBS.

4.3 HUCPV and HUVEC characterisation

4.3.1 Immunophenotyping

HUCPV cells and HUVECs can be efficiently immunophenotyped by confirming the expression of specific markers *via* flow cytometry. Considering the location and the surroundings of HUCPV cells and HUVECs in the umbilical cord, the potential contamination from local cell types (*e.g.*, blood cells) was also considered. Thus, in the immunophenotyping, the cluster of differentiation (CD) 31, CD 90 and CD

105 were applied as positive controls (full molecule names can be found in Table 8). Moreover, CD 45 and CD 31 were used as negative controls for hematopoietic and endothelial (only in the HUCPV cell isolate) contamination, respectively. The natural Y shape of an antibody can be divided into three sections, with the Fc section a binding region for endogenous Fc receptors on the cellular surface and the binding site for the secondary antibody⁹⁹. In addition to Fc, nonspecific adhesive material, as an example, might undesirably bind to the cell membrane. Therefore, to distinguish between positive and negative populations and between nonspecific and specific antibody signals¹⁰⁰, an isotype control containing corresponding mouse immunoglobulin G conjugated with the same fluorochrome was used. Thus, the isotype controls should match the primary antibody regarding the host species, the class of heavy and light chains and the fluorochrome conjugate and molecule number per immunoglobulin (IgG), as well as derive from the same manufacturing lot^{100,101}. Consequently, mouse immunoglobulin G (IgG) was used as an isotype control (Table 8).

Materials

Cells resuspended in PBS served as a blank control. BSA in PBS (1% w/v) was prepared for use as a staining buffer. All antibodies and isotypes were purchased from Thermo Fisher (Fisher Scientific GmbH, Germany), as listed in Table 7 and 8. All markers are distributed on the cell surface.

Table 7 Materials for flow cytometry

Product	Abbreviation	Supplier
Bovine serum albumin	BSA	Carl Roth, Karlsruhe, Germany
Phosphate-buffered saline	PBS	Thermo Scientific – Fisher Scientific GmbH, Langenselbold, Germany
0.05% Trypsin-EDTA	Trypsin	Life Technologies, Schwerte, Germany
Bio-Rad S3e™ Cell Sorter	Flow cytometer	Bio-Rad Laboratories, Munich, Germany
Round-bottom polystyrene tubes	Flow cytometer tubes	Bio-Rad Laboratories, Munich, Germany
Propidium iodide	PI	Bio-Rad Laboratories, Munich, Germany
Prosort™ software for S3e™ Cell Sorter, version 1.5	ProSort software	Bio-Rad Laboratories, Munich, Germany

Table 8 Antibody information

Population	Purpose	Marker	Antigen	Catalogue	Conjugate	Isotype	Reference
HUCPV	Control for endothelial contamination	CD 31	Platelet endothelial cell adhesion molecule-1	MA119769	PE	Mouse IgG1/#559320	[87]
	Control for hematopoietic cells	CD 45	Leukocyte common antigen	MA119569	FITC	Mouse IgG1/#555748	[102, 103]
	Negative control	CD34	Sialomucin-like adhesion molecule	MA119645	PE	Mouse IgG1/#559320	[104, 105]
		CD 54	Intercellular adhesion molecule 1	MA110250	PerCP	Mouse IgG2b/#558304	[87]
	Positive	CD 90	Thy-1 cell surface antigen	A15761	FITC	Mouse IgG1/#555748	[106]
		CD 105	Endoglin	MA119594	FITC	Mouse IgG2a/#555573	[87]
HUVEC	Control for hematopoietic cells	CD 45	Leukocyte common antigen	MA119569	FITC	Mouse IgG1/#555748	[107]
	Positive	CD 31	Platelet endothelial cell adhesion molecule-1	MA119769	PE	Mouse IgG1/#559320	[108]
		CD 105	Endoglin	MA119594	FITC	Mouse IgG2/#555573	[108]

Immunophenotyping is a process using antibodies to identify cells based on the types of antigens or markers on the surface of the cells. The cell population was identified by the expression of specific markers as positive, negative and isotype controls using flow cytometry. The schematic about immunophenotyping is introduced in Appendix (Fig. S1).

Procedures

- 1) Cells were dissociated by 0.05% trypsin-EDTA.
- 2) The dissociated cells were adjusted to 500,000 cells per 20 μL of staining buffer and stained with the following antibody solutions according to the flow cytometry panel designed for HUCPV cells and HUVECs (Table 8). The FL channels are dependent on the fluorescence spectrum of conjugated dyes and detection sensors.
 - a) CD 105: 5 μL for 5×10^5 cells, FITC (FL1 channel)
 - b) CD 54: 2 μL for 5×10^5 cells, PerCP (FL4 channel)
 - c) CD 31: 2 μL for 5×10^5 cells, PE (FL2 channel)
 - d) CD 34: 2 μL for 5×10^5 cells, PE
 - e) CD 45: 2 μL for 5×10^5 cells, FITC
 - f) CD 90: 2 μL for 5×10^5 cells, FITC
- 3) Samples were incubated at 4 °C for 30 min in darkness on ice.
- 4) Cells were washed once with warm staining buffer and centrifuged at 13,000 rpm for 5 min.
- 5) Samples were resuspended in a 5 mL of ice-cold PBS in round bottom flow cytometer tubes.
- 6) The forward scatter (FSC) and side scatter (SSC) were determined by blank controls. The diameter of the cell can be measured *via* FSC, which is proportional to the light diffraction around the cell. SSC can provide information about the internal complexity (*i.e.* granularity) of the cells¹⁰⁹. At some extent, FSC and SSC can represent the heterogeneity within the cell population.
- 7) The corresponding fluorescence intensity of different groups (positive, blank, negative and isotype) and their propidium iodide (PI) staining were detected *via* the collection of 5,000 to 10,000 events per assay.
- 8) Unspecific binding was excluded based on no significant difference between the isotype and blank controls. The results were obtained by compensating the marker expression with the blank controls, PI staining or single staining if cells were double stained with two fluorochromes. By gating >95% of the events in blank controls, the results were finally acquired after applying the gate to the other assays using ProSort™ software.

4.3.2 Differentiation potential

Osteogenesis inducement

To characterise further the mesenchymal stem cells, HUCPV osteogenic potential was induced in medium containing osteogenic components such as 1α , 25-dihydroxyvitamin D3 (Vit D3), β -glycerophosphate, L-ascorbic acid and dexamethasone. Method 1, 2 and 3 contain different osteogenic components were applied to validate the osteogenesis potential of isolated HUCPV cells^{91, 110}. HUCPV cells (passage 5th to 8th) were seeded as 5,000 cells/cm² in 24-well plates for 21 days. Every 7 days, the supernatant and cells were used for investigating DNA, alkaline phosphatase (ALP) activity and ARS staining.

Angiogenesis inducement

The ability to develop capillary structure is a vital step during angiogenesis¹¹¹. To form three-dimensional vascular networks (capillary-like networks), specific molecules in the “matrix-integrin-cytoskeletal signalling axis” are involved in such angiogenesis assembly¹¹². The tube formation assay is a typical platform to investigate this reorganisation stage. This assay needs to be optimised because of the variation induced by cell types, experimental media and treatment compounds. HUVECs were first expanded to 70-80% confluence (exponential phase) to obtain more activated cells¹¹³ and then starved in ECGM-complete medium supplemented with low FBS (1%) for 24 h to synchronise the life cycle in the G0/G1 phase. One requirement for EC capillary development is the extracellular matrix (ECM). The usual ECM coating requires a large amount of matrix to create a thick layer on a flat surface because the matrix is viscous. An adapted thin-layer assay (TLA)¹¹⁴ was applied, as indicated in tube formation assay (refer to Fig. 8 in section 4.13).

4.4 Cell expansion

HUVECs were cultured in ECGM-complete medium as 5,000 cells/cm² in physiological conditions until 90% confluence or up to passage 6. The HUCPV cells were cultured in α -MEM-complete medium (α -MEM plus 15% SC-FBS and 1% P/S) as 2,000 cells/cm² in physiological conditions before 80% confluence or up to passage 12.

4.5 Coculture system

To understand the cytokine effects and contact dependency during coculture, HUCPV cells and HUVECs were cocultured as non-contact (transwell) and contact (cell mixed) coculture models, respectively (Fig. 5). The well areas of the low chamber and insert were 2 and 0.33 cm², respectively. The well areas of the 24- and 96-well plates were 2 and 0.32 cm², respectively. Based on the results of the medium test (Section 5.2), the α -MEM-complete medium was applied as the coculture medium.

In the non-contact or transwell coculture and the wound healing assay, HUCPV cells and HUVECs (80,000:20,000 cells per well) were seeded in the inserts and the bottom chamber of 24-well plates respectively. Culture medium at a volume of 1.5 mL and containing or not containing Mg degradation product was refreshed every 3 days.

In direct-contact (*i.e.*, contacting) coculture, HUCPV cells and HUVECs (5,000:1,000 cells per well) were seeded together in 96-well plates for ELISA and DNA assays. HUCPV cells and HUVECs (80,000:20,000 cells per well) were seeded in 24-well plates for flow cytometry, Alizarin Red S staining (ARS) and the determination of alkaline phosphatase (ALP) activity. Two hundred microlitres of culture medium or Mg degradation product was used in 96-well plates or 1.5 mL in 24-well plates and refreshed every 3 days. The continuous presence of HUCPV cells and HUVECs in the direct-contact coculture throughout the culture period was monitored by the phenotypic expression of specific surface markers (CD 90 (Thy1 cell surface antigen) and CD 31 (platelet endothelial cell adhesion molecule-1) for HUVEC and HUCPV cells, respectively) *via* flow cytometry.

Both coculture models were used under physiological conditions. Hypoxia and normoxia were obtained under 5% and 20% O₂, respectively. All further assays or sample collections were performed on days 1, 4 and 7. Eventually, the continuous presence of HUCPV cells and HUVECs in the direct-contact coculture was monitored up to 7 days by the phenotypic expression of specific markers (CD 90 and CD 31 for HUVECs and HUCPV cells, respectively) *via* flow cytometry.

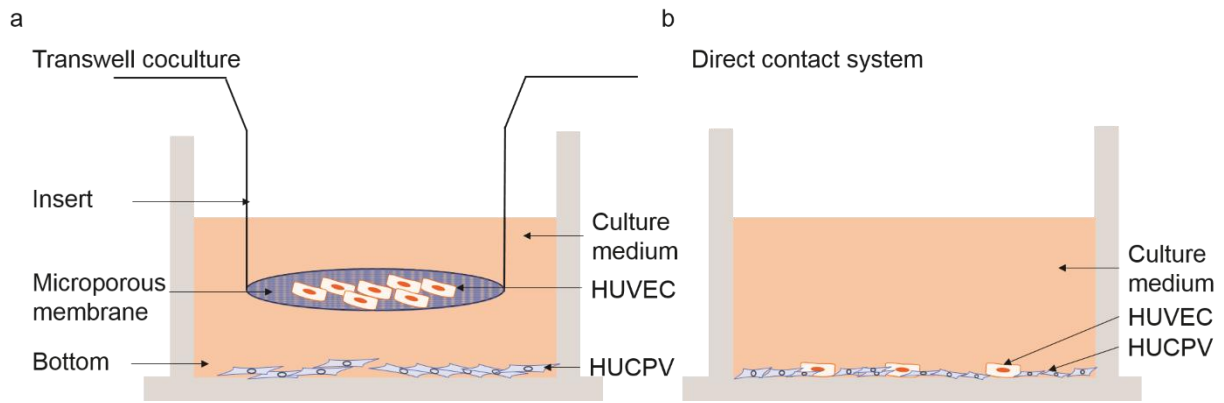


Fig. 5 The coculture systems: (a) transwell coculture and (b) direct-contact coculture.

4.6 Deoxyribonucleic acid (DNA) quantification

4.6.1 Materials

Table 9 Materials for DNA quantification

Name	Abbreviation	Supplier
2'-(4-Ethoxyphenyl)-6-(4-methyl-1-piperazinyl)-1H,3'H-2,5'-bibenzimidazole	Bisbenzimidide	Sigma-Aldrich, Munich, Germany
Sodium hydroxide pellets	NaOH	Sigma-Aldrich, Munich, Germany
Ethylenediaminetetraacetic acid	EDTA	Sigma-Aldrich, Munich, Germany
Tris(hydroxymethyl)aminomethane	Tris	Sigma-Aldrich, Munich, Germany
Human genomic DNA	gDNA	Sigma-Aldrich, Munich, Germany
Sodium chloride	NaCl	Merck, Darmstadt, Germany
Hydrochloric acid	HCl	Merck, Darmstadt, Germany
NanoDrop™ 2000c spectrophotometer	Nanodrop	Thermo Scientific – Fisher Scientific GmbH, Langenselbold, Germany
Thermomixer® comfort	Thermomixer	Eppendorf, Hamburg, Germany
VICTOR ³ multilabel plate reader	Plate reader	PerkinElmer, Waltham, USA
Cellstar® 24-well cell culture plate	24-Well plate	Greiner Bio-One, Kremsmünster, Austria
Minimum essential medium, Eagle-alpha modification	α-MEM	Fisher Scientific GmbH, Schwerte, Germany
Kimberly-Clark™ professional tissue wipers	Low-lint paper	Thermo Scientific – Fisher Scientific GmbH, Langenselbold, Germany

4.6.2 Procedures

Cell proliferation can assess physiological cell health and responses to foreign substances. DNA levels, synthesis, or cellular metabolism as well as proliferation-specific proteins can be typical markers. DNA investigation is accurate and simple because the amount of DNA in each cell remains constant for a given cell line or cell type. The DNA content can be quantified by spectrophotometry (*e.g.*, Nanodrop technique) or fluorometry (*e.g.*, bisbenzimidide fluorochrome). The bisbenzimidide was chosen for DNA quantification because of the more stable DNA results observed with bisbenzimidide.

The bisbenzimidide method was performed with the following steps:

- 1) Various treated cells were extracted in lysis buffer (25 mM NaOH, 0.2 mM EDTA) and incubated for 5 min at 37 °C.
- 2) Lysate was heated and centrifuged on the thermomixer at 98 °C and 1,000 rpm for 1 h and cooled

to 15 °C at 700 rpm.

- 3) Lysate was buffered with an equal volume of neutralisation solution (40 mM Tris/HCl, pH 5.5) and centrifuged at 13,000 rpm for 1 min.
- 4) Depending on the predicted DNA concentration and the linear range of standard curves, lysate was diluted with varying quantities of dilution buffer (2.5 M NaCl, 19 mM sodium citrate, pH 7). DNA standard curves were calculated by the fluorescence intensities and the concentrations of 1:2 serial dilutions of the genomic DNA (gDNA).
- 5) Lysis buffer and neutralisation solution were used as the blank control. Diluted samples (including standards and blank controls), DNA working buffer (2 M NaCl, 15 mM sodium citrate, pH 7) and bisbenzimidazole solution (2 µg/mL bisbenzimidazole in DNA working buffer) were prepared in a 2:1:1 ratio in 200 µL and ultimately pipetted into 96-well plates.
- 6) Then, the mixed solutions were incubated in the dark for 15 min. The DNA content was quantified by reading the bisbenzimidazole fluorescence with a plate reader at excitation (Ex) 355 nm and emission (Em) 460 nm. The DNA concentration was calculated with a fluorescence standard curve for DNA content. The same amount of vehicle buffers was applied as that used in the blank controls.

4.7 Metabolism assay

4.7.1 Materials

Table 10 Materials for mitochondrial susceptibility and membrane potential assays

Name	Content	Supplier
Digitonin detergent solution for permeabilising cells	Digitonin	Thermo Scientific – Fisher Scientific GmbH, Langenselbold, Germany
Antimycin A from Streptomyces species	Antimycin A	Sigma-Aldrich, Munich, Germany
Rhodamine 123	R123	Sigma-Aldrich, Munich, Germany
VICTOR3 multilabel plate reader	Plate reader	PerkinElmer, Waltham, USA
Sunrise™ Tecan microplate reader	Microplate reader	Tecan, Männedorf, Switzerland
PreMix WST-1 Cell Proliferation Assay System	WST-1 kit	Takara Bio Inc., Kusatsu, Japan

4.7.2 Metabolism

Mitochondria play a vital role in eukaryotic cellular metabolism since the majority of ATP is generated through oxidative phosphorylation in mitochondria¹¹⁵. During energisation, electrons are transported, crossing from electron donors (complex I to IV in Fig. 6) to electron acceptors such as oxygen. The mitochondrial electron transport chain creates an electrochemical gradient and generates the mitochondrial membrane potential ($\Delta\Psi_m$).

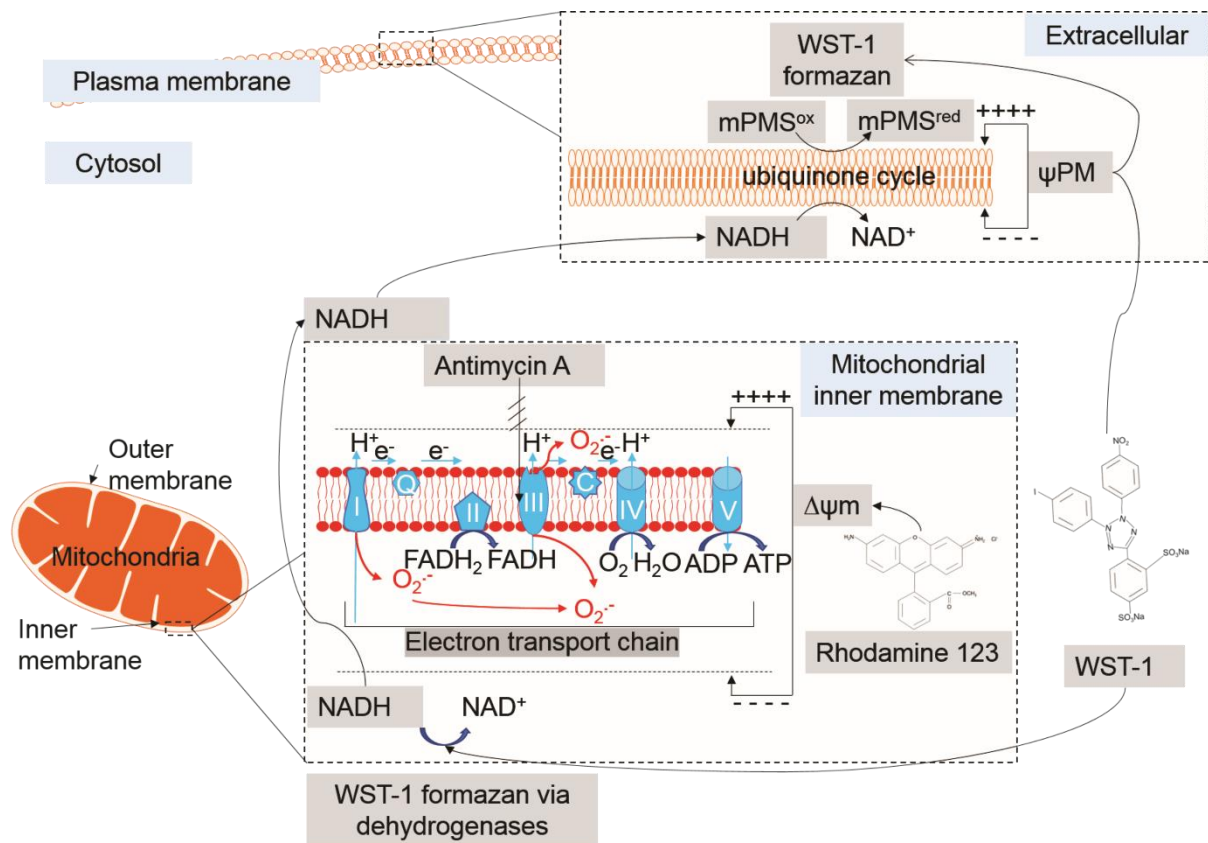


Fig. 6 WST-1 and rhodamine 123 involvement in metabolism.

Rhodamine 123 and WST-1 were used to investigate cellular metabolism. Because the mitochondrial inner membrane is negatively charged *via* the electron transport chain, and rhodamine 123 (R123) is cationic and lipophilic, R123 can diffuse through and selectively accumulate across the mitochondrial membrane in proportion to the membrane potential¹¹⁶. As an inhibitor of mitochondrial electron transport between cytochromes B and C (complex III)¹¹⁷, antimycin A eliminates the selective mitochondrial association with rhodamine 123, which triggers loss of $\Delta\psi_m$ ^{118, 119}. The application of rhodamine 123 in fluorescence microscopy to monitor $\Delta\psi_m$ has been reported in individual living cells¹¹⁶. Digitonin effectively water-solubilises lipid and can solubilise membrane proteins in the lipidic double layer, precipitate cholesterol and permeabilise cell membranes^{120, 121}. Digitonin did not affect the mitochondrial membrane in cytofluorometric analysis¹²². WST-1, as a classical tetrazolium salt, can be cleaved by complex I in the mitochondrial, changing from a slight pink material into yellow formazan (Fig. 6). Additionally, recent studies indicate that WST-1 can undergo transformation by the ubiquinone cycle in the cytoplasm represented by the cytoplasm membrane potential.

The effects of glucose and galactose on mitochondria-related experiments must be considered because

two ways are involved in generating ATP in mammalian cells, namely mitochondrial (oxidative phosphorylation) and non-mitochondrial (glycolysis). To increase the detection of xenobiotic-induced mitochondrial effects, cells have been forced to rely on mitochondrial oxidative phosphorylation rather than glycolysis¹²³. Thus, a further mitochondrial-related assay was performed under galactose-excluded conditions.

4.7.3 Rhodamine 123 assay

The mitochondrial membrane potential ($\Delta\psi_m$) in HUVEC monoculture model was measured by the retention of R123 fluorescence. HUVEC monocultures were seeded as 5,000 cells per well in 96-well plates. The cocultures were built as described in the “Coculture system” section. All the samples were cultured with Mg degradation products or α -MEM-complete medium (as control) at 37°C in 20 or 5% O₂. After the treatment period (e.g., on Day 1, 4 and 7), 30 nM of digitonin was added to each well, and the plates were incubated for 5 min on ice¹²². Rhodamine 123 (10 μ g/mL in PBS) was added to each well, and the plates were incubated for 10 min at room temperature (RT). Rhodamine 123 was excited (λ_{Ex}) at 510 nm, and the fluorescence emission was detected (λ_{Em}) at 534 nm with a plate reader as Rh T0. Antimycin A was added at a concentration of 10 μ M to the cells for 1 min on ice, and the fluorescence was detected after every 2 min for 3 times as Rh T2, T4 and T6. The value of $\Delta\psi_m$ was calculated by the difference between T0 and the average of T2 to T6. The variation induced by cell numbers between each treatment was normalised by the DNA content.

4.7.4 WST-1 assay

The metabolism represented by WST-1 was determined from the amount of formazan produced (Fig. 6). HUVEC monocultures were seeded as 5,000 cells per well in 96-well plates. Cocultures were seeded as described in the “Coculture system” section. All samples were cultured with Mg degradation products or α -MEM-complete medium (as control) at 37 °C in 20 or 5% O₂. After the treatment period (e.g., on Days 1, 4 and 7), WST-1 solution (1:10 in fresh control medium) was added as 500 μ L per well to 24-well plates, and the plates were incubated for 30 min in 20% and 5% O₂. The absorbance of 100 μ L of each sample was measured using a microplate reader at 450 nm. The variation induced by cell number differences between treatments was normalised by the DNA content. Absorbance was normalised by

the DNA content from a DNA quantification assay performed to reduce the variation in cell numbers.

4.8 Real-time quantitative polymerase chain reaction (RT-qPCR)

To investigate gene regulation, a particular RNA was quantified by two-step RT-qPCR. First, RNA was transcribed into complementary DNA (cDNA) from a total RNA sample. cDNA was then detected *via* measuring the amplification of DNA with SYBR Green fluorescent dye. Translation and RT-qPCR are introduced in Appendix (Fig. S2).

4.8.1 Materials

Table 11 Materials for RT-qPCR

Material	Abbreviation	Supplier
RNeasy mini kit	RNeasy kit	Qiagen, Hilden, Germany
Omniscript RT kit	RT kit	Qiagen, Hilden, Germany
cDNA primer (Table 13)	Primer	Eurofins MWG Operon, Ebersberg, Germany
SsoFast™ Evagreen® supermix	Ssofast supermix	Bio-Rad Laboratories, Munich, Germany
CFX96 Touch™ real-time PCR detection system	PCR detector	Bio-Rad Laboratories, Munich, Germany
CFX Manager™ software version 3.1	CFX software	Bio-Rad Laboratories, Munich, Germany
NanoDrop™ spectrophotometer	Nanodrop	Thermo Scientific – Fisher Scientific GmbH, Langensfeld, Germany

4.8.2 Ribonucleic acid (RNA) extraction and quality control of RNA

First, total RNA was extracted by binding RNA to silicon-based columns and washing off other fat and proteins using the QIAshredder and RNeasy kit. The RNA concentration was measured using a Nanodrop spectrophotometer. The RNA concentration was measured by the absorbance at 260 nm (A₂₆₀). The ratio of the absorbance at 260 to that at 280 nm (A_{260/280}) was used to ensure its purity.

4.8.3 Complementary DNA (cDNA) synthesis

cDNA was produced *via* reverse transcription (RT). The cocktail for each sample of the same treatment was prepared with the same amount of RNA (50-100 ng) to produce comparable results. The cocktail was prepared with the RT kit and incubated at 37 °C for 60 min by the PCR detector (Table 12). The

cDNA product was diluted 1:40 with nuclease-free water and stored at -20 °C until use.

Table 12 Cocktail for cDNA synthesis in RT

Name	Amount
10x Buffer RT	2 µL
dNTP mix	2 µL
RNase inhibitor	1 µL
Omniscript reverse transcriptase	1 µL
RNA template	50 or 100 ng
RNase-free water	Compensated for RNA volume
Cocktail final volume	20 µL

4.8.4 Primers and RT-qPCR

Primers were designed *via* Primer 3 (version 4.0.0) or found in the RTPimerDB database and purchased from Eurofins NDSC Food Testing Germany GmbH (Hamburg, Germany). The following targets were used, and their sequences are presented in Table 13. Beta-2-microglobulin (*B2M*) and actin beta (*ACTB*) were used as reference genes.

Table 13 Primers for RT-qPCR. Annealing temperature was 60°C for all designed primers.

Full name	Abbreviation	Sequence
Angiogenin	ANG	Forward: 5'-CATCATGAGGAGACGGGG-3' Reverse: 5'-TCCAAGTGGACAGGTAAGCC-3'
vascular cell adhesion molecule 1	VCAM1	Forward: 5'-CGTCTTGGTCAGCCCTTCT-3' Reverse: 5'-ACATTCATATACTCCCGCATCCTTC-3'
Vascular endothelial growth factor B isoform	VEGFB186	Forward: 5'-GCTCTTCTGCCATCCCTTGT-3' Reverse: 5'-TAGTGAGGGGAGGAAGAGCC-3'
Vascular endothelial growth factor receptor 1	FLT1/VEGFR1	Forward: 5'-GGGCTGAAACCATGTGCAAG-3' Reverse: 5'-GCCAAAGATGCACTCCTCCT-3'
Vascular endothelial growth factor receptor 2	KDR/VEGFR2	Forward: 5'-GGCATGGGGTCTGTTCTGAA-3' Forward: 5'-TTGGCCAGGAGACACGTAAC-3'
Transmembrane 4	CD9	Forward: 5'-CCTGCTGTTTCGGATTTAACTTCA-3' Forward: 5'-TGGTCTGAGAGTCGAATCGGA-3'
Ezrin	EZR	Forward: 5'-ATGCCCCACGTCTGAGAATC-3' Forward: 5'-TCCTGCGGCGCATATACAAC-3'
Integrin subunit alpha 1	ITGA1	Forward: 5'-GTGCTTATTGGTTCTCCGTTAGT-3' Reverse: 5'-GCCACAAGCCAGAAATCCT-3'
Integrin subunit alpha 2	ITGA2	Forward: 5'-TGTTGTTTGGCCTACAATGTTGG-3' Reverse: 5'-CAACCAGTAACCAGTTGCCTT-3'
Integrin subunit alpha 3	ITGA3	Forward: 5'-GGGATCCTGCCTAAGTTGTCT-3' Reverse: 5'-CCTTCTTTCTAGTTCCTTTGCTGTTG-3'

Table 13 (Continued)

Full name	Abbreviation	Sequence
Integrin subunit alpha M	ITGAM	Forward: 5'-GTGAAGCCAATAACGCAGC-3' Reverse: 5'-TCTCCATCCGTGATGACAAC-3'
Interleukin 8	IL8	Forward: 5'-ATAAAGACATACTCCAAACCTTTCCAC-3' Reverse: 5'-AAGCTTTACAATAATTTCTGTGTTGGC-3'
Matrix metalloproteinase 13	MMP13	Forward: 5'-TTTCAACGGACCCATACAGTTTG-3' Reverse: 5'-CATGACGCGAACAATACGGTTA-3'
TIMP metalloproteinase inhibitor 1	TIMP1	Forward: 5'-GGAGAGTGTCTGCCGATACTTC-3' Reverse: 5'-GCAGGTAGTGATGTGCAAGAGTC-3'
Hypoxia-inducible factor 1 alpha subunit	HIF1A	Forward: 5'-GGCGGAACGACAAGAAAAAG-3' Reverse: 5'-CCTTATCAAGATGCGAACTCACA-3'
Hypoxia-inducible factor 2 alpha subunit	HIF2A	Forward: 5'-TACAAGGAGCCCCTGCTGTC-3' Reverse: 5'-TGCTGGATTGGTTCACACATG-3'
Basic fibroblast growth factor	FGFb/FGF2	Forward: 5'-AAAAGGCAAGATGCAGGAGA-3' Reverse: 5'-TTTTGCAGCCTTACCCAATC-3'
Interferon gamma	IFN γ	Forward: 5'-TCGGTAACTGACTTGAATGTCCA-3' Reverse: 5'-TCCTTTTTTCGCTTCCCTGTTTT-3'
Ca-activated neutral protease 1	CAPN1	Forward: 5'-GGTGCGGCTAGAGACCATGT-3' Reverse: 5'-CTTGGCAGACGAGGAGGGAG-3'
Claudin 16	CLD16	Forward: 5'-TGGTAACTCGAGCGTTGATG-3' Reverse: 5'-TTCACGCAGTCAAGACCAAG-3'
Nitric oxide synthase	NOS2	Forward: 5'-ATGCTCAGCTCATCCGCTAT-3' Reverse: 5'-CGATGCACAGCTGAGTGAAT-3'
Cytohesin2	CYTH2	Forward: 5'-GAGGACGGCTCTATGAACC-3' Reverse: 5'-ACCTCGCTCATGGCTTCAC-3'
Selectin	SELE	Forward: 5'-TGTGGGTCTGGGTAGGAACC-3' Reverse: 5'-AGCTGTGTAGCATAGGGCAAG-3'
Bone morphogenetic protein 4	BMP4	Forward: 5'-ATGATTCCTGGTAACCGAATGC-3' Reverse: 5'-CCCCGTCTCAGGTATCAAAC-3'
Bone morphogenetic protein 6	BMP6	Forward: 5'-AGCGACACCACAAAGAGTTCA-3' Reverse: 5'-GCTGATGCTCCTGTAAGACTTGA-3'
Platelet-derived growth factor aa	PDGFA/PDGFaa	Forward: 5'-CCAGCGACTCCTGGAGATAGA-3' Reverse: 5'-CTTCTCGGGCACATGCTTAGT-3'
Osteoprotegerin	OPG	Forward: 5'-CGCTCGTGTCTGACAT-3' Reverse: 5'-GGACATTTGTCACACAACAGC-3'
Collagen type XII alpha 1 chain	Col12A1	Forward: 5'-CAGGTTCCGGCTAACACATT-3' Reverse: 5'-GCGCAAACATCTCAGAAAACA-3'
Endothelial differentiation related factor 1	EDF1	Forward: 5'-GCAAGGGGCTTACGCAGAA-3' Reverse: 5'-CGCTCTCATAGTCCGCGAT-3'
Integrin subunit alpha 1	ITGA1	Forward: 5'-GTGCTTATTGGTTCTCCGTTAGT-3' Reverse: 5'-GCCACAAGCCAGAAATCCT-3'
Collagen type I alpha 1 chain	COL1A1	Forward: 5'-AAGACATCCCACCAATCACC-3' Reverse: 5'-GCAGTCTTGGTCTCGTCCAC-3'

Table 13 (Continued)

Full name	Abbreviation	Sequence
TIMP metalloproteinase inhibitor 2	TIMP2	Forward: 5'-ACCCTCTGTGACTTCATCGTGC-3' Reverse: 5'-GGAGATGTAGCACGGGATCATG-3'
C-C motif chemokine ligand 2	CCL2	Forward: 5'-AGAATCACCAGCAGCAAGTGTC-3' Reverse: 5'-TCCTGAACCCACTTCTGCTTGG-3'
Beta-2-microglobulin	B2M	Forward: 5'-TGCTGTCTCCATGTTTGATGTATCT-3' Reverse: 5'-TCTCTGCTCCCCACCTCTAAGT-3'
Actin beta	Actin β	Forward: 5'-CTTCTGGGCATGGAGTC-3' Reverse: 5'-TGATCTTCATTGTGCTGGGT-3'
Glyceraldehyde 3-phosphate dehydrogenase	GAPDH	Forward: 5'-GTCGGAGTCAACGGATTTG-3' Reverse: 5'-TGGGTGGAATCATATTGGAA-3'
Bone morphogenetic protein receptor type 1a	BMPR1A	Forward: 5'-ACTGCCCCCTGTTGTCATAG-3' Reverse: 5'-AATGAGCAAAACCAGCCATC-3'
Fibronectin	FN1	Forward: 5'-AGTGGACACCACCAATGTT-3' Reverse: 5'-TTCATTGGTCCGGTCTTCTC-3'

RT-qPCRs were performed using SsoFast™ EvaGreen® Supermix with the CFX96 Touch real-time PCR detection system and CFX Manager software (version 3.1). The RT-qPCR cocktail was prepared according to Table 14. The thermal cycling conditions consisted of an initial denaturation at 95 °C for 3 min, followed by 40 of the following additional cycles: 20 s denaturation at 95 °C, 20 s annealing at 60 °C and 30 s elongation at 75 °C. A melting curve step (95 °C for 30 s and heating from 65 to 95 °C in 0.5 °C increments of 5 s) was set to confirm the melting temperature (T_m) of the PCR products. No-treatment controls (NTC, only primer) were performed to exclude reaction contamination and primer dimerisation.

Table 14 Composition of the RT-qPCR cocktail.

Name	Amount (μ L)
Ssofast supermix	5
Forward primer	0.5
Reverse primer	0.5
cDNA	0.625
Purified H ₂ O	9.0
Total final volume	10

The quantification of gene expression was performed by the 2(-Delta CT) method ($\Delta\Delta C_t$) and reported as the fold difference in comparison to the internal controls and the control samples (set to 1).

4.9 ALP activity

4.9.1 Materials

Table 15 Materials and equipment for the ALP assay.

Chemical	Abbreviation	Supplier
Quantichrome™ alkaline phosphatase assay kit	ALP kit	BioAssay Systems, Hayward, USA
Sunrise™ microplate reader	Microplate reader	Tecan, Männedorf, Switzerland

4.9.2 The principle and procedure

The ALP, also known as tissue non-specific alkaline phosphatase (TNAP), is an ubiquitous enzyme in numerous tissues such as liver, kidney and bone. The quantification of ALP can indicate bone formation or mineralisation. ALP catalyses the hydrolysis of phosphate esters and produces both organic radicals and inorganic phosphate. For instance, p-nitrophenyl phosphate (pNPP) can be hydrolysed by ALP to produce a yellow product, which has an absorbance peak at 405 nm; the rate of production was directly proportional to the enzyme activity. Thus, ALP activity can be quantified via measuring the optical density of p-nitrophenol.

HUCPV cell monocultures were seeded as 20,000 cells per well in 24-well plates. Direct-contact and transwell cocultures were seeded as described in the “Coculture system” section. All the groups were cultured in Mg degradation products or α -MEM-complete medium (as control) at 37 °C in 20 or 5% O₂. On Days 1, 4 and 7, the supernatant was collected and stored at -80 °C for further assays. The variation in results induced by proliferation was normalised by the DNA concentration of HUCPV cells. DNA from the direct-contact coculture of HUCPV cells was calculated by from the flow cytometry and DNA quantification results.

4.10 ARS staining

4.10.1 Materials

Table 16 Materials and equipment for ARS staining

Name	Abbreviation	Supplier
Alizarin Red S	ARS	Sigma-Aldrich, Munich, Germany
Nikon inverted microscope system, Ti-S/L100	Inverted microscope	Nikon, Minato, Japan
Sunrise™ microplate reader	Microplate reader	Tecan, Männedorf, Switzerland

4.10.2 Procedures

Alizarin Red S (ARS) is an anthraquinone dye that can react with both pure and ionic Ca to form Alizarin Red S-Ca precipitates with sulfonic acid and/or OH groups¹²⁴. Alizarin Red S has been applied in many studies related to bone growth and calcium deposition - mineralisation (*i.e.*, hydroxyapatite [a form of $\text{Ca}_{10}(\text{PO}_4)_6(\text{OH})_2$]) in mesenchymal stem cells¹²⁴. HUCPV cells were seeded as 20,000 cells per well in 24-well plates as a monoculture. All mono- and cocultures were grown at 37 °C in 20% and 5% O₂ in Mg degradation products or α -MEM medium (as control). On days 1, 4 and 7, ARS staining was performed, and the staining pattern was visualised by inverted microscopy.

4.11 Enzyme-linked immunosorbent assay (ELISA)

ELISA (enzyme-linked immunosorbent assay) is a colorimetric assay reaction designed for quantifying a ligand (commonly a protein). Here, sandwich ELISA was performed to quantify cytokines. The principle of sandwich ELISA is introduced in Appendix (Fig. S3).

4.11.1 Materials

The following solutions were prepared based on Table 17:

- Wash buffer: 0.05% (v/v) Tween® 20 in PBS, pH 7.3, adjusted with 20% (v/v) HCl
- Block buffer: 1% BSA in PBS, pH 7.3, 0.2 μm filtered
- Substrate solution: 1:1 mix of H₂O₂ and TMB
- Stop solution: 2 N H₂SO₄

- Capture antibody solution: reconstitute with no-protein PBS (the lyophilised antibody with epitope responding to the antigen of interest)
- Detection antibody: was reconstituted in reagent diluent (biotinylated primary antibodies that respond to antigens with another epitope comparable to that of capture antibody)
- Streptavidin-HRP: was reconstituted in reagent diluent (secondary antibodies conjugated with and responsive to primary antibodies)

Table 17 Materials and kits for ELISA

Content	Name	Supplier
Human FGF basic DuoSet® ELISA	FGFb	
Human IL-8/CXCL8 DuoSet® ELISA	IL8	
Human CCL2/MCP-1 DuoSet® ELISA	CCL2	
Human Total MMP-13 DuoSet® ELISA	MMP13	
Human TIMP-1 DuoSet® ELISA	TIMP1	
Human eNOS DuoSet® ELISA	eNOS/NOS3	
Human VEGFA DuoSet® ELISA	VEGFA	R&D Systems, Abingdon, UK
Human PDGF-AA DuoSet® ELISA	PDGFaa	
Human TGFβ1 DuoSet® ELISA	TGFβ1	
Stabilised hydrogen peroxide (H ₂ O ₂), stabilised with tetramethylbenzidine (TMB)	Substrate solution	
Plate sealer	Sealers	
A comprehensive collection of reagents and plates	Reagent buffer	
Phosphate-buffered saline buffer	PBS	
Nalgene syringe filter, sterile, SFCA membrane, 0.2 µm	0.2 µm filter	Thermo Scientific – Fisher Scientific GmbH, Langenselbold, Germany
Microplate with clear polystyrene wells and flat bottom	Nunc™ 96-well plate	
Polyethylene glycol sorbitan monolaurate	Tween® 20	Sigma-Aldrich, Munich, Germany
Bio-Plex Pro™ wash station	Autowasher	Bio-Rad Laboratories, Munich, Germany
Sunrise™ microplate reader	Plate reader	Tecan, Männedorf, Switzerland

4.11.2 Procedures

- 1) Capture antibody solution (50 µL) was added on the polystyrene surface in 96-well plates for 12 h at room temperature (RT).
- 2) The nonbinding antibody was washed 2 times with 150 µL of wash buffer by an autowasher using crosswise aspiration.
- 3) The remaining nonspecific surface was blocked with 50 µL of block buffer for 1 h at RT.

- 4) Block buffer was washed 2 times with 150 μL of wash buffer by an autowasher using crosswise aspiration.
- 5) Antigens (samples or standards) were bound with 50 μL of capture antibodies for 1 h at RT. Depending on the antigen concentration, samples were diluted to avoid results fall beyond the linear range of the standard curve.
- 6) Unbound antigen was washed 2 times with 150 μL of wash buffer by an autowasher using crosswise aspiration.
- 7) Detection antibodies (50 μL) were bound to antigens for 1 h at RT.
- 8) Unbound detection antibodies were washed 2 times with 150 μL of wash buffer by an autowasher using crosswise aspiration.
- 9) Streptavidin-HRP (50 μL , supplied in each ELISA kit) was added to detect antibodies for 20 min at RT with no direct light.
- 10) Unbound streptavidin-HRP was washed 2 times with 150 μL of wash buffer by an autowasher using crosswise aspiration.
- 11) Streptavidin-HRP was incubated for 20 min with 50 μL of substrate solution at RT with no direct light.
- 12) The reaction was terminated with 25 μL of the stop solution.
- 13) The plates were shaken thoroughly, and the optical density of each well was determined using a plate reader at 450 nm wavelength, with 540 nm as the reference wavelength.

4.12 Wound healing assay

The EC migration process involves the development of angiogenesis through the enzymatic degradation of the capillary basement membrane, endothelial cell (EC) proliferation and the directed migration of ECs (Fig. 3). More specifically, endothelial cell migration is a mechanically integrated molecular process that involves cell adhesion, signal transduction and cytoskeletal organisation.

To investigate cellular edge extension during the migration of HUVECs, a wound healing assay was performed to elucidate differences in the wound closure area influenced by magnesium degradation products compared to that influenced by hypoxia, as indicated in Fig. 7. Cells were maintained in ECGM-complete medium until approaching 80% confluence to obtain more activated cells in the exponential growth phase¹¹³. To achieve more reproducible results, HUVECs were first starved in ECGM with 1% FBS to synchronise the cellular life cycle in the G0/G1 phase and increase the reproducibility of cell responses. Then, HUVECs were treated with 10 $\mu\text{g}/\text{mL}$ of mitomycin C, which can inhibit proliferation *via* cross-linking double-stranded DNA at its aminoquinone group¹²⁵. Additionally, because mitomycin C does not affect RNA and protein synthesis, cytokine secretion and gene regulation, *e.g.*, chemoattractant, can be analysed further based on wound healing samples¹²⁶.

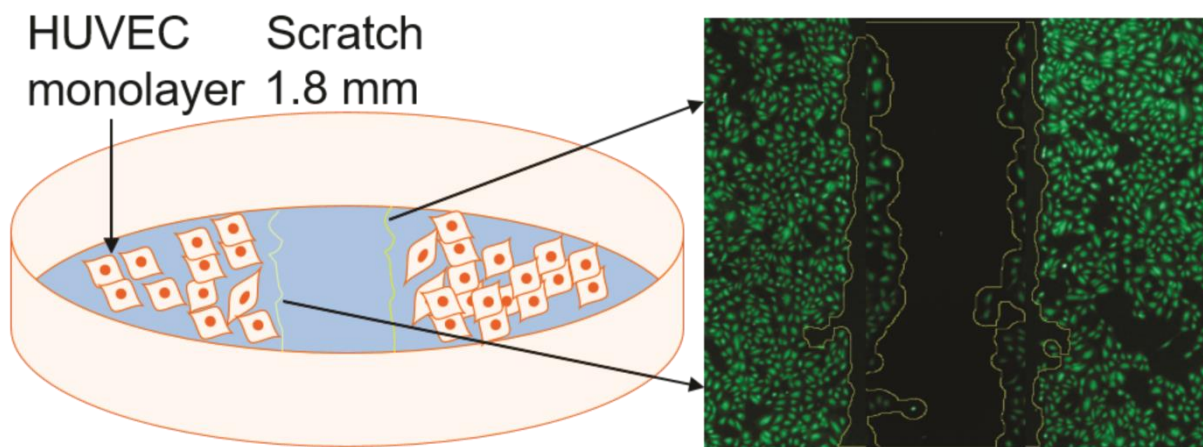


Fig. 7 Schematic of HUVEC wound healing.

4.12.1 Materials

Table 18 Materials for the wound healing assay

Name	Abbreviation	Supplier
Endothelial cell growth medium with 1% FBS	Low FBS ECGM	PromoCell, Heidelberg
Endothelial cell growth supplement	ECGS kit	PromoCell, Heidelberg
LIVE/DEAD viability kit for mammalian cells	Calcein AM	Thermo Scientific – Fisher Scientific GmbH, Langenselbold, Germany
Trypsin-EDTA (0.05%), phenol red	Trypsin	Thermo Scientific – Fisher Scientific GmbH, Langenselbold, Germany
Mitomycin C from <i>Streptomyces</i>	Mitomycin C	Sigma-Aldrich, Munich, Germany
Costar® TC-treated multiple-well plates	24-Well plate	Sigma-Aldrich, Munich, Germany
Eppendorf® epT.IPS standard pipette tips, 1 mL	1 mL Pipette tip	Sigma-Aldrich, Munich, Germany
Eclipse Ti-S inverted microscope system	Inverted microscope	Nikon, Minato, Japan
Image processing and analysis in java, version 1.51b	ImageJ	National Institutes of Health, Bethesda, USA

4.12.2 Procedures

HUVECs were seeded in 24-well plates and cultured until reaching 80% confluence.

- 1) Day 0: The HUVEC monolayer was starved in ECGM-complete medium without extra FBS for 24 h.
- 2) Day 1: The monolayer of HUVECs was treated with 10 µg/mL of mitomycin C for 2 h. Wounds were produced using a standard 1 mL pipette tip on the cell monolayer. Pictures were acquired at 0 h with an inverted microscope as basic values (T0). Wounds were cultured in Mg degradation products under 20 and 5% O₂ for 24 h.
- 3) Day 2: Wounds were observed at 24 h, when pictures were acquired with an inverted microscope to represent the migration results (T24). The wound healing closure was calculated from the difference in scratch between T0 and T24 using ImageJ with the MRI plugin.

4.13 Tube formation assay

An adapted thin-layer assay (TLA)¹¹⁴ was applied, as indicated in Fig. 8, to acquire RNA extract and images more easily and economically. TLAs do not need high-resolution/single-cell microscopy for image acquisition or matrix digestion with dispase for extracting mRNA but retain their performance for anchoring and differentiating HUVECs¹¹⁴. To preclude potential interference between cell and matrix, the basement membrane matrix was free of LDEV and reduced in growth factor. The density of cell seeding is a determinant factor since subconfluent density can ensure a monolayer to re-establish the tube reorganisation^{127–130}. After plating, HUVECs were adhered, permitting their migration by mechanical forces to the ECM coating. The adhered cells created paths where cells migrated and ultimately formed capillary-like structures. These capillary structures were quantified by their number and length as well as the area of cell cords and hollow lumens in microscope images. The observations and supernatant collection were performed within 6 h (decided by section 5.2), since the interconnected network would thereafter diminish by low-cell-density-induced apoptosis. Since non-endothelial cell types also demonstrate tube formation¹¹¹, this assay was only performed with HUVECs in monoculture and transwell coculture.

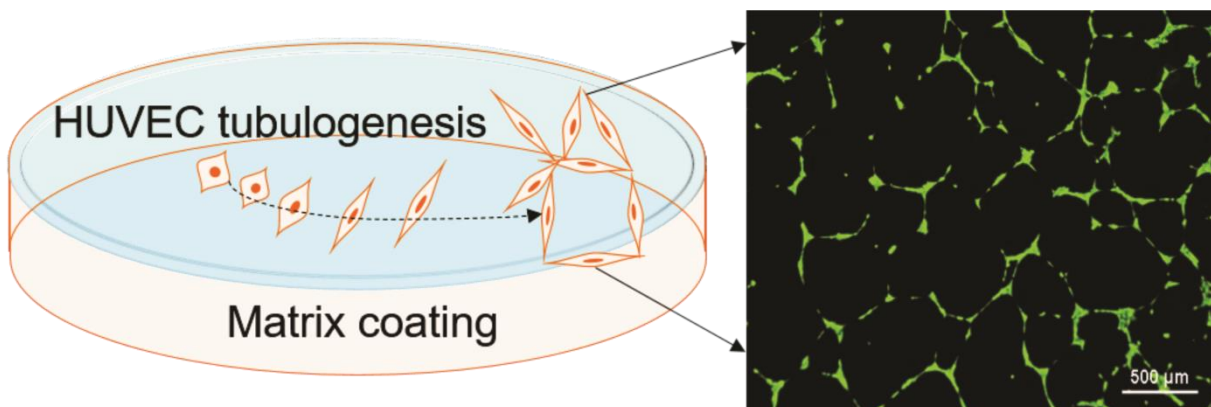


Fig. 8 Schematic of HUVEC tube formation.

4.13.1 Materials

Table 19 Materials for tube formation assay.

Name	Abbreviation	Supplier
Endothelial cell growth medium with 1% FBS (low FBS ECGM)	Low FBS ECGM	PromoCell, Heidelberg, Germany
Endothelial cell growth supplement	ECGS kit	PromoCell, Heidelberg, Germany
Minimum essential medium, Eagle-alpha modification	α -MEM	Fisher Scientific GmbH, Schwerte, Germany
LIVE/DEAD viability/cytotoxicity kit for mammalian cells	Calcein AM	Thermo Scientific – Fisher Scientific GmbH, Langenselbold, Germany
Geltrex® LDEV-free reduced growth factor basement membrane matrix	Matrix	Thermo Scientific – Fisher Scientific GmbH, Langenselbold, Germany
Trypsin-EDTA (0.05%), phenol red	Trypsin	Thermo Scientific – Fisher Scientific GmbH, Langenselbold, Germany
Corning® Costar® TC-treated multiple-well plates	24-well plate	Sigma-Aldrich, Munich, Germany
Eppendorf® Combitips Advanced® pipette tips, quality grade, 0.5 mL	Combitip	Sigma-Aldrich, Munich, Germany
Eclipse Ti-S inverted microscope system, Ti-S/L100	Inverted microscope	Nikon, Minato, Japan
Image processing and analysis in java, version 1.51b	ImageJ	National Institutes of Health, Bethesda, USA

4.13.2 Procedures

- 1) Day 0: matrix was thawed on ice at 4 °C overnight.
- 2) Day 1: 10 μ L of matrix was spread evenly within 30 s in each well of 24-well plates with the insert end of a combitip while avoiding any the production of bubbles in the monolayer (bubbles can disrupt tube formation). During the whole experiment, the matrix was on ice to avoid its degradation. HUVECs were seeded as 40,000 cells per well with α -MEM-complete medium in 24-well plates. After 30 min of cell adhesion, culture medium was replaced with Mg degradation products or control medium accordingly.
- 3) Day 1+6 h: after supernatant collection, cells were stained with diluted Calcein AM (1:2500 (v/v) in PBS) and incubated in 20% or 5% O₂ for 30 min. PBS was added, and pictures of 3 different fields of each sample was taken under an inverted microscope.
- 4) Images were analysed using ImageJ (1.51b, National Institutes of Health, USA) with the Angiogenesis Analyzer Plugin.

4.14 Statistical analysis

The results of section 5.1 (immunophenotyping) and section 5.5 (ALP activity of HUCPV cell monoculture) were collected from two technical replicates of three independent experiments (n=3). The results of section 5.3 were collected from two independent experiments with two replicates of two donors (n=4). Other results were acquired from two technical replicates of two independent experiments from three donors (n=6). The results are presented as the average and standard deviation (SD). If not specifically mentioned, the data were analysed with either one-way ANOVA or one-way ANOVA after ranking based on the distribution of data *via* SigmaPlot 13.0 (version 13.0; Systat Software GmbH, Erkrath, Germany). The following post hoc multiple comparisons were based on the Dunnett's or Student-Newman-Keuls (SNK) test ($\alpha=0.05$) when equal variance was assumed or not, respectively. For RT-qPCR, to detect differential expression, a t-test ($\alpha=0.05$, $P\leq 0.05$) was employed, and differential expression was directly calculated using CFX manager software (version 3.1; Bio-Rad, Munich, Germany).

5 Results

5.1 The isolation, validation and differentiation potential of existing HUCPV and HUVEC

According to the cell distribution of the umbilical cord, HUCPV cells were isolated from the perivascular WJ covering the artery surface. Additionally, HUVECs were extracted from the inner lumen layer of the vein using collagenase type IA. To ensure purity and the osteogenesis and angiogenesis potential, HUCPV cells and HUVECs were labelled with antibodies or isotypes, as listed in Table 8. Isolated HUCPV cells and HUVECs show typical “fibroblast” and “cobblestone” morphology (Figs. 9a and 9b). In HUCPV cells, positive CD 105 and CD 90 markers suggest a highly purified population, and endothelial contamination is excluded by a negative CD 31 result, presented in Fig. 9c. The high positive CD 105 and CD 31 values indicate purified HUVECs, for which hematopoietic contamination is excluded by the negative result for CD 45 (Fig. 9d).

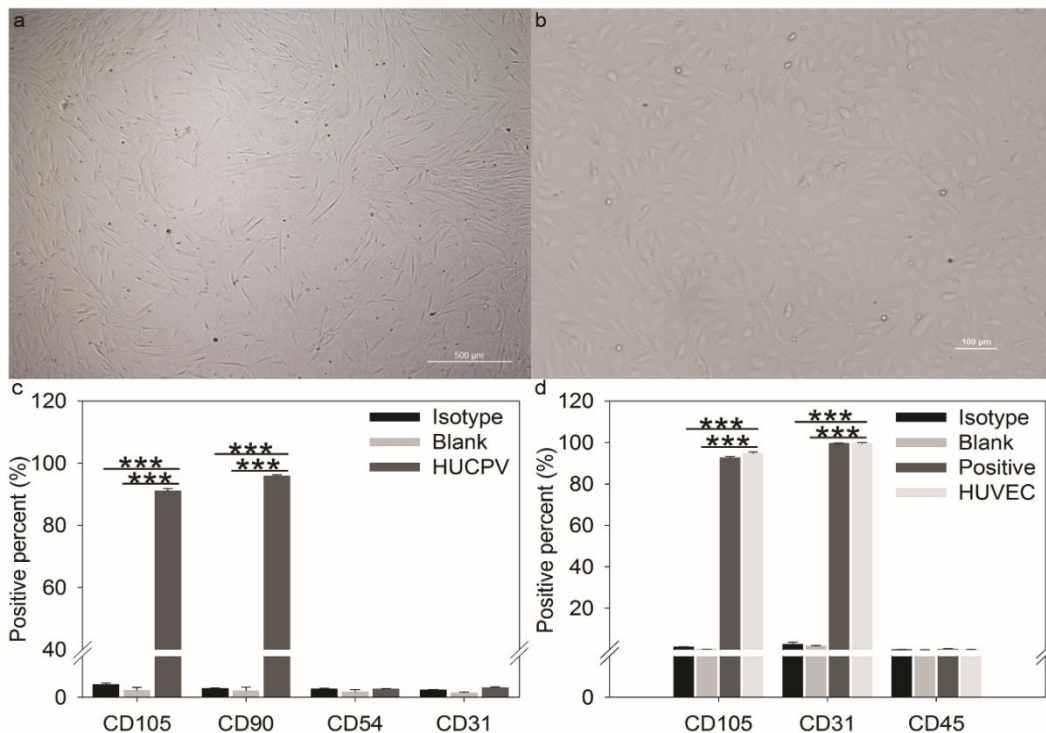


Fig. 9 HUCPV cell and HUVEC characterisation: a) HUCPV cell fibroblastic morphology, b) HUVEC cobblestone morphology, and summaries of the surface markers for (c) HUCPV cells and HUVECs (d). Statistical significance was tested by ANOVA with Dunnett's test ($\alpha=0.05$, $***P\leq 0.001$).

Method 1, 2 and 3 contain different osteogenic components to induce the osteogenesis of isolated HUCPV cells^{91, 110}. As shown in Fig. 10, the DNA content on day 7 was significantly increased by method 2. On day 14, the DNA content was decreased by method 1 but significantly increased by method 2. On day 21, the DNA content for method 1 was significantly reduced. Methods 2 and 3 almost induced less ALP activity at all three timepoints. The ALP activity induced by method 1 was significantly higher on days 14 and 21. The mineralisation (Fig. 11) indicated by ARS staining for all treatments, especially for methods 2 and 3, was obviously higher on days 14 and 21. The tube formation by HUVECs (Fig. 12) suggested that the observation window should be 6 h.

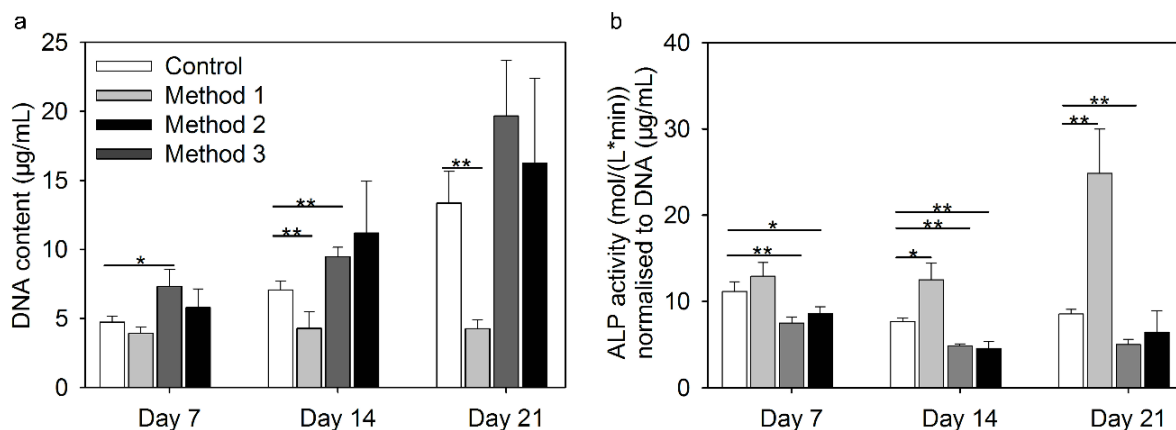


Fig. 10 DNA content and ALP activity of HUCPV cells during the 21 days of differentiation: (a) DNA, (b) ALP. The asterisks indicate significance by ANOVA ($\alpha=0.05$, $*P \leq 0.05$, $**P \leq 0.01$).

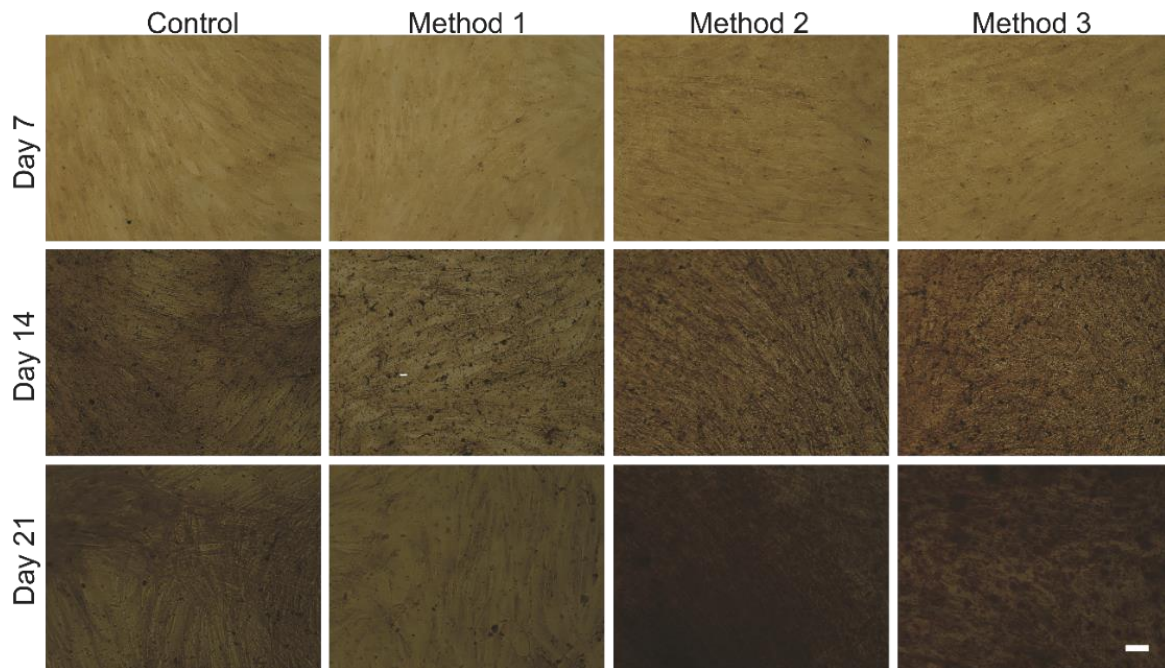


Fig. 11 ARS staining of HUCPV cells for 21 days. The scale represents 100 μm . The HUCPV cells were seeded as 5,000 cells/ cm^2 in different media containing osteogenic chemicals.

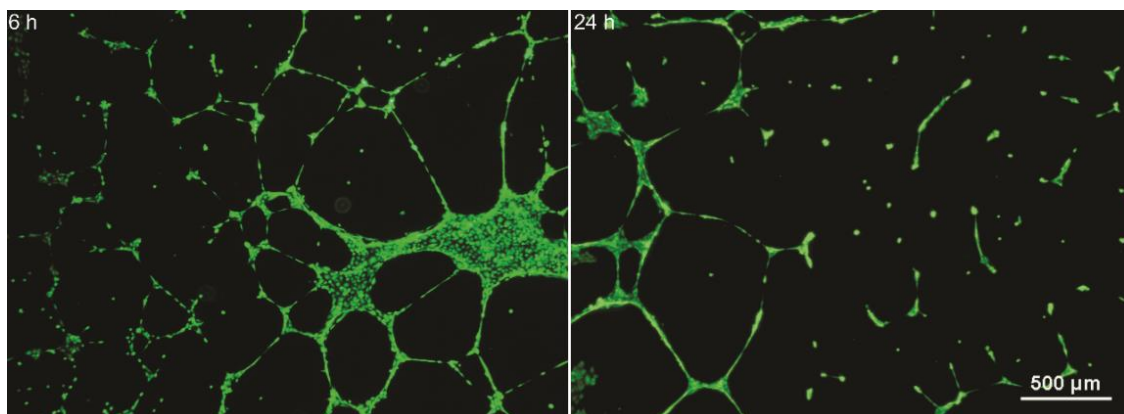


Fig. 12 Tube formation of isolated HUVEC. HUVEC were seed as 50,000 cells/ cm^2 in 24-well-plate and cultured for 6 and 24 h. Tubes were stained with Calcein AM in PBS and observed under inverted microscope.

According to the CD 105⁺, CD 90⁺, CD 54⁻ and CD 31⁻ expression levels and the fibroblastic shape of the HUCPV cells, their isolation from human umbilical cord vein can reliably produce MSCs without endothelial contamination for further study. The ARS staining and the ALP and proliferation levels induced by the different osteogenic chemicals indicate the osteogenesis potential of isolated HUCPV cells. The typical morphology and the CD 105⁺, CD 31⁺ and CD 45⁻ markers of the isolated HUVECs suggest that collagenase digestion in the vein lumen of human umbilical cord can dependably produce ECs without blood contamination. Furthermore, the capillary structure formed by the tube formation assay suggests the differentiation of isolated HUVECs.

5.2 Optimisation and validation of the coculture system

The α -MEM- and ECGM-complete media were originally used as culture media for the HUCPV cells and HUVECs, respectively. α -MEM and ECGM contain 0.814 and 10mM background Mg. The possible influence of α -MEM on EC growth induction should be measured. The proliferation and metabolism of HUCPV cells and HUVECs when cultured in α -MEM and ECGM are presented in Figs. 13 and 14. The HUCPV cells were incubated in α -MEM-complete medium and ECGM-complete medium for 9 days. On days 3, 6 and 9, the DNA concentration was measured by the fluorescence of bisbenzimidazole. On days 3, 6 and 9, the metabolic activity was quantified *via* culturing cells in WST-1 solution (1:10 v/v, water-soluble tetrazolium salt-1) supplemented with the corresponding medium for 30 min.

During the expansion of direct-contact coculture, HUCPV cells and HUVECs will contact each other and compete for the bottom surface of the cell culture plate or flask. According to the HUCPV cell growth in α -MEM and observation during the direct-contact coculture trial under bright field, HUCPV cells seem to proliferate faster and occupy more culture area compared to HUVECs. Moreover, the 7-days-coculture was chosen because proliferation and metabolism were significantly decreased in α -MEM on day 9 (Figs. 13 and 14). Thus, to assure the consistent existence of HUCPV cells and HUVECs up to 7 days, the direct coculture was simultaneously labelled with CD 90 and CD 31 in flow cytometry. Single staining with CD 90 and CD 31 was applied respectively for fluorescence compensation of the analysis results. The positive percentage of CD 90 and CD 31 represents HUCPV cells and HUVECs, respectively, in Fig. 15.

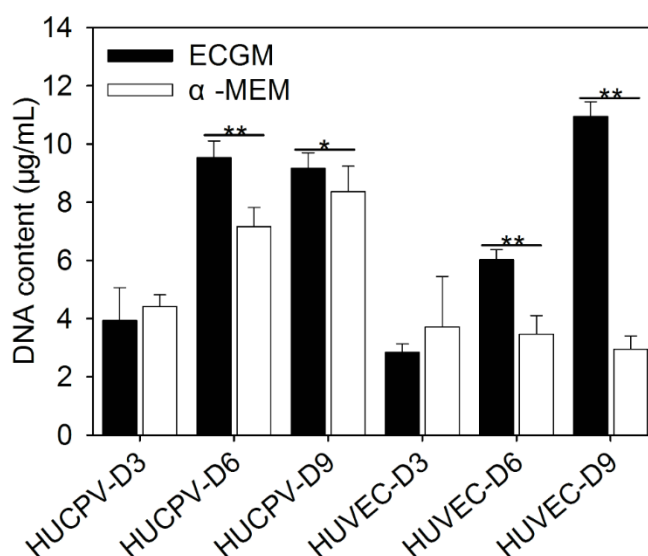


Fig. 13 DNA content of HUCPV cells and HUVECs in ECGM- and α -MEM-complete media by bisbenzimidazole. The asterisk indicates significance by t test ($\alpha=0.05$, * $P\leq 0.05$, ** $P\leq 0.01$).

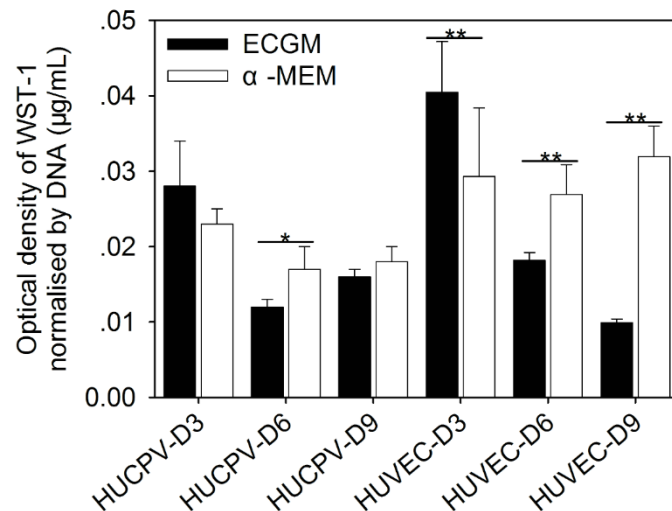


Fig. 14 Metabolic activity of HUICPV cells and HUVECs in ECGM- and α -MEM-complete media by WST-1 assay. The asterisk indicates significance by t test ($\alpha=0.05$, $*P\leq 0.05$, $**P\leq 0.01$).

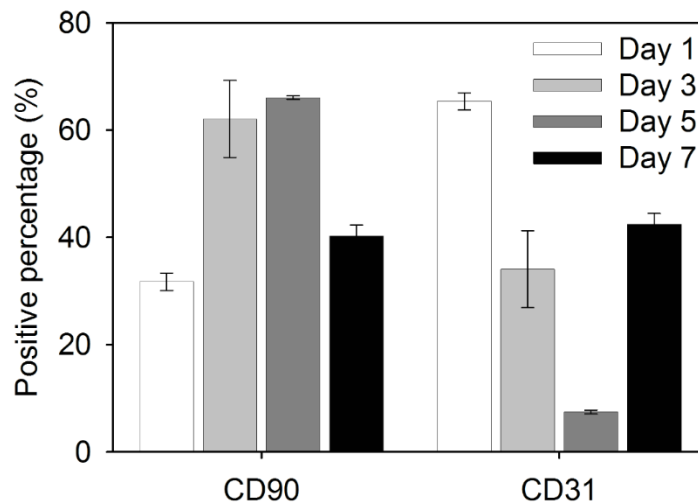


Fig. 15 The quantification of HUICPV cells and HUVECs in the total population of direct-contact cocultures. To suggest the percentage of HUICPV cells and HUVEC, direct-contact cocultures were stained with CD 90 and CD 31, respectively, and investigated through flow cytometry.

The results in the “medium test” section indicate the possible growth of both HUICPV cells and HUVECs in α -MEM for at least 9 days. The results (Figs. 13 and 14) also suggest that the growth of HUICPV cells and HUVECs cocultured in transwell with α -MEM for up to 9 days can be possible. The possible influence of background Mg in ECGM on cell growth should be investigated because plans exist to study a low dose of Mg for its proven effect on ECs⁷⁰. Therefore, considering the heightened metabolism in α -MEM and the potential effect of a low dose of Mg⁷⁰, α -MEM was hereafter applied as the coculture medium. The existence of HUICPV cells and HUVECs in direct-contact cocultures was assured by the expression of CD 90⁺ and CD 31⁺ for at least 7 days.

5.3 Magnesium degradation products and hypoxia influenced the HUVEC angiogenesis stage

5.3.1 Proliferation of HUVECs indicated by DNA quantification

Proliferation was assessed by the DNA content. No significant change in the DNA content was measured with Mg at 20% O₂. However, under 5% O₂, HUVECs cultured with 4 and 8 mM Mg degradation products exhibited an increased DNA content compared to that of the control (Fig. 16a). According to multiple comparison testing (Fig. 16b), the 4 mM and 8 mM Mg treatments under hypoxia had a higher DNA content than those measured at different Mg concentrations under 20% O₂ (except 4 mM 5% vs Ctr 20%).

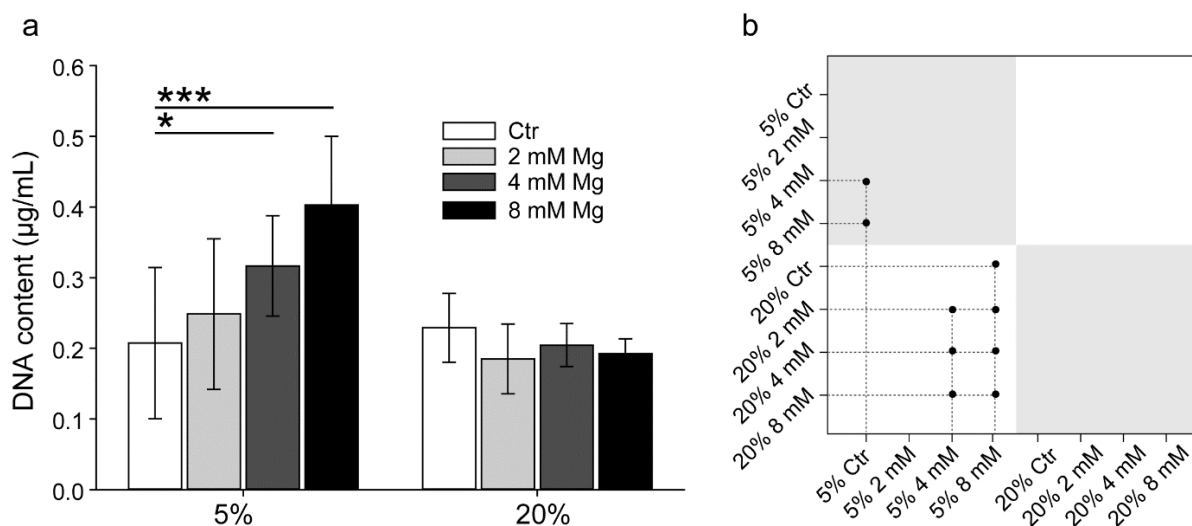


Fig. 16 Proliferation of HUVECs indicated by DNA contents: (a) significance between treatments was tested by ANOVA and indicated by an asterisk ($*P \leq 0.05$ and $***P \leq 0.001$) and (b) post hoc multiple comparisons between each treatment. A solid dot represents a significant difference.

5.3.2 Metabolism measured via WST-1 assay and rhodamine 123

The tetrazolium salt WST-1 (4-[3-(4-iodophenyl)-2-(4-nitrophenyl)-2H-5-tetrazolio]-1,3-benzene disulfonate) can be cleaved into formazan dye, which can in turn quantitatively represent the metabolic activity of cells. Normalising the results of the WST-1 and R123 assays with DNA content, *i.e.*, cell number, enables a comparison of the influence of magnesium degradation products on HUVEC metabolism. Under 5% O₂, statistically significant decreases can be seen at the 4 and 8 mM Mg levels

compared to the control and between the 2 and 8 mM treatments (Fig. 17).

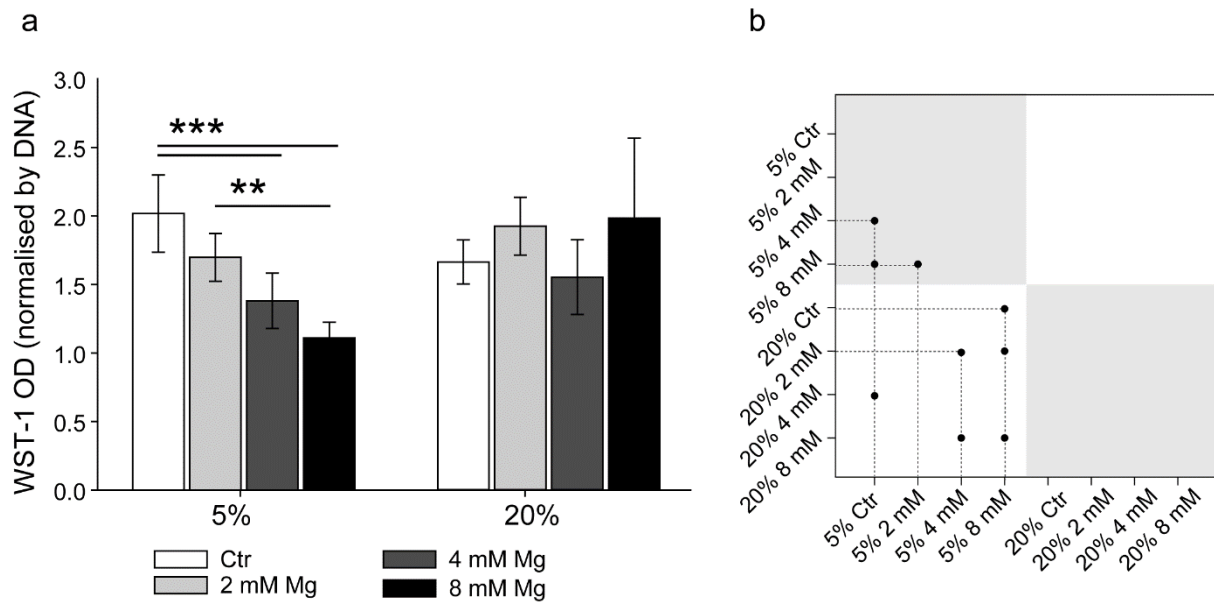


Fig. 17 Metabolic activity of HUVEC measured by the WST-1 assay: (a) significance between treatments was tested by ANOVA and indicated by an asterisk (** $P \leq 0.01$ and *** $P \leq 0.001$) and (b) post hoc multiple comparisons between each treatment. The solid dots represent significant differences.

Mitochondrial membrane potential ($\Delta\psi_m$) indicated by rhodamine 123

The fluorescence of rhodamine 123 staining can indicate the change of $\Delta\psi_m$, which relates to the metabolism of HUVECs. To measure the influence of Mg degradation products and the O₂ content on mitochondrial membrane energisation, the mitochondrial membrane potential gradient was measured. Adenosine triphosphate (ATP) synthesis by F₀F₁ATPase during cellular respiration originates from an electrochemical gradient created by a difference in proton (H⁺) concentration across the mitochondrial membrane (*i.e.*, a potential)¹³¹. The quenching of R123 fluorescence is induced by inhibiting mitochondrial energisation; therefore, the measurement of $\Delta\psi_m$ is possible because $\Delta\psi_m$ is proportional to the fluorescence decay rate¹³². R123 is a fluorescent cationic dye capable of binding to mitochondrial and other plasma membranes. Digitonin can increase the sensitivity of R123 probes by permeabilising the cell plasma membrane, allowing access to the inner membrane¹²². Antimycin A, an inhibitor of complex III in the respiratory chain, can rapidly collapse the energy-linked absorbance¹³³. Therefore, the combination of digitonin, R123 and antimycin A permits an assessment of mitochondrial energisation in intact cells and the exclusion of non-mitochondrial staining by subtracting the fluorescence after antimycin A treatment (Fig. 18a). HUVECs treated with 2 and 4 mM Mg under 20% O₂ showed significantly increased R123 retention. However, under 5% O₂, all the Mg doses markedly

decreased $\Delta\Psi_m$ (Fig. 18b). Multiple comparison tests (Fig. 18c) indicated a role for hypoxia compared with normoxia (20% O_2) in increasing $\Delta\Psi_m$.

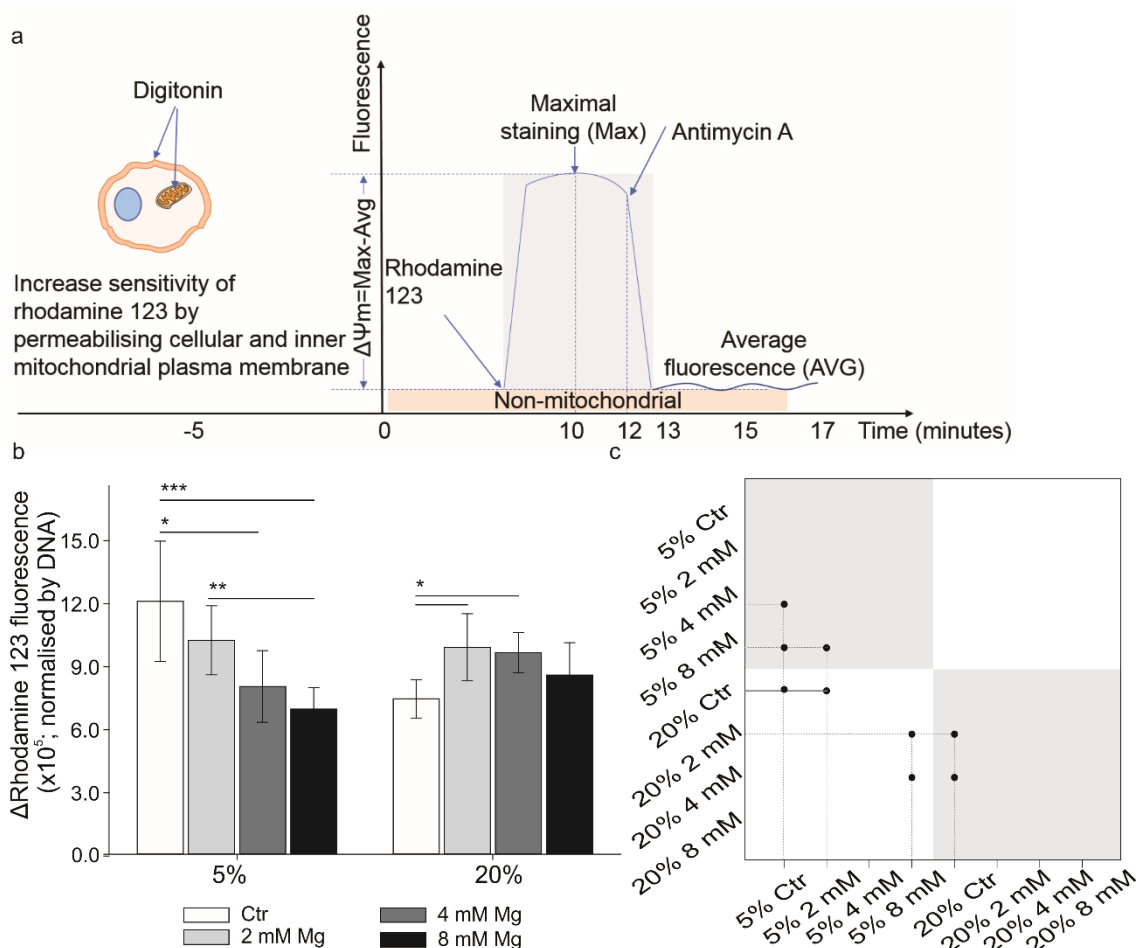


Fig. 18 Mitochondrial membrane potential of HUVEC measured by R123 fluorescence quenching in the presence of Mg degradation products: (a) principles and procedural overview of $\Delta\Psi_m$ tests, (b) significance between treatments tested by ANOVA indicated by an asterisk ($*P \leq 0.05$, $**P \leq 0.01$ and $***P \leq 0.001$) and (c) post hoc multiple comparisons between each treatment. Solid dots represent a significant difference.

5.3.3 Migration ability was increased by Mg in normoxia

The wound closure was calculated from the difference in scratch areas between 0 and 24 h to assess the influence of Mg on the cell migration ability. Under 5% O_2 and compared to a 5% control, the Mg degradation products did not influence the closure area or cell migration (Fig. 19). However, cell migration was increased with the Mg products at 20% O_2 (significantly with 2 mM Mg compared to the 20% control). Even with a bell-shaped curve, migration may be increased at a low concentration of Mg extract and decreased at high concentration (Fig. 19a).

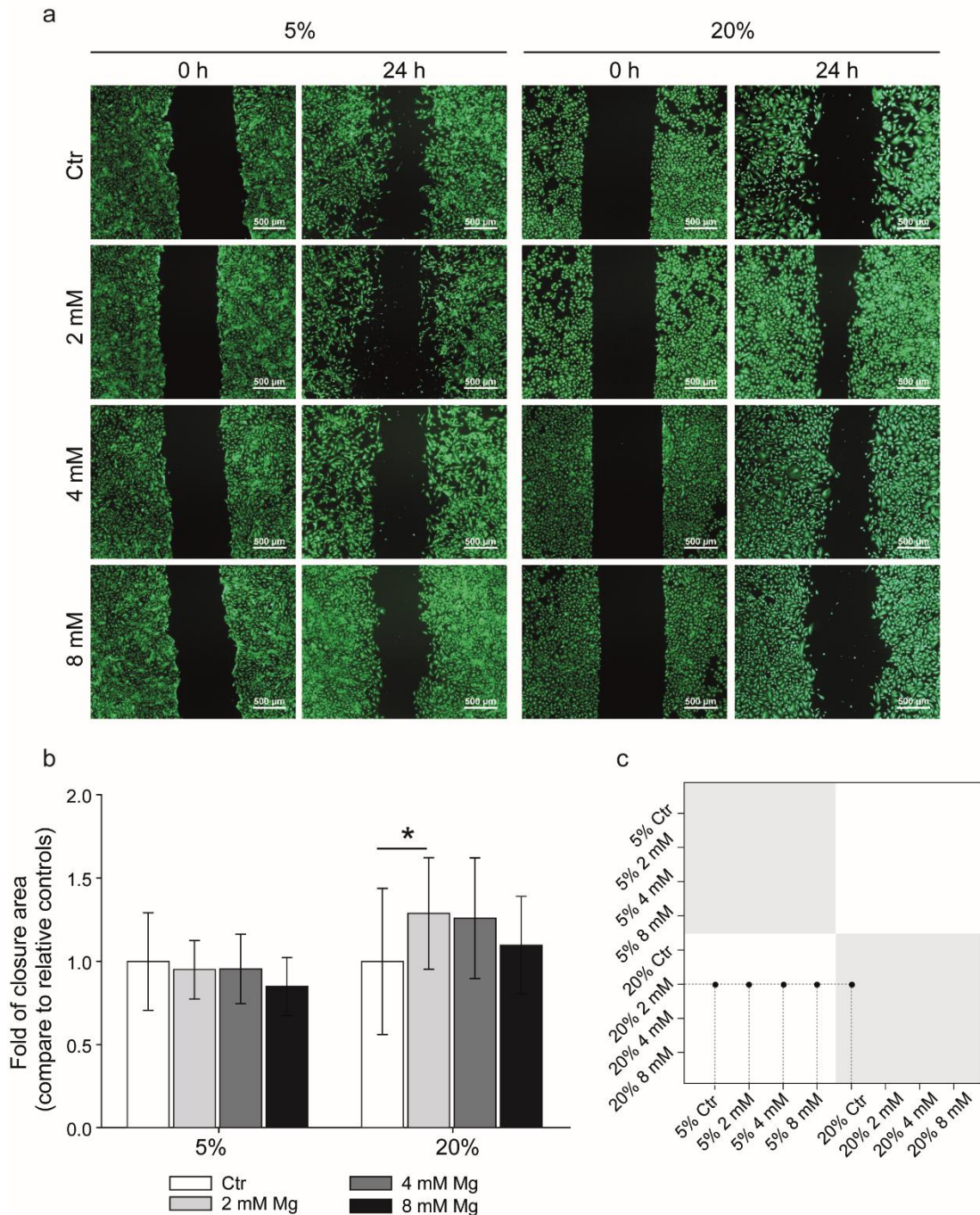


Fig. 19 Wound healing closure of HUVECs in the presence of Mg degradation products under hypoxia (5% O₂) or normoxia (20% O₂). (a) Pictures were acquired with an inverted microscope at 0 and 24 h, and the wound closure area was analysed with ImageJ. (b) Values represent the no-cell-area difference between 24 and 0 h, further normalised to relative controls. Significance between treatments was tested by ANOVA and indicated by an asterisk (* $P \leq 0.05$). (c) Post hoc multiple comparisons were performed between each treatment, with solid dots representing a significant difference ($P \leq 0.05$).

5.3.4 Tube formation was decreased by Mg in normoxia

An obvious reduction in the total length of tubes and the number of branches at 4 and 8 mM Mg (Fig. 20a) was observed under 20% O₂ after 6 h. However, under 5% O₂, no significant change occurred (Fig. 20a). Post hoc tests did not indicate significant effects induced by Mg between the 20 and 5% O₂ levels (Figs. 20b and 20c).

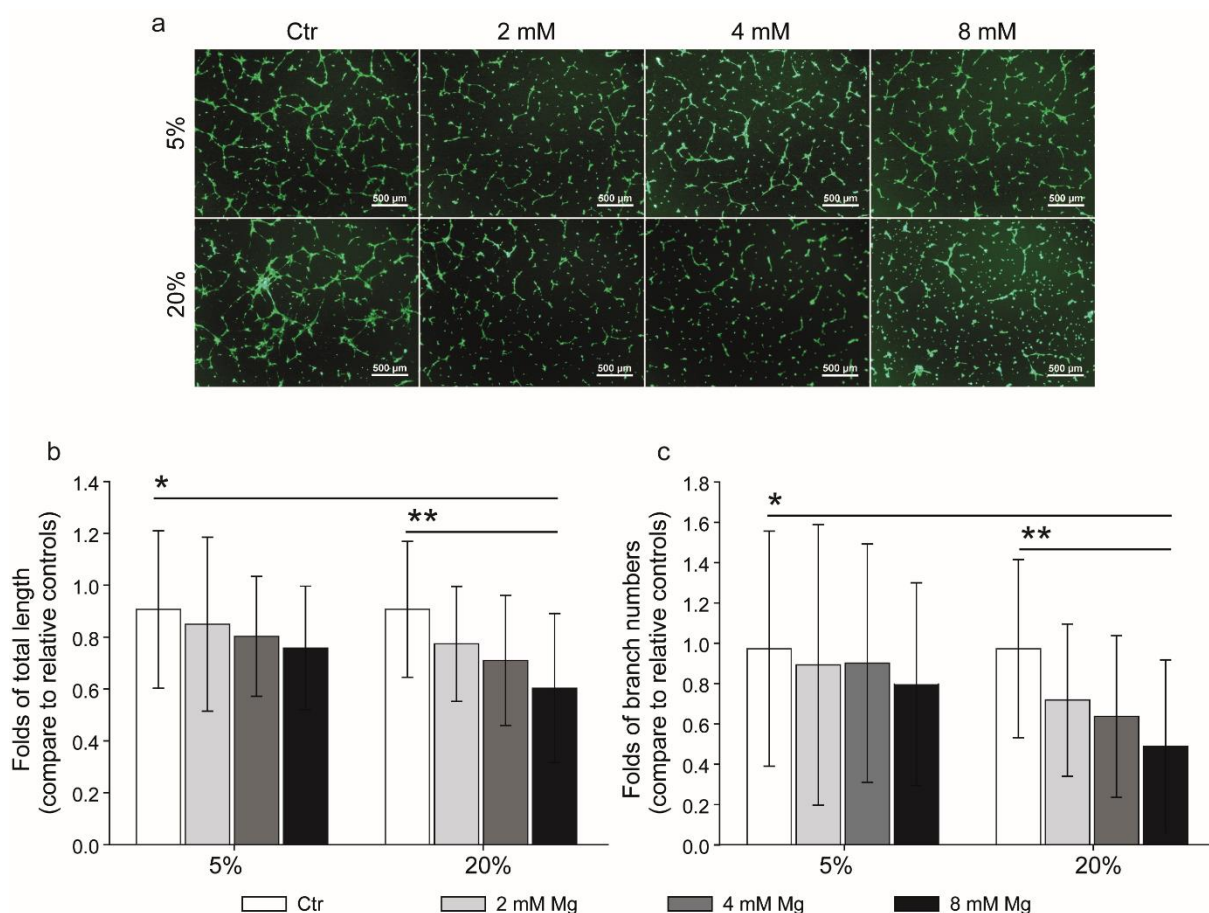


Fig. 20 Tube formation of HUVECs in magnesium degradation products. After 6 h, tubes were stained with calcein AM, and images were taken with an inverted microscope (a). With ImageJ and the angiogenesis analyser plugin, the total length of tubes (b) and the number of branches (c) were calculated. Significance between treatments was tested by ANOVA and indicated by an asterisk (* $P \leq 0.05$ and ** $P \leq 0.01$).

5.3.5 Gene regulation during migration and tube formation was influenced by Mg and hypoxia

To explore the gene regulation potentially influenced by Mg degradation products and hypoxia during the migration of HUVECs, specific gene expression levels were studied. Significantly regulated genes are presented in Table 20. Under 5% O₂, most of the selected genes were downregulated, but not in a

dose-dependent manner. These results are in accordance with the phenotypic observations during wound healing (*i.e.*, no effect observed under hypoxia and increased Mg extract concentrations). Under 20% O₂, fewer genes were regulated. However, the bell shape previously observed in wound healing can be related to certain gene expression levels. Indeed, some genes (*e.g.*, those coding for vascular endothelial growth factor B isoform (*VEGFB186*) and interleukin 8 (*IL8* or chemokine (C-X-C motif) ligand 8, *CXCL8*)) exhibited an increased and then a decreased expression as the Mg concentrations increased. Other genes, such as those coding for angiogenin (*ANG*) and tissue inhibitors of metalloproteinase 1 (*TIMP1s*), were upregulated only at 2 mM. To produce an exhaustive results description and highlight potential relationships, regulated genes were classified into 6 groups.

- i. **Cell surface and cytoskeleton organisation.** Under 20% O₂, *ANG* and ezrin (*EZR*) were upregulated in 2 mM Mg. Vascular cell adhesion molecule 1 (*VCAM1*) was upregulated by 4 mM Mg. *VEGFB186* and vascular endothelial growth factor receptor 1 (*FLT1*) were upregulated by 2 and 4 mM Mg but downregulated by 8 mM Mg. Vascular endothelial growth factor receptor 2 (*KDR*) was upregulated in 2 and 4 mM Mg. Transmembrane 4 (*CD9*) was upregulated and downregulated in 2 and 8 mM Mg, respectively. Under 5% O₂, all these genes were increasingly downregulated from 2 to 8 mM Mg.
- ii. **Adhesion.** Integrin subunit alpha 2 (*ITGA2*) and integrin subunit alpha M (*ITGAM*) was upregulated in 2 mM but *ITGA2* was also downregulated in 8 mM at 20% O₂. Under hypoxia, *ITGA2* was downregulated in 2 to 8 mM and *ITGAM* was downregulated in 2 and 4 mM.
- iii. **Migration and precondition for vessels.** At 20% O₂, *IL8* was upregulated in 2 and 4 mM Mg while downregulated in 8 mM. Matrix metalloproteinase 13 (*MMP13*) was upregulated in 2 and 4 mM Mg. *TIMP1* was upregulated in 2 mM Mg. Under hypoxia, *IL8*, *MMP13* and *TIMP1* were all downregulated under the influence of 2 to 8 mM Mg.
- iv. **HUVEC differentiation and hypoxia sensors.** Basic fibroblast growth factor (*FGFb*), hypoxia-inducible factor 1 alpha subunit (*HIF1A*) and Interferon gamma (*IFN γ*) were upregulated in 2 mM at 20% O₂; however, these factors were downregulated by Mg at 5% O₂. *HIF2A* was downregulated in 8 mM Mg under 20% O₂ and also downregulated in 2 to 8 mM Mg under hypoxia. The *IFN γ* was upregulated in 2 mM at 20% O₂ while downregulated in 2 and 4 mM Mg in 5% O₂.

- v. **Ca²⁺ and Mg²⁺ flux, cell mobility and blood vessel diameter.** Ca-activated neutral protease 1 (*CAPN1*) was observed to be upregulated at 20% O₂ in 2 mM Mg but then to be markedly downregulated in up to 8 mM Mg under 5% O₂. Claudin 16 (*CLD16*) was significantly downregulated under hypoxia.
- vi. **Vascularity protection and adaptive effect.** Nitric oxide synthase (*NOS2*) was upregulated under 20% O₂ while significantly downregulated in 2 and 4 mM Mg under 5% O₂.

The regulation of selected genes influenced during tube formation by Mg degradation products and O₂ content was investigated. Specific targets were tested and the significant changes were present in Table 20. During tube formation, only ANG and ITGA3 were upregulated by Mg degradation products under 20% O₂; however, 11 genes were downregulated. Under hypoxia, downregulation was tempered, and four genes were even upregulated. Only MMP13 was downregulated in 5% O₂. In addition, the highly regulated genes were classified into 6 classes.

- i. **Cell surface and cytoskeleton organisation.** No obvious regulation of *ANG* was observed under 5% O₂, but significant upregulation occurred under 20% O₂ in 2 mM Mg. *VEGFB186* was downregulated under 20% O₂ in 4 and 8 mM but upregulated under 5% O₂ in 8 mM Mg. Both *FLT1* and *KDR* were downregulated under 20% O₂ in 4 and 8 mM concentrations while upregulated in 2 mM Mg under hypoxia. No significant regulation of *CD9* and *EZR* was observed under hypoxia. *CD9* was downregulated under 20% O₂ in 4 and 8 mM Mg. *EZR* was downregulated in 4 mM Mg under 20% O₂.
- ii. **Adhesion.** Mg extract did not influence the expression of *ITGA2* or *ITGAM* under either 20 or 5% O₂. *ITGA3* was upregulated in 2 mM Mg under 20%.
- iii. **Migration and precondition for vessels.** *IL8* and *MMP13* were downregulated by 4 mM Mg degradation products in 20 and 5% O₂. *TIMP1* was strongly downregulated in 4 and 8 mM Mg degradation products.
- iv. **HUVEC differentiation and hypoxia sensors.** Both *HIF1A* and *HIF2A* expression were upregulated by 2 mM Mg but downregulated in 4 mM Mg under 20% O₂. However, *HIF1A* was downregulated in 4 mM Mg and upregulated in 8 mM Mg under hypoxia. *IFN γ* was downregulated in 4 mM Mg under 20% O₂.

- v. **Ca²⁺ and Mg²⁺ flux, cell mobility and blood vessel diameter.** *CAPN1* and *CLD16* were downregulated in 4 and 8 mM Mg under 20% O₂.
- vi. **Vascularity protection and adaptive effect.** *NOS2* was downregulated in 4 and 8 mM Mg under 20% O₂.

Table 20 Gene expression changes with Mg degradation product concentration and hypoxia. Slashes “/” indicate non-significant regulation. Asterisks represent * $P \leq 0.05$ or ** $P \leq 0.01$.

Function	Name	Mg content (mM)	Wound healing		Tube formation	
			5% O ₂	20% O ₂	5% O ₂	20% O ₂
Cell surface organisation; cytoskeleton activity	Angiogenin (<i>ANG</i>)	2	-3.033**	+1.966**	/	+4.283**
		4	-4.200**	/	/	/
		8	-4.306**	/	/	/
	Vascular cell adhesion molecule 1 (<i>VCAM1</i>)	2	-2.393**	/	/	/
		4	-2.750**	+2.220**	/	/
		8	-2.002**	/	/	/
	Vascular endothelial growth factor B isoform (<i>VEGFB186</i>)	2	-3.626**	+1.931**	/	/
		4	-5.509**	+1.560**	/	-1.838**
		8	-4.189**	-1.503**	+2.402*	-1.863**
	Vascular endothelial growth factor receptor 1 (<i>FLT1</i>)	2	-3.293**	+1.909**	+2.476*	/
		4	-4.757**	+1.581**	/	-2.974*
		8	-3.766**	-1.382**	+2.521*	-2.027*
	Vascular endothelial growth factor receptor 2 (<i>KDR</i>)	2	-3.647**	+1.819**	+2.373*	/
		4	-4.892**	+1.445**	/	-3.997**
		8	-3.998**	/	+2.322*	-2.229**
	Transmembrane 4 (<i>CD9</i>)	2	-3.616**	+1.851**	/	/
		4	-4.890**	/	/	-2.298*
		8	-4.249**	-1.501*	/	-2.750*
Ezrin (<i>EZR</i>)	2	-3.975**	+2.067**	/	/	
	4	-5.629**	/	/	-3.953	
	8	-2.771**	/	/	/	
Integrin subunit alpha 2 (<i>ITGA2</i>)	2	-3.330**	+1.681**	/	/	
	4	-5.707**	/	/	/	
	8	-4.235**	-1.414**	/	/	
Adhesion	Integrin subunit alpha 3 (<i>ITGA3</i>)	2	/	/	/	+2.028*
		4	/	/	/	/
		8	/	/	/	/

Table 20 (Continued)

Function	Name	Mg content (mM)	Wound healing		Tube formation	
			5% O ₂	20% O ₂	5% O ₂	20% O ₂
Adhesion	Integrin subunit alpha M (<i>ITGAM</i>)	2	-2.810**	+3.138*	/	/
		4	-2.935**	/	/	/
		8	/	/	/	/
	C-X-C motif ligand 8 (<i>CXCL8</i> , <i>IL8</i>)	2	-3.546**	+1.893*	/	/
		4	-4.749**	+1.523*	/	-1.934*
		8	-3.182**	-1.854**	/	/
Chemotaxis; collagen degradation	Matrix metalloproteinase 13 (<i>MMP13</i>)	2	-5.321**	+2.706**	/	/
		4	-6.037**	+2.722*	-2.554*	/
		8	-4.378**	/	/	/
	Tissue inhibitors of metalloproteinase 1 (<i>TIMP1</i>)	2	-4.003**	+1.343**	/	/
		4	-5.209**	/	/	-2.943**
		8	-3.299**	/	/	-1.867*
	Hypoxia-inducible factor 1 alpha (<i>HIF1A</i>)	2	-2.536**	+1.448*	/	+2.271*
		4	-2.618**	/	-1.465*	-2.260*
		8	-2.027**	-1.392*	+1.904**	/
Regulation of HUVECs differentiation	Hypoxia-inducible factor 2 alpha (<i>HIF2A</i> , <i>EPAS1</i>)	2	-2.825**	/	/	+2.405**
		4	-3.175**	/	/	-2.335**
		8	-2.321**	-1.977**	/	/
	Basic fibroblast growth factor (FGFb)	2	-2.683**	+1.861*	/	/
		4	-4.040**	/	/	/
		8	-3.716**	-1.630*	/	/
	Interferon gamma (IFN γ)	2	-2.611**	+2.250**	/	/
		4	-3.312**	/	/	-2.274*
		8	/	/	/	/
Mg ²⁺ and Ca ²⁺ flux; blood vessel diameter	Calpain 1 (<i>CAPN1</i>)	2	-3.067**	+1.626*	/	/
		4	-5.346**	/	/	-4.118*
		8	-3.975**	-1.962**	/	-3.485**
Vascularity protection and adaptivity	Claudin 16 (<i>CLD16</i>)	2	/	/	/	/
		4	-3.773**	/	/	-3.605**
		8	-2.560**	/	/	-1.990*
	Nitric oxide synthase 2 (<i>NOS2</i>)	2	-4.614**	+2.974**	/	/
		4	-8.479**	-3.697**	/	-3.697**
		8	/	-5.965*	/	-5.965*

5.3.6 VEGFA and VEGFB levels during migration and tube formation indicated by

ELISA

To determine whether the influence of Mg and oxygen conditions on the capillary formation and cell migration is mediated through VEGFA and/or VEGFB, two angiogenic factors from the VEGF family, their concentrations were quantified in the supernatant from the wound healing and tube formation experiments at their endpoints: 6 and 24 h, respectively.

For VEGFA in wound healing and tube formation, no differences were observed under hypoxia. However, under normoxia, a dose-dependent decrease was detected for VEGFA in wound healing (with statistically significant decreases for 8 mM Mg vs Ctr and 2 mM Mg). For tube formation, approximately the same level of statistically significant downregulated VEGFA was detected for all the Mg concentrations vs Ctr. During wound healing (Fig. 21c), a dose-dependent decrease and increase in VEGFB levels were observed for normoxia and hypoxia, respectively. Similar results were found for tube formation: a decreased VEGFB level in normoxia (20% O₂), while all the VEGFB levels were upregulated in an (Mg) dose-dependent manner under hypoxia (with Ctr vs 4 mM and 8 mM showing statistically significant differences).

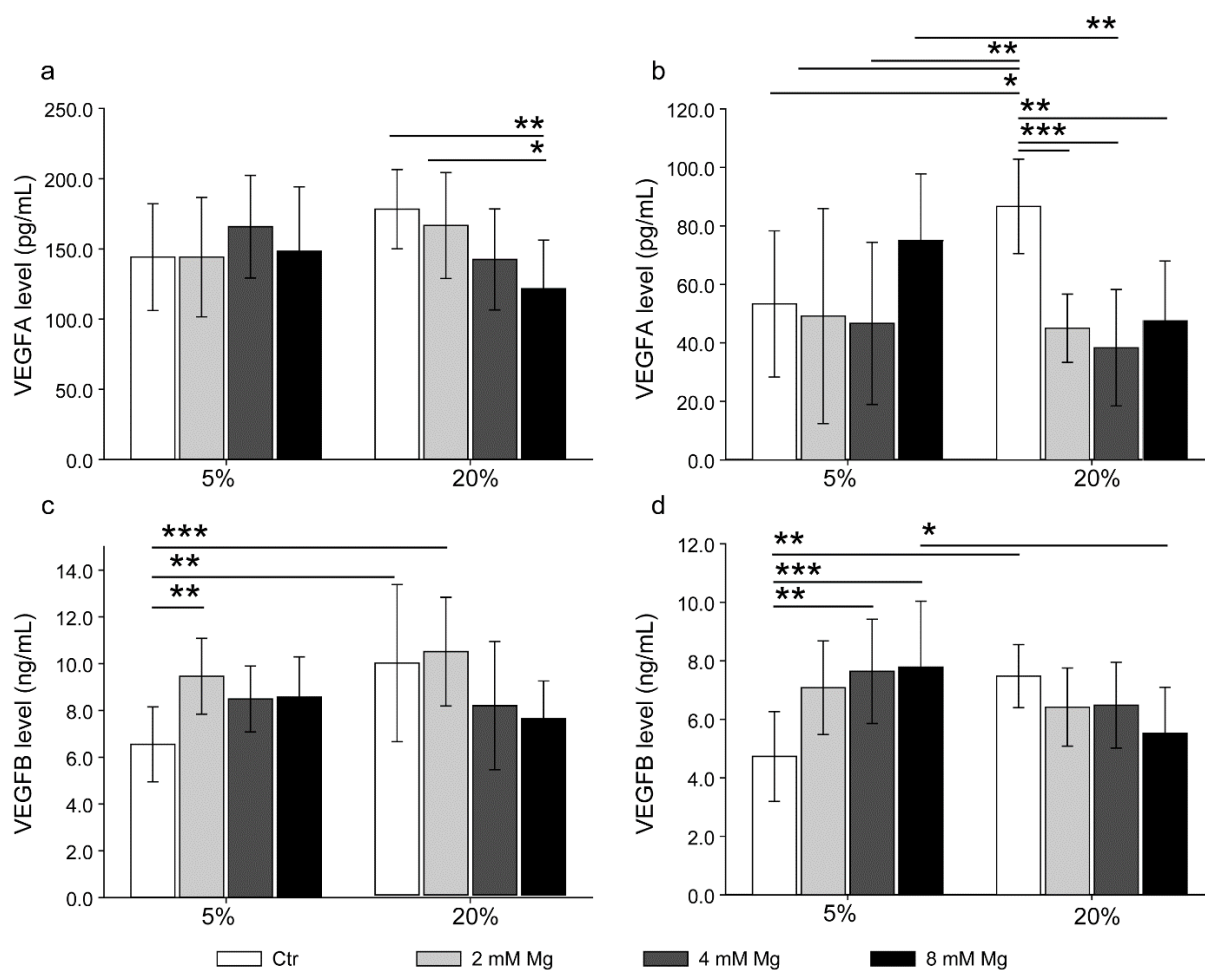


Fig. 21 VEGFA and VEGFB levels secreted in the wound healing (a and c, respectively) and tube formation (b and d, respectively) assays. An asterisk represents a significant difference between the Mg groups and controls with the same oxygen setting ($*P \leq 0.05$ and $**P \leq 0.01$) by ANOVA test.

5.4 Magnesium degradation products and hypoxia influenced the intermediate stage of HUCPV cells and HUVECs

5.4.1 Proliferation of HUCPV cells and HUVECs in transwell coculture

As indicated in Fig. 22a, the total DNA content increased on day 1 in an Mg-concentration-dependent manner. On days 4 and 7, this content increased compared to day 1 and remained relatively constant (except day 4 with 8 mM Mg). While analysing the HUCPV-HUVEC proportions, clearly enhanced HUVEC and decreased HUCPV cell proliferation (occurring in an Mg-concentration-dependent manner) was measured on day 1. On day 4, while the HUCPV cell content remained stable, a slight increase in HUCPV cells could be observed. On day 7, both cell types remained relatively constant. Under normoxia (Fig. 22b), the total DNA content was comparatively constant during the 7-day assay, while it slightly decreased with an increasing Mg concentration on all the measurement days. The HUCPV-HUVEC ratios stayed stable on days 1 and 7. However, on day 4, enhanced HUCPV and decreased HUVEC proliferation (occurring in an Mg-concentration-dependent manner) were measured.

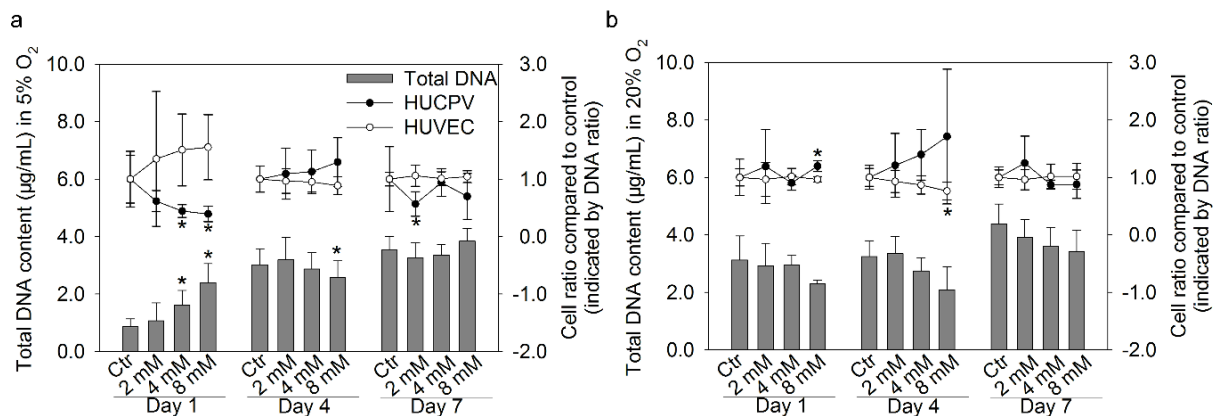


Fig. 22 DNA content and percentage of HUCPV cells and HUVECs in transwell coculture: DNA under 5% (a) and 20% O₂ (b) and cell percentage under 5% (c) and 20% O₂ (d). Dark grey and black asterisks indicate the significance of HUVECs and HUCPV cells, respectively, in ANOVA tests ($\alpha=0.05$, $*P\leq 0.05$). The DNA content was investigated by bisbenzimidazole fluorescence. Cell ratio was calculated by the DNA ratio between HUCPV cells and HUVECs.

5.4.2 Gene expression of HUCPV cells and HUVECs in 7-day-transwell coculture

To simultaneously explore their gene regulation, HUVECs (insert) and HUCPV cells (cell well bottom) were separately cultured in transwells for 7 days. The gene regulation folds and significance are summarised in Table 21 and 22, respectively. On day 1, under hypoxia in HUCPV cells, only *MMP13* was up- (2 mM Mg) or downregulated (4 and 8 mM Mg). However, under normoxia, the bone morphogenetic protein 4 (*BMP4*), *IL8*, *MMP13*, *PDGFA* and *TIMP1* expression levels were increased by up to 4 mM Mg (and at 8 mM, *BMP4* and *MMP13* were downregulated). On day 4, under hypoxia, *BMP4*, *EPAS1/HIF2A*, *MMP13*, *OPG* and *PDGFA* were upregulated under different Mg concentrations. However, these increased expression levels were instead downregulated under normoxia, (except *MMP13* and *PDGFA*). *COL1A1* was downregulated on day 4 with 4 or 8 mM Mg under both normoxia and hypoxia, while *IL8* was only downregulated under hypoxia on day 4. On day 7, *BMP4*, *IL8*, *MMP13*, *OPG* and *TIMP1* expression was decreased by 2 or 4 mM Mg under hypoxia. *CCL2* was downregulated by 2 mM but upregulated by 8 mM Mg under hypoxia. Under normoxia, all the genes except *OPG* were downregulated by up to 8 mM Mg.

On day 1, HUVEC, *ANG*, *IL8*, *ITGA1*, *MMP13* and *TIMP1* were all decreased under hypoxia by up to 8 mM Mg. By contrast, *KDR* and *VEGFB186* were downregulated by 2 and 4 mM Mg. Under normoxia, the expression on day 1 for *ANG*, *IL8*, *ITGA1*, *KDR*, *MMP13*, *TIMP1* and *VEGFB186* was not decreased from 4 mM Mg but was increased by 8 mM Mg. On day 4, *EPAS1/HIF2A* was upregulated by 4 mM Mg, while *VEGFB186* was increased by 2 and 4 mM Mg but decreased by 8 mM Mg under hypoxia. However, under normoxia, *ANG*, *CCL2*, *IL8*, *KDR*, *VEGFB186*, *EPAS1/HIF2A* and *MMP13* were all upregulated for HUVECs by 4 and 8 mM Mg. On day 7, only *MMP13* was significantly regulated in hypoxia (increased by 2 mM but decreased by 4 and 8 mM Mg). Under normoxia, *MMP13* and *EPAS1/HIF2A* were decreased by 2 or 4 mM Mg, while *MMP13* expression was upregulated by 8 mM Mg.

Table 21 Summary of gene regulation in HUCPV cells during 7 days of non-contact or transwell coculture. The slash “/” means non-significant regulation. Positive and negative numbers mean up- and downregulation, respectively. Significance between treatments was analysed by t tests and is indicated by asterisks ($\alpha=0.05$, * $P\leq 0.05$, ** $P\leq 0.01$ and *** $P\leq 0.001$).

Oxygen	Day	Mg (mM)	Gene									
			<i>BMP4</i>	<i>CCL2</i>	<i>COL1A1</i>	<i>EPAS1/ HIF2A</i>	<i>IL8</i>	<i>MMP13</i>	<i>OPG</i>	<i>PDGFA</i>	<i>TIMP1</i>	
5%	1	2	/	/	/	/	/	3.1*	/	/	/	
		4	/	/	/	/	/	-1.4*	/	/	/	
		8	/	/	/	/	/	-1.7*	/	/	/	
	4	2	3.1**	/	/	8.6***	-1.0*	4.3*	2.4*	2.8*	/	
		4	/	/	-8.8***	3.8***	-2.5*	4.2*	/	2.7*	/	
		8	/	/	-3.7***	7.7***	-1.7*	/	1.8*	2.9*	/	
		7	2	-1.9*	-1.5***	/	/	-1.4*	-2.3*	-3.9**	/	-1.6**
			4	/	/	/	/	/	-1.3*	/	/	/
			8	/	1.6***	/	/	/	/	/	/	/
20%	1	2	5.6**	/	/	/	4.8*	3.1*	/	5.2*	4.9*	
		4	3.5**	/	/	/	/	3.3*	/	2.9*	3.8*	
		8	-3.3*	/	/	/	/	-6.3*	/	/	/	
	4	2	-2.1**	/	/	/	/	-1.6*	/	/	/	
		4	/	/	-5.0***	/	/	1.5*	/	-1.2*	/	
		8	/	/	/	-2.1*	/	-2.1*	/	1.1*	/	
		7	2	/	-1.2*	/	/	/	/	/	/	/
			4	-3.3***	-1.6***	/	-4.4***	/	/	/	/	/
			8	-7.8***	-5.6***	-6.5***	-12.5***	-4.1**	-7.4**	/	-5.5**	-4.9***

Table 22 Summary of HUVEC gene regulation in 7 days of non-contact or transwell coculture. The slash “/” means non-significant regulation. Positive and negative numbers mean up- and downregulation, respectively. Significance between treatments was analysed by t tests and is indicated by asterisks ($\alpha=0.05$, * $P\leq 0.05$, ** $P\leq 0.01$ and *** $P\leq 0.001$).

Oxygen	Day	Mg (mM)	Gene								
			ANG	CCL2	EPAS1 /HIF2A	IL8	ITGA1	KDR	MMP13	TIMP1	VEGFB186
5%	1	2	-6.4***	/	/	-3.7**	-3.7***	-1.92*	-3.8***	-4.1***	-2.2***
		4	-3.7***	/	/	-5.9**	-4.8***	-3.2**	-4.7***	-3.5***	-1.6**
		8	-2.5***	/	/	-3.9**	-3.3**	/	-2.5*	-2.5***	/
	4	2	/	/	/	/	/	/	/	/	1.0*
		4	/	/	1.9**	/	/	/	/	/	1.1*
		8	/	/	/	/	/	/	/	/	-1.8*
	7	2	/	/	/	/	/	/	1.3*	/	/
		4	/	/	/	/	/	/	-1.1*	/	/
		8	/	/	/	/	/	/	-1.0*	/	/
20%	1	2	-1.5*	/	/	-2.6***	-1.7*	-1.9***	-2.1*	-2.7***	-1.9***
		4	/	/	/	/	/	/	/	/	/
		8	2.1***	/	/	/	3.6**	1.9***	3.1**	1.8***	2.6***
	4	2	/	/	/	/	/	/	/	/	/
		4	2.2*	2.3*	/	1.9*	/	2.6***	/	/	1.5*
		8	3.8**	4.0*	2.5***	5.4*	/	2.0**	20.8***	/	4.4**
	7	2	/	/	-1.4*	/	/	/	-1.1*	/	/
		4	/	/	/	/	/	/	-1.0*	/	/
		8	/	/	/	/	/	/	1.4*	/	/

5.4.3 Cytokine levels in transwell coculture up to 7 days

The levels of cytokines acting as regulators of migration, angiogenesis and osteogenesis were investigated using ELISA. The results (fold changes and significances compared to a relative control) for migratory cytokines (CCL2, IL8, MMP13 and TIMP1) and key regulators of angiogenesis and osteoblastogenesis (PDGFA, VEGFA, FGFb and eNOS) are summarised in Fig. 23 and Table 23. Under hypoxia, expression was high on day 1, decreased on day 4 and increased again on day 7 (except for eNOS and FGFb). On day 1 (except for PDGF), a decreased expression with increased Mg concentration was observed (statistically significant for VEGFA, FGFb, TIMP1, MMP13, IL8 and CCL2). On day 4, the cytokine levels remained rather low and constant independently of the Mg concentrations. On day 7, expression increased, and the inhibition from an increasing Mg concentration was no longer observed. Indeed, for eNOS, FGFb and CCL2, increased cytokine levels could be seen as the Mg

concentrations increased.

Under normoxia, the overall decreased expression was not observed. By contrast, the expression remained rather constant (VEGFA, eNOS and FGFb) or increased on day 7 (e.g., PDGFA and CCL2). Furthermore, in certain cases (except for PDGF), increased Mg concentrations increased cytokine expression (e.g., a statistically significant increase for MM13 on day 1 comparing control vs 8 mM Mg).

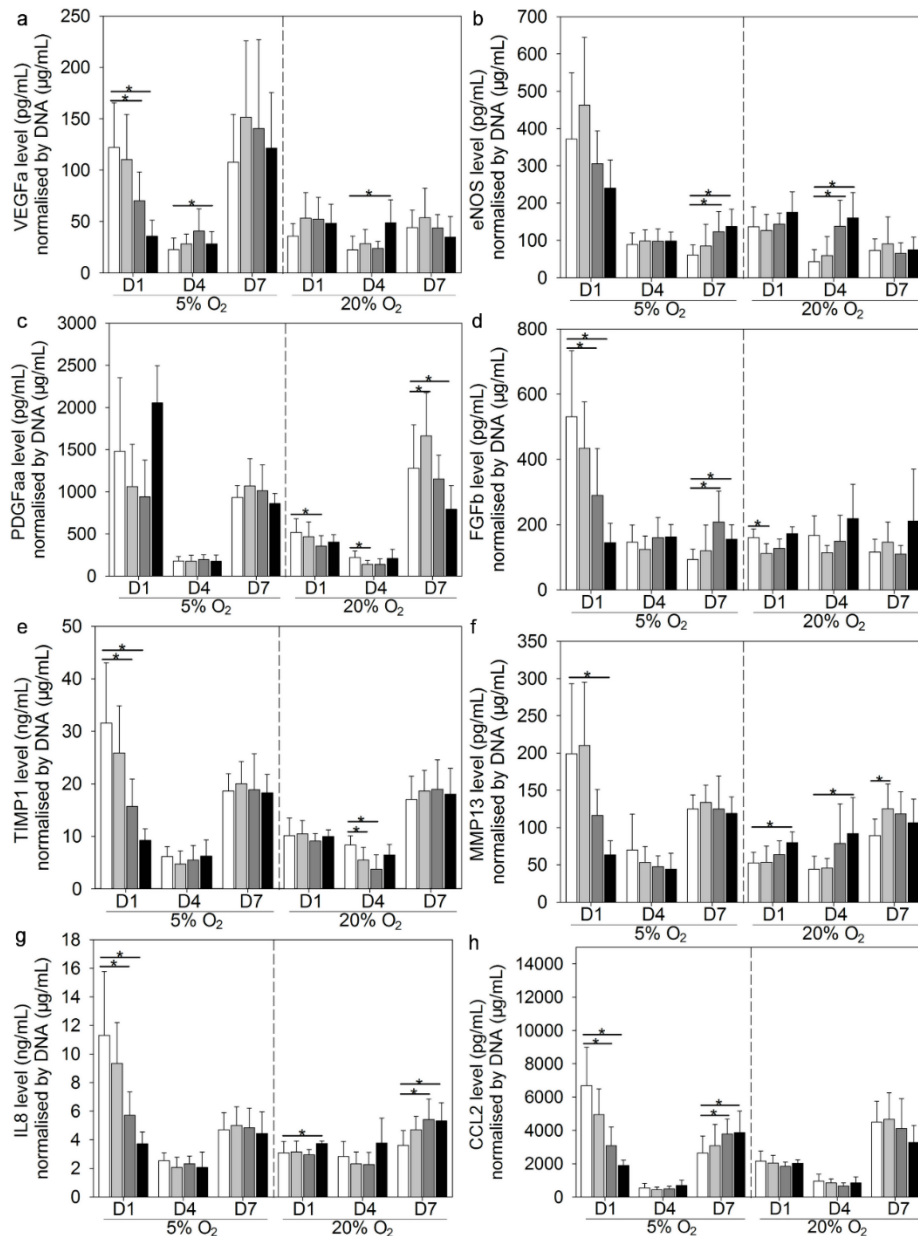


Fig. 23 Cytokine levels in the supernatant after 7 days of non-contact or transwell coculture. The control and 2, 4, and 8 mM Mg treatments are indicated in white, grey, dark grey and black, respectively. (a) VEGFA, (b) eNOS, (c) PDGFA, (d) FGFb, (e) TIMP1, (f) MMP13, (g) IL8 and (h) CCL2 expression. Cytokine concentrations were measured by sandwich ELISA, and results were normalised by the total DNA content of HUVEC cells and HUVECs. Significance between treatments was tested by ANOVA and indicated by an asterisk ($\alpha=0.05$, $*P\leq 0.05$).

Table 23 Summary of cytokines in transwell cocultures with Mg degradation products. The “↑, ↓ and ↓↑” arrows indicate a significant increase, decrease and reversal from decrease to increase, respectively.

Field	Mechanism	Cytokine	5% O ₂			20% O ₂		
			D1	D4	D7	D1	D4	D7
Regulate angiogenesis and osteogenesis <i>via</i> paracrine signalling	Pro-angiogenic activity	VEGFA	↓	↑	-	-	↑	-
	Endothelial activation and MSC migration	eNOS	-	-	↑	-	↑	-
	MSC migration, tyrosine kinase activity, protein kinase C and intracellular calcium signalling pathways; angiogenic signals such as VEGF	PDGFaa	-	-	-	↓	↓	↑↓
	VEGF, FGF receptors and following pathways	FGFb	↓	-	↑	↓	-	-
	Protect MSC or perivascular niche <i>via</i> Inhibiting MMPs	TIMP1	↓	-	-	-	↓	-
Cell contact, cell morphology, cell stress, migration	Differentiation of MSC, migration, cell-cell surface adhesion	MMP13	↓	-	-	↑	↑	↑
	Proliferation, migration and tube-formation <i>via</i> mediating VEGF and MMPs	IL8	↓	-	-	↑	-	↑
	Migration of MSC and EC, cell contact	CCL2	↓	-	↑	-	-	-

5.4.4 HUCPV cell migration and gene regulation

To measure whether the recruitment of HUCPV cells by HUVECs is influenced by oxygen content and Mg degradation products, the migration ability of HUCPV cells was measured *via* a wound healing assay. Therefore, HUCPV cells were cultured on the well bottom, with HUVECs cultured in the inserts to permit cytokine sharing without direct cellular contact. The migration of HUCPV cells at 0 and 24 h was measured by the wound healing assay in Mg degradation products, with 20 and 5% oxygen concentrations. The wound edge at 24 h is indicated in Fig. 24a. An obvious increase in wound closure occurred for HUCPV cells under 5% O₂ in 4 and 8 mM Mg (Fig. 24b). However, Mg showed no significant impact under 20% O₂. Black lines were used to indicate the wound edge of HUCPV cells at 24 h. A numerical value for wound closure was calculated from the pixel change between 0 and 24 h. The gene expression of HUCPV cells and HUVECs is indicated in Tables 24 and 25. Under hypoxia in HUCPV cells, *ANG*, *IL8*, and *VEGFB186* were all increased by 8 mM Mg. Moreover, *BMPR1A* was upregulated

by 2 and 8 mM Mg, and PDGFA was upregulated by 4 mM Mg. Under normoxia, a significant expression of *ANG* was not found, but *BMP4* was markedly increased by 2 mM Mg. *BMPR1A* and *FN1* were upregulated by up to 8 mM Mg. Expression of *FGFb*, *HIF1A* and *TIMP1* was increased by 4 and 8 mM Mg. *COL1A1* and *PDGFA* were upregulated by 4 mM Mg, while *VEGFB186* was increased by 8 mM Mg. Under hypoxia in HUVECs, all targets of interest were significantly regulated by Mg, except *VEGFB186*. *ANG* was increased by 8 mM Mg, but *IL8* was decreased by 4 mM Mg. *TIMP1* was increased by 2 mM Mg while downregulated by 8 mM Mg. The expression of *BMPR1A*, *HIF1A* and *PDGFA* was upregulated by up to 8 mM Mg. Under normoxia, *ANG*, *BMPR1A*, *HIF1A*, *PDGFA* or *TIMP1* all showed changes in regulation; under hypoxia, no changes were observed for 8 mM Mg. *ANG* was increased by 2 mM Mg, whereas *BMPR1A*, *HIF1A*, *PDGFA*, *TIMP1* and *VEGFB186* were upregulated by 2 and 4 mM Mg. No influence of Mg on *IL8* was found under normoxia.

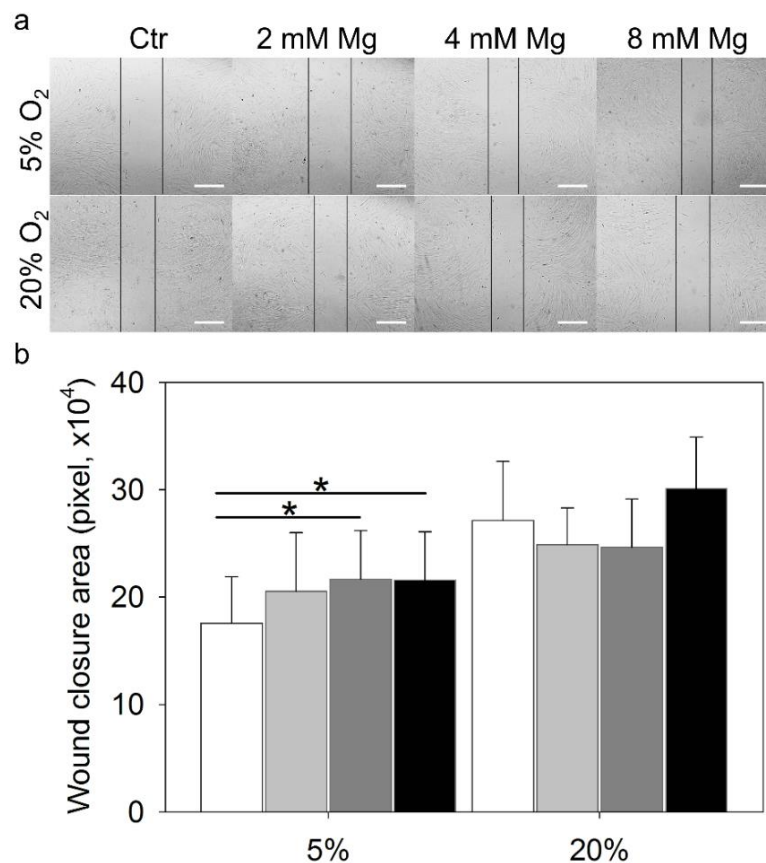


Fig. 24 Wound healing closure of HUVECs in the presence of Mg degradation products under hypoxia (5% O₂) or normoxia (20% O₂). Control and 2, 4, and 8 mM Mg treatments are indicated in white, grey, dark grey and black, respectively. (a) Pictures were acquired with an inverted microscope at 0 and 24 h, and the wound closure area was analysed with ImageJ. Scale bar=500 μ m. (b) Values represent the no-cell-area difference between 24 and 0 h. Significance between treatments was tested by ANOVA and is indicated by an asterisk ($\alpha=0.05$, $*P\leq 0.05$).

Table 24 Gene regulation in HUCPV cells during wound healing in transwell coculture. The slash “/” means non-significant regulation. Positive and negative numbers mean up- and downregulation, respectively. Significance between treatments was tested by ANOVA and is indicated by asterisks ($\alpha=0.05$, * $P\leq 0.05$, ** $P\leq 0.01$ and *** $P\leq 0.001$).

Oxygen	Mg (mM)	Gene										
		ANG	BMP4	BMPR1A	COL1A1	FGFb	FN1	HIF1A	IL8	PDGFA	TIMP1	VEGFB186
5%	2	/	/	1.6***	/	/	/	/	/	/	/	/
	4	/	/	/	/	/	/	/	/	1.3*	/	/
	8	1.6**	/	1.1**	/	/	/	/	3.4***	/	/	2.1*
20%	2	/	4.2**	1.3**	/	/	1.7*	/	/	/	/	/
	4	/	/	1.5***	2.1***	1.6**	2.1**	1.6*	/	1.7*	1.6**	/
	8	/	/	1.3***	/	2.1***	1.9**	2.0***	19.0***	/	2.2**	1.9*

Table 25 Gene regulation in HUVECs during wound healing in transwell coculture. The slash “/” means non-significant regulation. Positive and negative numbers mean up- and downregulation, respectively. The significance between treatments was tested by ANOVA and is indicated by asterisks ($\alpha=0.05$, * $P\leq 0.05$, ** $P\leq 0.01$ and *** $P\leq 0.001$).

Oxygen	Mg (mM)	Gene						
		ANG	BMPR1A	HIF1A	IL8	PDGFA	TIMP1	VEGFB186
5%	2	/	3.7***	4.0***	/	5.6*	2.5***	/
	4	/	3.2***	3.2**	-1.6*	2.5*	/	/
	8	2.7*	9.0***	9.2***	/	3.2*	-1.3*	/
20%	2	3.2*	2.2***	1.9**	/	1.9*	3.0***	3.1**
	4	/	9.6***	8.0***	/	4.2*	2.9**	4.2**
	8	/	6.5***	4.8***	-1.7*	3.8*	5.9***	3.3**

5.5 Magnesium degradation products and hypoxia influenced osteogenesis and the cytokine environment after HUCPV/HUVEC direct-contact coculture

5.5.1 Proliferation in direct-contact coculture investigated by DNA content and flow cytometry

To investigate the effects of Mg and hypoxia when influenced by heterotypic cell contact, HUCPV cells and HUVECs were seeded as mixtures to achieve direct cellular contact. Under hypoxia (Fig. 25a), the total DNA content remained low on day 1, with a significant effect of Mg increasing the concentrations. On the next days, even if the effect of Mg was still evident, an increase in the total DNA contents was measured (especially on day 4). While analysing cell ratios, the HUCPV cell and HUVEC amounts remained constant on day 1. Afterwards, on day 4, the HUCPV cell number strongly increased and HUVEC numbers decreased in an Mg-concentration-dependent manner. The same trend, but damped, could be observed on day 7. Under normoxia (Fig. 25b), the total DNA content remained rather constant over days, and some negative influence of Mg could be measured (e.g., a significant decrease on day 4 with 8 mM Mg). While analysing the cell ratios, the HUCPV cells also remained relatively constant over days. On day 4, compared to the control, increased HUCPV cell numbers could be measured with Mg, whereas a decrease was measured with 8 mM Mg on day 7. In contrast, HUVECs dramatically decreased in an Mg-concentration-dependent manner on days 4 and 7 (except day 7 with 8 mM Mg).

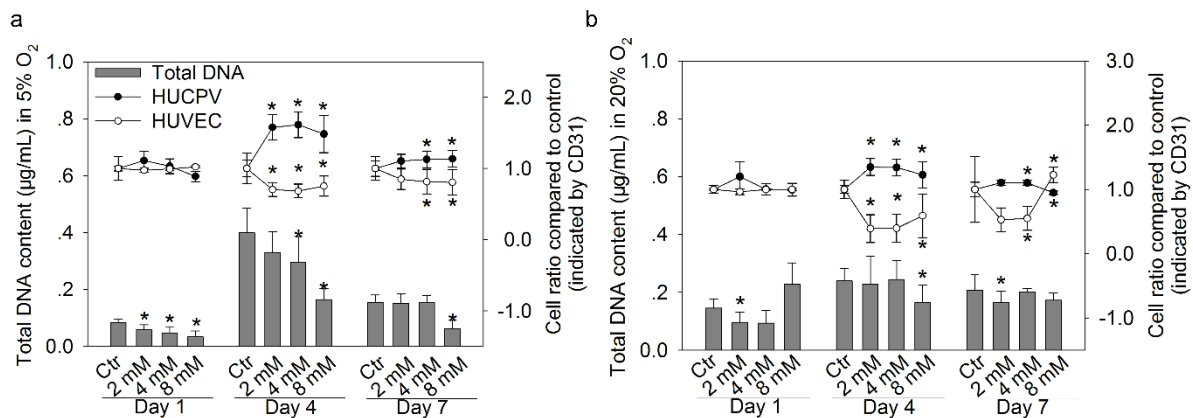


Fig. 25 Total DNA content and the ratio in direct-contact coculture. An asterisk indicates significance in comparison to the control for the corresponding day. (a) 5% O₂ and (b) 20% O₂. DNA content was investigated by bisbenzimidazole fluorescence (left abscissa). Cell ratios were calculated by the CD 31 ratio and compared to controls; Significance was determined by the ANOVA test ($\alpha=0.05$, $*P\leq 0.05$).

5.5.2 Cytokine levels of direct-contact coculture in ELISA tests

In the direct-contact system, Mg degradation products resulted in a common influence on cell migration, angiogenesis and osteogenesis regulators. Under 5% O₂, Mg obviously increased the levels of these cytokines (Fig. 26). However, under 20% O₂, Mg decreased the level of the following migration-related cytokines: TIMP1, IL8, CCL2 and MMP13. Additionally, under 20% O₂, the VEGFA, PDGFA and FGFb regulator were decreased by 4 or 8 mM Mg on day 1 and 7. PDGFA and eNOS were increased under 20% O₂ by 2 or 4 mM Mg. The significant changes in cytokine levels are summarised in Table 26.

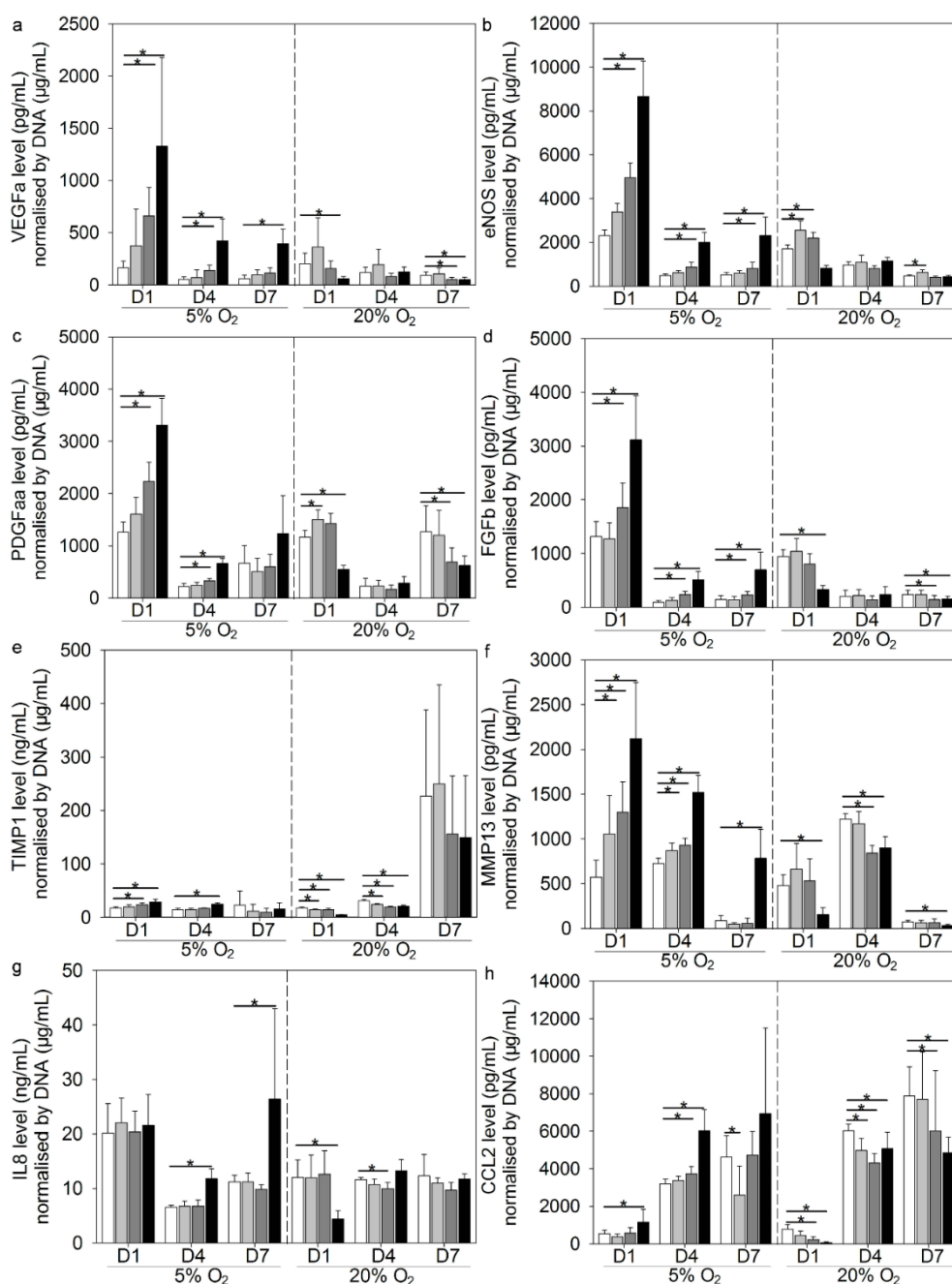


Fig. 26 Cytokine levels in supernatant for up to 7 days in contact or direct coculture. Control and 2, 4,

and 8 mM Mg treatments are indicated in white, grey, dark grey and black, respectively. (a) VEGFA, (b) eNOS, (c) PDGFA, (d) FGFb, (e) TIMP1, (f) MMP13, (g) IL8 and (h) CCL2 expression levels. Cytokine concentrations were measured by sandwich ELISA and results were normalised by the total DNA content of HUCPV cells and HUVECs. Significance between treatments was tested by ANOVA and indicated by an asterisk ($\alpha=0.05$, $*P\leq 0.05$).

Table 26 Summary of cytokine expression in direct-contact coculture. The “↑, ↓ and ↓↑” arrows indicate a significant increase, decrease and reversal from decrease to increase, respectively.

Field	Mechanism	Cytokine	5% O ₂			20% O ₂		
Regulate angiogenesis and osteogenesis via paracrine signalling	Pro-angiogenic activity	VEGFA	↑	↑	↑	↓	-	↓
	Endothelial activation and MSC migration	eNOS	↑	↑	↑	↑	-	↑
	MSC migration, tyrosine kinase activity, protein kinase C and intracellular calcium signalling pathways; angiogenic signals such as VEGF	PDGFaa	↑	↑	-	↑	-	↓
	VEGF, FGF receptors and following pathways	FGFb	↑	↑	↑	↓	-	↓
Cell contact, cell morphology, cell stress, migration	Protect MSC or perivascular niche via Inhibiting MMPs	TIMP1	↑	↑	-	↓	↓	-
	Differentiation of MSC, migration, cell-cell surface adhesion	MMP13	↑	↑	↑	↓	↓	↓
	Proliferation, migration and tube-formation via mediating VEGF and MMPs	IL8	-	↑	↑	↓	↓	-
	Migration of MSC and EC, cell contact	CCL2	↑	↑	↓	↓	↓	↓

5.5.3 Osteogenesis investigated by ARS staining and ALP activity

Since heterotypic cell contact and hypoxia were suggested to enhance osteoblastogenesis, the propensity of HUCPV cells to mineralise was evaluated in the non-contact and contact cell culture models (osteogenic inducement). The calcium composition and ALP activity are both key indicators of osteogenesis maturity. Calcium was determined by the ARS-Ca module. ALP activity was quantified in linear relation to the optical density (OD) of p-nitrophenol. The ALP activity (Fig. 27a) and calcium deposits (in the form of ARS-stained hydroxyapatite) (Fig. 27b) are key markers for mature osteoblasts. Referring to Fig. 27a, compared to HUCPV cells alone or in the transwell coculture, the values of the ALP activities were higher in the direct-contact coculture, especially under hypoxia. While Mg concentrations had disparate effects in the transwell system (e.g., both increased and decreased with 2 mM Mg in 5 and 20% O₂, respectively), statistical increases were measured with 8 mM in the contact

system. Compared to the HUCPV cell monoculture (Fig. 27b), ARS staining was obviously stronger in the direct-contact coculture with 8 mM Mg on day 7, especially in hypoxia.

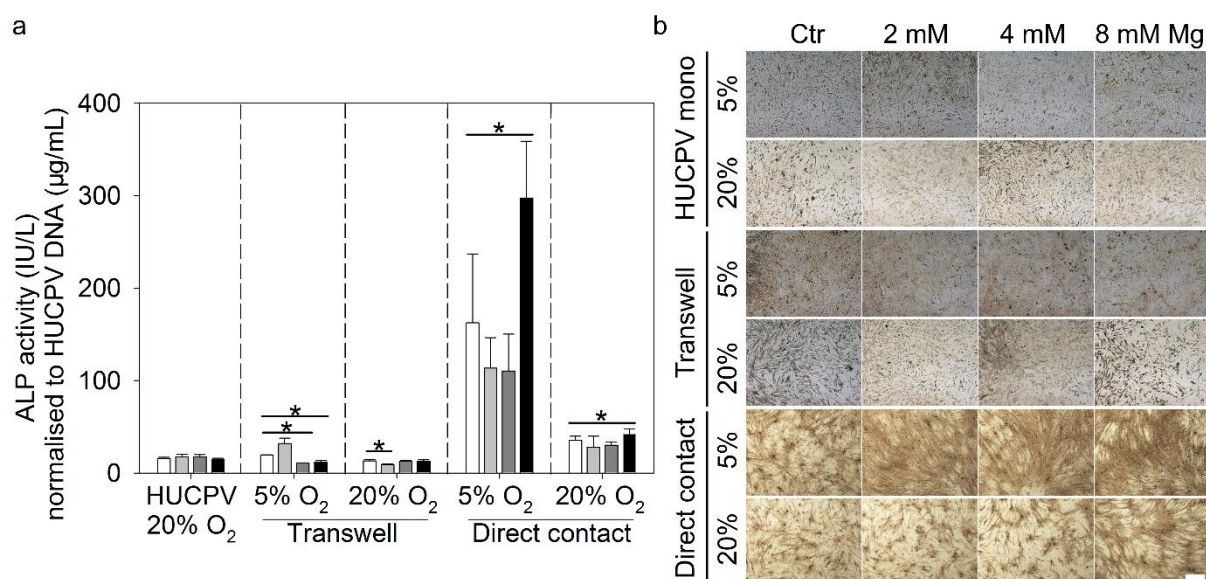


Fig. 27 Mineralisation in HUCPV cell monoculture and transwell and direct-contact coculture on day 7: (a) alkaline phosphatase activity and (b) Alizarin Red S staining. Scale bar represents 500 μm . Significance was determined by the ANOVA test ($\alpha=0.05$, $*P\leq 0.05$).

6 Discussion

Magnesium biodegradable implants are investigated extensively in regenerative medicine for tissue engineering and repairing, which depends on its excellent manufacturing, biocompatibility and biodegradability. To develop biodegradable implants, their bioactivity has to be understood. The interplay between implants and local *in vivo* protagonists is complex, but their interaction is also intriguing, especially the fate of stromal cells when interacting with environmental factors and implant degradation products. The bone fracture environment is controlled and nuanced by many cascades in the intricate hierarchical structure of bones. Endothelial and mesenchymal stem cells represent two protagonists in bone marrow fostering angiogenesis and osteogenesis. EC-induced angiogenesis can bring nutrients, oxygen and bone-forming cells (*e.g.*, MSCs) into the fracture site for healing the host integratively. Bone fracture events, such as inflammation, blood clotting and the generation of highly proliferated cell populations (such as MSCs), can trigger hypoxic conditions^{134,135}. Hypoxia has been proven to affect enzymatic reactions, including mitochondrial respiration and responses involved in tissue development and homeostasis^{136,137}. Hypoxia can be dynamic since Mg degradation is oxygen-dependent. Thus, the collective effect of Mg and hypoxia was investigated in the MSC-EC monoculture and coculture systems.

The purity of HUCPV cells and HUVECs was validated by the high positive ratios of CD 31, CD 90 and CD 105 and the negative ones of CD 45 and CD 54. The differentiation potential of MSCs was assured by their osteogenesis in different osteogenesis media. To refine the cell culture conditions to achieve optimal mitochondrial responsiveness, HUCPV cells and HUVECs were documented to generate ATP by mitochondrial oxidative phosphorylation. HUVEC proliferation, metabolism, tube formation and wound healing were investigated by their monoculture. Moreover, the gene and VEGF mechanism of action were studied. Concentrations of 2, 4 and 8 mM Mg ions were applied, considering 1.0 mM Mg to be circulating physiologic level, 2 mM Mg to fall at the physiological/pathophysiological transition and 10 mM Mg to be a high dose for *in vitro* studies^{138, 139}.

After a fracture, angiogenesis is one of the early processes of tissue healing and can be influenced by its environment (*e.g.*, hypoxia). Angiogenesis defines new blood vessel formation, which is vital to

vascular remodelling, the regeneration of bone fracture and tissue healing. For instance, ECs act in crucial roles affecting haemostasis, vascular tone, medial smooth muscle cell growth, immune response, coagulation, growth regulation, the modulation of blood flow and the production of extracellular matrix^{131,140,141}. To achieve a greater understanding through the entire angiogenesis process, ECs were exposed to Mg degradation product in monoculture models mimicking the stages of angiogenesis. The migration and morphogenesis abilities, as well as the related gene and cytokine regulation can be interpreted in these specific steps. Additionally, ECs located along the entire inner endothelium of a vessel interact with MSCs during cellular translocation in blood vessels and the physiological events of fracture healing⁷⁰. Two mechanisms exist for communication between ECs and MSCs: paracrine secretion and heterotypic cell contact¹⁴². Various paracrine factors, such as cytokines, are produced by local cells into the immediate extracellular environment and then influence nearby cells. Heterotypic contact defines the interaction between heterogeneous cell populations. For example, cell-cell adhesion is led by the surface “cadherin switch”¹⁴³ and local cytoskeletal reorganisation¹⁴². Heterotypic contact also mediates serial physiological and pathological cascades, such as the regulation of prostaglandin action by OB-EC proximity¹⁴² and the E-cadherin/N-cadherin-moderated adhesion between fibroblasts and cancer cells that can drive cancer cell invasion¹⁴⁴. Moreover, the study of cellular contact is vital for improving the biological activity in 3D bioprinting and the stem cell niche environment, where different cell populations interact, communicate and undergo storage¹⁴⁵.

6.1 Magnesium and hypoxia influence the angiogenesis of HUVECs

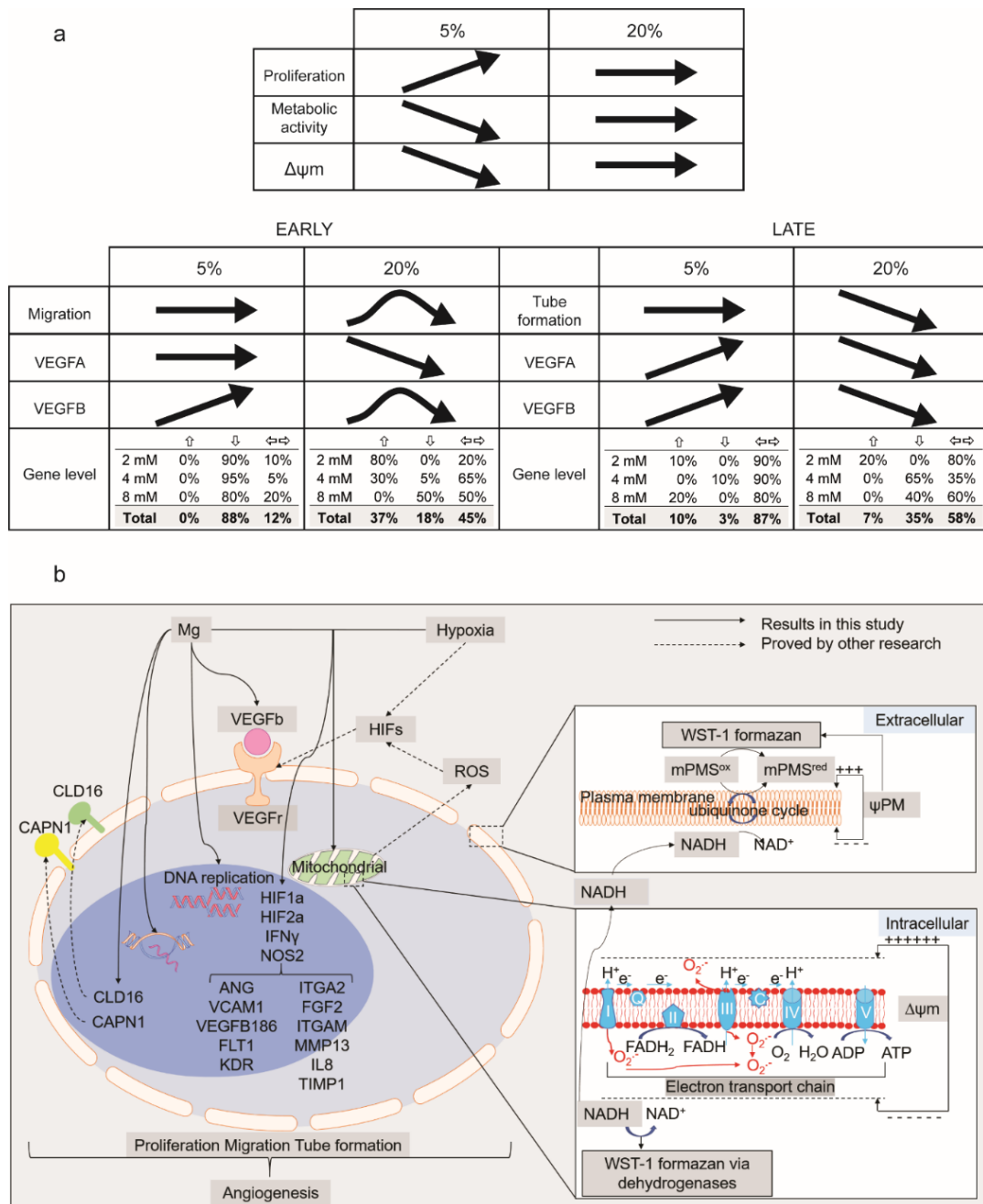


Fig. 28 Summary of HUVEC angiogenesis in Mg degradation products (a) and schematic overview of HUVEC angiogenesis and effects of Mg and oxygen contents (b). Abbreviations: plasma membrane surface potential (ψ_{PM}), mitochondrial membrane potential ($\Delta\psi_m$) and 1-methoxy-5-methylphenazinium methyl sulfate (mPMS^{ox}) as an oxidative intermediate electron acceptor.

The basic steps of (sprouting) angiogenesis involve stages such as the enzymatic degradation of the capillary basement; endothelial cell proliferation, directed migration, and reorganisation as a tube structure (tube formation); vessel fusion and pruning; and pericyte stabilisation¹⁴⁶. Hypoxia can be induced and influenced by several parameters near the bone fracture and implantation area, therefore,

affecting tissue development and homeostasis¹³⁷. The effect of Mg degradation on the underlying molecular events of angiogenesis still needs to be better understood. However, a few studies elaborate on the effects of Mg under hypoxic conditions on specific angiogenesis steps. Under normoxia, Mg exerts a positive effect on endothelial migration^{147,70}. Even though such stimulation is abolished under hypoxia, the decreased endothelial migration could be a target of interest for inhibiting tumours through the suppression of microvessel formation, which is vital to tumour metastasis¹⁴⁸. Nevertheless, tube formation increased with Mg concentration and hypoxia strength, indicates the beneficial role of Mg in fracture healing cooperating with its effects on MSC fate, osteogenesis and vascularisation near a transplant¹⁴⁹.

The present findings indicate that under hypoxia, Mg extracts do not interfere with angiogenesis but can influence angiogenic factors. During bone healing, hypoxia is temporary but is maintained because Mg degradation is oxygen-dependent. Thus, due to the increased proliferation of ECs, increased angiogenesis could be expected. However, the antagonist effects of hypoxia and Mg would associate to sustain abnormal angiogenesis in pathologic neovascularisation and haemangiomas.

Increased proliferation was measured with Mg extracts under hypoxia but not under normoxia. A previous study reported that MgSO₄ (up to 10 mM) can increase the proliferation of endothelial cells¹³⁷. However, such enhanced proliferation was not observed here under normoxia, only under hypoxia, which suggests a synergistic effect of hypoxia and HIF expression. Another explanation for this discrepancy may be the form of Mg studied. Indeed, different effects of MgCl₂ and Mg extracts have already been observed during osteogenesis and osteoclastogenesis, suggesting a high complexity for the composition and properties of the Mg extract^{68,150}. After ion influx, Mg²⁺ is an important modulator of biological response due to its similarity with other biologically important metal ions (such as Mn²⁺, Ca²⁺ and Zn⁺) regarding radius, coordination sphere¹⁵¹ and borderline hard–soft character^{152–154}. Mg²⁺ most likely displaces other metal ions from functional biomolecules, such as enzyme cofactors or enzymes affecting DNA activity^{155,156}. The catalytic steps of DNA topoisomerases and the enzyme–DNA cleavage complex both provide basic structural insight regarding the mechanisms by which Mg could influence cell proliferation¹⁵¹. Mg reportedly acts as an essential cofactor in nucleotide excision repair, mismatch repair, the removal of damaged DNA and the intracellular regulation of the cell cycle and apoptosis¹⁵⁷.

HUVEC vitality was assessed *via* two different techniques: (1) by measuring the activity of enzymes or oxidoreductases with WST-1 and (2) by determining the mitochondrial membrane potential based on R123 staining. Recent research indicates that NADH is responsible for most tetrazolium (WST-1) reduction but that the reduction sites are not only in mitochondria but also in the cytoplasm, endosome/lysosome membranes and the plasma membrane on the cellular surface^{157,158}. Moreover, the membrane potential in respiring mitochondria is not always consistent (as judged by the extent of lipophilic ion uptake) with the level of respiration^{159,160}. Therefore, R123 can be applied to obtain a more specific mitochondrial level, since R123 is a lipophilic cation whose cellular accumulation within the mitochondrial matrix occurs in accordance with the Nernst equation reflecting $\Delta\Psi_m$ (aerobic respiration)-linked ion potential changes via complex III in the electron transport chain^{122,133}. The increased cellular metabolism measured during normoxia and higher Mg concentrations are probably due to Mg-induced metabolic adaptations: protein, carbohydrate synthesis¹⁵¹ and the hydrolysis of ATPase^{161,162}. Copper (Cu^{2+}) and iron ions ($\text{Fe}^{2+/3+}$) are functional components of respiratory enzyme complexes I, III and IV. Ca plays roles in activating NADH dehydrogenase, phosphate carrier and the cytochrome oxidase complex^{163–165}. In consequence, the gradient potential can be changed by the interference between metal ions. Because of its hydration shell, Mg can be a non-competitive antagonism of cations, such as Ca^{2+} , Na^+ , and K^+ ⁶. Mg could increase the positively charged inner membrane proton gradient, which pumps protons and holds the energy to drive the ATP synthesis by $\text{F}_0\text{F}_1\text{ATPase}$ in the respiratory chains¹³¹. Eventually, Mg changes the mitochondrial membrane potential according to the electrochemical potential gradient.

Under normoxia and with Mg extracts, HUVEC migration exhibited a bell-shaped curve. The same pattern was observed with VEGFB expression, while VEGFA was constantly downregulated. Under hypoxia, migration and the VEGFA levels remained constant. However, VEGFB was upregulated. Similarly, under normoxia, tube formation and VEGFA and VEGFB levels were downregulated. Nevertheless, under hypoxia, tube formation again remained constant, while VEGFA and VEGFB were upregulated.

The HIF pathway is proven to be a responder and core regulator of most transcriptional responses and other angiogenic factors under hypoxia¹⁶⁶. Our results indicate the regulatory roles of VEGFB during

hypoxia and Mg degradation and suggest their cell stage dependence. Compared to VEGFA, the effects of VEGFB on angiogenesis remain mainly unexplored. The difference in hypoxia effects on migration and tube formation when influenced by Mg degradation relies on HIF downregulation. Studies suggest that HIF can upregulate the gene and protein expression of MMPs, TIMPs, NOS, VEGFs and VEGFRs, which play major roles in angiogenesis^{167,168}. VEGFRs can be mediated by HIF *via* the FLT1 promoter or through post-translational mechanisms^{169–172}. Hypoxia downregulated the expression of NOS. The hypoxia–attenuated, VEGF-stimulated activation of NOS2 has been reported as a consequence of nitric oxide release in endothelial migration and proliferation^{172,173}. Our results suggest that the effects of Mg and hypoxia can be cell stage dependent. Other reports indicate that the effects of hypoxia may depend on cell types^{174–178}.

Cellular migration begins with detachment from the primary site by reducing adhesion, approaching and attaching to the secondary site by motility and increased adhesion¹⁷⁹. For example, some cytoskeletal proteins can facilitate adhesion but impair chemotaxis through regulating chemotactic signalling or hindering the formation of new adhesion to finish the migration. Adhesion often facilitates migration to new sites to adapt new tissues by physical links between cell and ECM¹⁸⁰. For instance, integrin is a known adhesion receptor family. With combinations of the α and β subunits, multiple heterodimers can bind to specific ligands of ECMs^{181,182}. Moreover, an adhesion event is also a complex process that involves multiple events, such as receptor–ligand binding and the modulation of cytoskeletal assembly¹⁸³. ECM and its degradation by collagenases, such as the activity of MMPs and tissue MMPs inhibitors are also involved^{184,185}. ECMs are produced around cells, and the main components include glycosaminoglycans, perlecan, aggrecan, fibronectin, laminins, tenascin and collagens¹⁸⁶. ECM is a highly dynamic structure. This matrix serves diverse functions in the cellular microenvironment but is indispensable during the restructuring of tissue architecture, for example, regulating stem cell niches and branching morphogenesis^{187,188}. Generally, studies have suggested that ECMs support cellular adhesion, migration, proliferation, differentiation, the growth and death of vasculature and bone regeneration, which may occur through upregulating molecules such as TGF β and transmitting mechanical support or stresses^{189–192}. ANG can support endothelial adhesion, providing a substratum for interacting with ECM molecules and then inducing basement membrane degradation, mainly through activating protein kinase B/Akt signalling^{193–195}. MMPs, as the most prominent family of ECM enzymes

and their inhibitors, such as TIMPs, perform vital roles in the turnover of ECMs, for example, collagen degradation to allow ductal progression through the basement membrane¹⁹⁶. MMPs also cleave many growth factors, cytokines and cell adhesion molecules and modulate their functions^{197–199}. Some investigation suggests that the sensitivity of MMPs to Mg, which associates with TIMPs, activates NFκB and protein tyrosine kinase^{197–199}. Binding to tyrosine kinase receptors, VEGF can induce cell migration and new vessel formation as a highly specific mitogen for endothelial cells²⁰⁰. MMPs could also be influenced by Mg²⁺ because MMPs are zinc-dependent endopeptidases in which Mg²⁺ could interfere with Zn²⁺ because of ion radius similarity^{201,202}. Some reports indicate a role of IL8 in pro-inflammation and delayed wound closure^{203,204}. IL8 can be formed in highly inflammatory conditions and produced in endothelial cells to attract cells through activating the phosphoinositide 3-kinase-Rac1/RhoA pathway²⁰⁵. In contrast, IL8 can promote wound healing and initiate immune responses^{203,204}.

Mitochondrial potential, as a factor in mitochondrial function, is suggested to relate to the cell migration through dynamin-1-like protein (Drp1)-dependent mitochondrial fission or HIF1a accumulation from increased ROS^{206,207}. The stimulated metabolism under hypoxia suggests mechanisms by which hypoxia can influence the effects of Mg on endothelial metabolism. The elevated mitochondrial membrane potential detected in the highly migratory HUVECs also suggests an increased need for mitochondrial activity, such as ATP synthesis during migration¹¹⁶. Hypoxia could decrease such migration induced by Mg, potentially *via* suppressing ATPase by Ca²⁺ release-activated Ca²⁺ (CRAC) channels and AMP-activated protein kinase (AMPK) activation²⁰⁸.

The present findings also suggest roles for transporters related to the Mg ion. Though the extracellular Mg is high, the alteration of intracellular Mg²⁺ requires Mg²⁺ transport with ion transporters or channels such as TRPM6 and TRPM7^{209–211}. CAPN1 can influence intracellular Mg²⁺ by decreasing TRPM7 and degrading tyrosine phosphatases, such as PTPN23^{209,212,213}. Claudins are transmembrane tight junction proteins that are directly responsible for forming ion-selective channels or pores. CLD16 was formerly reported to play a critical role in the re-absorption of magnesium²¹⁴. Oxygen stress can influence the downregulation of CAPN1 and CLD16 in HUVECs. Cell morphology is changed in response to adhesion and movement during both endothelial migration⁷³ and tube formation²¹⁵. Reports have suggested that the Mg²⁺ state is dynamically regulated by actin cytoskeleton rearrangement during cell morphology

changes⁷⁴. Mg can enhance migration while decreasing tubule formation by regulating cytoskeleton-related genes such as ANG, VCAM1, EZR and CD9. These results are consistent with former reports that Mg can significantly induce the cytoskeletal reorganisation of HUVECs^{216,217}. Hypoxia can induce actin rearrangement and actin stress fibre assembly during cytoskeleton organisation *via* Rho GTPase signalling²¹⁸ and modify the integration of matrix information²¹⁸. In endothelial adhesion, growth factors and their interaction with adhesion factors can mediate angiogenesis through similar pathways²¹⁸. Adhesion is primarily mediated through integrins binding to the extracellular matrix (ECM), a process involving the recognition of specific ECM ligands⁷³. For example, integrin $\beta 1$ regulates angiogenic cell survival and differentiation^{219,220}. Integrins directly interact with growth factor receptors, thereby regulating the capacity of integrin–growth factor receptor complexes to propagate downstream signalling²²¹. For instance, integrin $\alpha \nu \beta 3$ can cooperate with KDR²²⁰. Additionally, angiogenesis can be induced by epidermal growth factor (EGF), platelet-derived growth factor (PDGF), insulin, FGFb and VEGFs, which requires or relates to the functions of integrin $\alpha 1 \beta 1$, $\alpha 2 \beta 1$, $\alpha 5 \beta 1$, $\alpha \nu \beta 3$ and $\alpha \nu \beta 5$ ^{225–228}. Integrin $\alpha \nu \beta 3$ mediates angiogenesis depending on the ligation state of $\alpha 5 \beta 1$ to fibronectin²²⁹. VCAM1, as an endothelial adhesion receptor, can bind to integrins, which also can be upregulated by Mg²²⁹. Mg influenced angiogenesis *via* regulating CD9, which can support VCAM1 function as tetraspanin-enriched microdomains²²⁹.

Some clinic and epidemiology reports indicate the potency of Mg in the treatment of tumours because of its effects on endothelial proliferation and differentiation. Additional interesting but less efficient facts for application, are the pleiotropic and diverging effects on tumour growth²³⁰. Under normoxia, Mg presents a positive effect on endothelial migration, which accords with a former report¹⁴⁷. Even though such stimulation was abolished under hypoxia, the decreased endothelial migration could be a valuable hint regarding tumour inhibit through the suppression of microvessel formation, which is necessary for tumour metastasis. The migration dysfunction induced by Mg could also decrease the secretion of angiocrine factors, which normally promote tumour progression^{187,231}. Nevertheless, tube formation increased with Mg, and hypoxia strengthened the beneficial role of Mg in fracture healing, cooperating with its effects on MSC fate, osteogenesis and vascularisation around a transplant¹⁴⁹. Future work will focus on developing a more complex *in vitro* model (*e.g.*, coculture) to further study the interaction between MSC activity and angiogenesis.

6.2 Magnesium degradation products and hypoxia influence the EC-MSC interaction

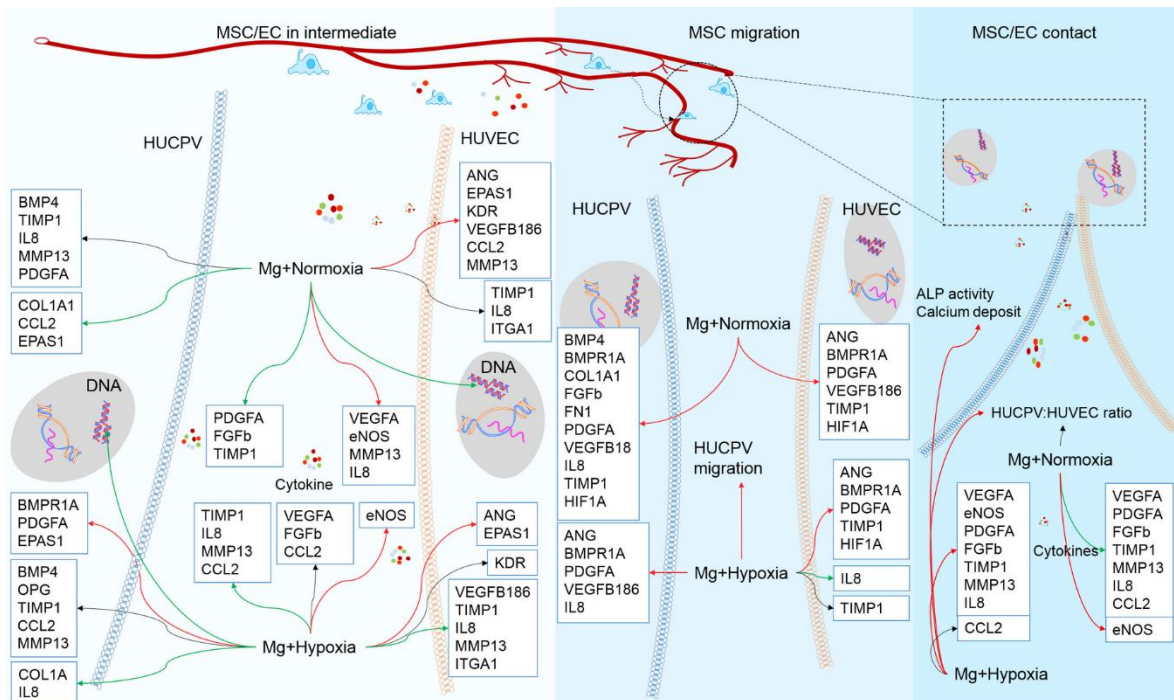


Fig. 29 Summary of the transwell and direct-contact coculture. Red and green arrow indicate the up- and downregulation, respectively. Black arrow represents both up- and downregulation.

After angiogenesis, MSCs can be recruited through blood vessels into fracture sites to support bone healing by their proliferation, secretion and differentiation. The bone fracture environment is controlled and nuanced by many cascades in the complex hierarchical structure of bones. The recent focus is on the cell niche formed by ECs, MSCs, hypoxia and proteins^{57,58}. The communication between MSCs and ECs can be classified into an MSC-EC intermediate stage (without contacting), MSC migration step and MSC-EC contact stage (Fig. 29) during fracture healing.

Furthermore, the findings regarding MSC-EC interaction can shed light on the value of Mg in stem cell therapy and tissue regeneration. MSCs have been applied in diverse tissue injuries within the field of regenerative medicine²³² because of their wide resources⁷⁵; multilineage differentiation potential⁷⁶ and cytokine modulatory effects on the host microenvironment^{76,233}. Implants are crucial carriers to act as biotic and abiotic graft scaffolds⁷⁵.

At present, the concerns regarding MSC fate most often indicated by many studies are MSC homing⁸⁰

and differentiation⁸¹ as well as the regulation of chemokine factors⁸³ and trophic factors²³⁴. Mg implants are an attractive biomaterial since Mg is a natural mineral component of bones⁸ and degrades in aqueous environments⁵⁴. Mg has been shown to improve cell motility²³⁵ and proliferation²³⁶, MSC fate¹⁴⁹ and EC activity⁴⁰. However, the effects (*i.e.*, molecular mechanisms) of Mg degradation products on MSC-EC communication, MSC migration and eventual MSC fate still need to be understood, especially when nuanced with dynamic hypoxia and successive heterotypic contacts.

The present results suggest that Mg could play roles in cellular proliferation, cytokine mechanisms and MSC-EC heterotypic contact (Fig. 29). In summary, Mg degradation products are beneficial for the microenvironment of MSCs and ECs such as the proliferation of MSCs, increased migration, improved expression of cytokines, ECM and HIF-related gene. From comparing the results between transwell (non-contact) and direct-contact coculture (contact), heterotypic contact can be crucial for Mg-increased osteogenesis.

Mg decreases MSC proliferation in transwells under hypoxia but increases proliferation in direct-contact coculture. Decreased proliferation of ECs is only found in direct-contact coculture. The influence of Mg on proliferation could be attributed to the chemical properties of metal ions, which are related to molecular or biological activities, as discussed in section 6.1. Mg could potentially influence other metal ions, such as Ca and Zn, that occur in metabolic or DNA enzymes^{152–154}. The Mg ion can influence cell proliferation *via* the displacement of these other ions from their biofunctional molecules, thus interfering, for example, with enzyme cofactors^{151,155}, DNA topoisomerases and enzyme–DNA cleavage complexes¹⁵¹.

6.2.1 The MSC-EC interaction in the intermediate stage is influenced by Mg and hypoxia

After angiogenesis, MSCs interact with ECs by sharing environmental factors, such as cytokines and hypoxia, before MSCs are recruited. The results of the 7-day-transwell cultures suggest that hypoxia and normoxia generally affect gene regulation in MSCs and ECs in opposite ways. In the long term, Mg degradation products are more beneficial to the cytokine environment under hypoxia than under normoxia. The similar influence of ECs on cytokines and EC genes suggests that ECs may act as

protagonists towards MSCs when influenced by Mg in the intermediate stage. Moreover, MSC-EC transplantation can be a promising therapeutic resource since these cells form the MSC-EC stromal niche. The undifferentiated and differentiated cells can exert equal therapeutic effects, such as cytokine secretion²³⁸. Thus, the cytokine expression during MSC-EC interaction was investigated in transwell coculture. Mg is reported to mediate osteogenesis and angiogenesis by regulating VEGFs and their subsequent signalling²³⁹. Besides the HIF axis, hypoxia is known to couple with VEGFs to improve osteogenesis and angiogenesis²⁴⁰. As a core regulator, VEGF can be released from both MSCs and ECs, which has been reported to promote revascularisation in injured tissues²⁴¹. Another important group of key regulators preferentially expressed under hypoxia is the family of hypoxia-inducible factors (HIFs). Hypoxia triggered HIFs and the subsequent cascades, e.g., the Notch, ANG²⁴² and VEGF axes²⁴³. ANG can counteract inflammation by reducing IL8 production²⁴⁴. PDGF, TGF β and NO regulate differentiation and the growth of MSCs²⁴⁵. In NO signalling, eNOS plays an important role in the NO biosynthesis of vascular endothelium²⁴⁶. Additionally, FGFs play crucial roles in self-renewal²⁴⁷, the multiline potential of MSCs^{248,249} and chemotaxis²⁵⁰. FGFb is also reported to protect MSCs in hypoxia conditions²⁵¹. FGFb and its high-affinity tyrosine kinase FGF receptors have been proven to regulate cell survival in angiogenesis and wound healing²⁵². The stimulation of FGFb in angiogenesis depends on the expression of the VEGF system, which is induced by Hedgehog activation²⁵³. Endothelial chemotaxis is triggered and modulated by VEGF and FGFb. CCL2 is critical for migration *via* cytoskeletal rearrangement and the activation of MAP kinase after binding to CCR2¹⁸⁵. Additionally, CCL2 serves as a potential therapy target since MSCs can influence inflammatory regulation *via* expressing CCL2 to B cells²⁵⁴ and NK cells²⁵⁵. Other important regulators in migration are the matrix metalloendopeptidases (MMPs), which breakdown ECM during tissue remodelling²⁵⁶. MMP13 is reported to regulate endothelial migration *via* activating NO signalling²⁵⁷ and mediating adhesion with the help of TIMPs²⁵⁸. The degradation and remodelling of MMP13 to ECMs may interact with Mg²⁺ since the endopeptidases are extracellular zinc-dependent enzymes²⁵⁹. The expression of MMPs can be directly enhanced by IL8, which depends on CXC chemokine receptor (CXCR) 1/2 expression²⁶⁰. PDGFs are mediators in proinflammation, tissue remodelling²⁶¹, wound healing^{262,263} migration²⁶⁴ tube formation²⁶⁵ and cell proliferation²⁶⁶. PDGFA can mediate EC relaxation *via* eNOS²⁵⁶. MSCs can secrete IL8 to promote endothelial proliferation, migration, and tube formation²⁶⁷.

6.2.2 MSC migration interaction with ECs is influenced by Mg and hypoxia

The migration of MSCs can be regulated by many cytokines. For instance, chemotaxis is directed by VEGF and FGFb. Haptotaxis is directed towards ligands such as integrins binding to ECMs. The MSC migration assays indicate that the influence of Mg is related to hypoxia, with migration generally higher under normoxia. The difference between oxygen levels can be ascribed to the influence of genes, such as migratory IL8, BMP and ECM pathways^{268,269}. CCL2 is a CC-type chemokine and can be synthesised by almost every cell type. Because this chemokine is limited by the distribution of its receptor CCR2 (in monocytes and macrophages, etc.), CCL2 performs inflammatory regulation *via* triggering intracellular Ca²⁺ mobilisation, cytoskeletal rearrangement and the activation of MAP kinase after binding to CCR2¹⁸⁵. Additionally, CCL2 proved to be critical for the migration process. Especially, CCL2 plays critical roles in the recruitment of monocytes across the vascular endothelium²⁷⁰ in the biomaterial implantation²⁷¹. MMP13, as a protease of MMPs, can breakdown ECMs in physiological and pathological processes that include tissue remodelling, arthritis and metastasis²⁵⁶. MMP13 can regulate endothelial migration through activating NO signalling²⁵⁷ and mediating adhesion *via* TIMPs and adhesion molecules²⁵⁸. eNOS plays an important role in NO biosynthesis in vascular endothelium²⁴⁶. IL8 can directly enhance EC proliferation, survival and MMP expression, which depends on CXCR1/2 expression²⁶⁰. Otherwise, IL8 indirectly triggers the angiogenesis of CXCR1/2 lacking ECs²⁷². FGFb and its high-affinity tyrosine kinase FGF receptors were proven to regulate cell proliferation, differentiation and survival during angiogenesis and wound healing²⁵². The stimulation of FGFb during angiogenesis depends on VEGF system expression, which is induced by Hedgehog activation²⁵³. TGFβ was shown to regulate the EC growth, differentiation and functions. Some data suggest that TGFβ can inhibit the EC growth of different cell sources²⁷³ *via* altering the cellular response to growth-stimulatory factors, such as epidermal growth factor (EGF), EGF-high-affinity receptors and EGF-induced growth regulatory genes²⁷⁴. However, TGFβ was also shown to promote angiogenesis *via* increasing PDGF and fibronectin as well as partly through an autocrine secretion of TGF-α activating PI3K/Akt and p42/p44 MAPK²⁷⁵. TGFβ can regulate EC plasticity²⁷⁵ and the EC synthesis of proteases such as MMPs^{276,277}. PDGFs are proinflammatory mediators known to contribute to cellular damage and tissue remodelling²⁶¹. PDGFs and their receptors are angiogenic in promoting wound healing^{262,263}, cell proliferation²⁶⁶, migration²⁶⁴, tube formation²⁶⁵ and mediating EC relaxation *via* eNOS²⁵⁶.

CCL2/CCR2 also can promote tumour growth with increasing MSC migration²⁷⁸. MSCs can also manipulate inflammatory regulation by expressing CCL2 to B cell²⁵⁴ and NK cells²⁵⁵, suggesting that CCL2 may serve as a potential target for MSC-based therapy. MMP13 was reported as a marker for the prediction and therapy of cancers. The degradation and remodelling roles to ECM of MMP13 can be predicted to interact with metal ions such as Mg^{2+} since its endopeptidases role is extracellular zinc-dependent²⁵⁹. MMP13 was also proven to be secreted by MSCs to mediate neovascular pathogenesis²⁷⁹. The exogenous MMPs can interact with MSCs at the cell surface to influence differentiation, angiogenesis, proliferation and migration and regulate the pericellular localisation of MMP activities²⁸⁰. The secretion of MMP13 in MSCs can be mediated by $TGF\beta^{281}$ and TIMPs²⁸². MSCs can secrete IL8 to promote endothelial proliferation, migration and tube formation in cancer-related angiogenesis²⁶⁷. The IL8 enhancement of angiogenesis has been reported to relate to VEGFs secretion in part *via* the PI3K/Akt and MAPK/ERK signal transduction pathways²⁴¹. VEGF, as a crucial regulator in angiogenesis, can be released from MSCs and contributes to the therapeutic effects of stem cells by regulating angiogenesis and promoting revascularisation in injured tissues²⁴¹. ANG is an angiogenic growth factor that can counteract inflammation *via* reducing IL8 production²⁴⁴. PDGF, $TGF-\beta$, NO and FGF signalling have been reported to regulate the differentiation and growth of MSCs²⁴⁵. FGFs play a crucial role in self-renewal²⁴⁷, the multiline potential of MSC^{248,249}, the immune response, the inflammatory response and the response to wounding and chemotaxis²⁵⁰. A transfection study suggests a role of FGFb in protecting MSCs under hypoxia conditions²⁵¹. The eNOS, which produces perivascular NO *via* activating Notch signalling, is mediated by PDGF²⁸³.

Referring to gene results, MSCs tend to be more regulated by Mg under normoxia. Unlike the results of the migration assay, the regulation of the EC gene is more significantly influenced by Mg under hypoxia. The Mg influence on MSC migration may depend on mediating MSC genes under normoxia but regulating EC involvement under hypoxia, such as increasing cytokine secretion by ECs.

6.2.3 Magnesium degradation products and hypoxia influence heterotypic EC-MSc contact

After migration or recruitment, MSCs reach the local fracture site. Direct contact between cells reportedly triggers signal transduction *via* widely distributed signalling on the cellular lipid bilayer¹³³. The present

comparison between proliferation and mineralisation of transwell and direct-contact cocultures and oxygen conditions support the existence of stimulatory roles for heterotypic contact and hypoxia in the differentiation of MSCs exposed to Mg degradation products. The improved results of direct contact may depend on enhanced MSC proliferation and osteogenesis^{284,285}, which depends on preventing apoptosis¹⁴². Moreover, cellular contact can improve osteogenesis and angiogenesis^{241,244,245} by binding cytokine receptors on the cellular surface and triggering signalling. MSC migration depends on cytokines such as IL8 and CCL2²⁸⁶ as well as MMP activation and reactive oxygen species (ROS)²⁸⁷. The MMP activity during migration is strongly related to the cellular surface of MSCs²⁸². The interaction between ECs and ECMs can regulate the production of MMPs through matrix-induced signalling, activate transcription and result in the formation of multiprotease complexes on the cell surface²⁸⁸. PDGF is indicated in the EC-induced recruitment, with heterotypic cell-cell interaction²⁷³. FGFs and VEGFs perform their functions during cell-cell interaction²⁵³ through specific binding to the surface receptors equipped with tyrosine kinase activity²⁸⁹. The Notch system is important to cell-cell communication for deciding EC fate, angiogenesis²⁹⁰, and osteogenesis²⁹¹. Notch signalling can be activated by perivascular NO²⁸³, which is synthesised by eNOS.

Another hypothesis for the different results between coculture models is other cellular communications, such as that based on exosomes or cell transitions. Exosomes are cell-derived vesicles believed to carry microRNA (miRNA) and proteins to regulate osteogenesis and angiogenesis by increasing MSC proliferation or the delivery of miRNA²⁹². The mobility of exosomes is restricted by the distance between neighbouring cells²⁹³ and can, therefore, be more efficient in direct-contact coculture. Endothelial-mesenchymal transition (EndMT) is a cellular interaction during angiogenesis and tissue development that can increase MSC proliferation²⁹⁴. VEGFA and FGFb experienced contrary influences in Mg under hypoxia in transwells on day 1, and these factors are reported to inhibit EndMT²⁹⁴. The mediator of EndMT is concentrated on the cell membrane, similar to ITGF β and MMPs²⁹⁵. Thus, the effects of Mg²⁺ on MSC-EC interaction could depend on cellular exosomes or EndMT *via* cytokine influences or signalling related to heterotypic cell contact.

7 Conclusion

Though natural hypoxia is dynamic, a relatively decreased oxygen environment can be maintained around the implant because the Mg degradation is oxygen-dependent. During angiogenesis steps, Mg extracts did not interfere under hypoxia. An explanatory hypothesis could include the increased proliferation of endothelial cells. Additionally, the antagonist effects of hypoxia and Mg would be associated to keep angiogenesis unaffected. Note that abnormally increased angiogenesis can also be pathological, such as in ocular neovascularisation and haemangiomas. The value of magnesium biomaterial for the orthopaedic application is emphasised and could be promising for regenerative medicine *via* improving the stem cell niche and tissue regeneration. Eventually, increased angiogenesis and osteogenesis could be expected. Heterotypic contact of stromal MSCs/ECs and hypoxia are important elements influencing the effects of Mg. Under hypoxia, Mg can affect proliferation and increase migration, angiogenic and other tropic cytokine secretions, as well as gene regulation in the MSC-EC cell niche. The effects of hypoxia are associated with MSC migration, VEGFs, ECM and HIF-related regulation and cytokines. However, due to limitations of the experiments' time scale, materials and methodology, the effects of Mg and hypoxia may be diminished, and the exact mechanism needs to be further clarified.

References

1. Gerteis, J. *et al.* *Multiple chronic conditions chartbook*. Agency for Healthcare Research and Quality (2014).
2. Johnell, O. & Kanis, J. A. An estimate of the worldwide prevalence and disability associated with osteoporotic fractures. *Osteoporos. Int.* **17**, 1726–1733 (2006).
3. Colón-Emeric, C. S. & Saag, K. G. Osteoporotic fractures in older adults. *Best Pract. Res. Clin. Rheumatol.* **20**, 695–706 (2006).
4. Kelly, B. B., Narula, J. & Fuster, V. Recognizing global burden of cardiovascular disease and related chronic diseases. *Mt. Sinai J. Med.* **79**, 632–640 (2012).
5. Whang, R. & KW, R. Frequency of hypomagnesemia and hypermagnesemia: Requested vs routine. *JAMA* **263**, 3063–3064 (1990).
6. Jahnen-Dechent, W. & Ketteler, M. Magnesium basics. *Clin. Kidney J.* **5**, i3–i14 (2012).
7. Touyz, R. M. Magnesium in clinical medicine. *Front. Biosci.* **9**, 1278–1293 (2004).
8. Alfrey, A. C. & Miller, N. L. Bone magnesium pools in uremia. *J. Clin. Invest.* **52**, 3019–3027 (1973).
9. Castiglioni, S., Cazzaniga, A., Albisetti, W. & Maier, J. A. M. Magnesium and osteoporosis: Current state of knowledge and future research directions. *Nutrients* **5**, 3022–3033 (2013).
10. Malpuech-Brugere, C. *et al.* Accelerated thymus involution in magnesium-deficient rats is related to enhanced apoptosis and sensitivity to oxidative stress. *Br. J. Nutr.* **81**, 405–411 (1999).
11. Myrissa, A. *et al.* In vitro and in vivo comparison of binary Mg alloys and pure Mg. *Mater. Sci. Eng. C* **61**, 865–874 (2016).
12. Del Gobbo, L. C. *et al.* Circulating and dietary magnesium and risk of cardiovascular disease: A systematic review and meta-analysis of prospective studies. *Am. J. Clin. Nutr.* **98**, 160–173 (2013).
13. Barbagallo, M. & Dominguez, L. J. Magnesium and type 2 diabetes. *World J. Diabetes* **6**, 1152–1157 (2015).
14. Almozni-Sarafian, D. *et al.* Magnesium and C-reactive protein in heart failure: An anti-inflammatory effect of magnesium administration? *Eur. J. Nutr.* **46**, 230–237 (2007).
15. Swaminathan, R. Magnesium metabolism and its disorders. *Clin. Biochem. Rev.* **24**, 47 (2003).
16. Sonna, L. A., Hirshman, C. A. & Croxton, T. L. Role of calcium channel blockade in relaxation of tracheal smooth muscle by extracellular Mg²⁺. *Am. J. Physiol.* **271**, L251–L257 (1996).
17. Iseri, L. T. & French, J. H. Magnesium: Nature's physiologic calcium blocker. *Am. Heart J.* **108**, 188–193 (1984).
18. Slone, R. M., Heare, M. M., Vander Griend, R. A. & Montgomery, W. J. Orthopedic fixation devices. *Radiographics* **11**, 823–847 (1991).
19. Xiao, H., Lu, W. & Yeh, J.-T. Crystallization behavior of fully biodegradable poly(lactic acid)/poly(butylene adipate-co-terephthalate) blends. *J. Appl. Polym. Sci.* **112**, 3754–3763 (2009).
20. Ridzwan, M. I. Z., Shuib, S., Hassan, A. Y., Shokri, A. A. & Ibrahim, M. N. M. Problem of stress shielding and improvement to the hip implant designs: A review. *J. Med. Sci* **7**, 460–467 (2007).

21. Buly, R. L., Huo, M. H., Salvati, E., Brien, W. & Bansal, M. Titanium wear debris in failed cemented total hip arthroplasty: An analysis of 71 cases. *J. Arthroplasty* **7**, 315–323 (1992).
22. Frigg, R. Development of the locking compression plate. *Injury* **34**, B6-10 (2003).
23. Daubs, B. M., McLaughlin, R. M., Silverman, E. & Rizon, J. Evaluation of compression generated by self compressing Orthofix bone pins and lag screws in simulated lateral humeral condylar fractures. *Vet. Comp. Orthop. Traumatol.* **20**, 175–179 (2007).
24. Hsu, J.-T. *et al.* The number of screws, bone quality, and friction coefficient affect acetabular cup stability. *Med. Eng. Phys.* **29**, 1089–1095 (2007).
25. Hope, P. G., Williamson, D. M., Coates, C. J. & Cole, W. G. Biodegradable pin fixation of elbow fractures in children. A randomised trial. *J. Bone Joint Surg. Br.* **73**, 965–968 (1991).
26. Board, T. N., Yang, L. & Saleh, M. Why fine-wire fixators work: An analysis of pressure distribution at the wire–bone interface. *J. Biomech.* **40**, 20–25 (2007).
27. Hynes, M. C. & Giddins, G. E. B. Dynamic external fixation for pilon fractures of the interphalangeal joints. *J. Hand Surg. Br. Eur. Vol.* **26**, 122–124 (2001).
28. Green, S. A. Complications of external skeletal fixation. *Clin. Orthop. Relat. Res.* 109–116 (1983).
29. Witte, F. The history of biodegradable magnesium implants: A review. *Acta Biomater.* **6**, 1680–1692 (2010).
30. Armour, K. J. *et al.* Activation of the inducible nitric oxide synthase pathway contributes to inflammation-induced osteoporosis by suppressing bone formation and causing osteoblast apoptosis. *Arthritis Rheum.* **44**, 2790–2796 (2001).
31. Hermawan, H. Updates on the research and development of absorbable metals for biomedical applications. *Prog. Biomater.* **7**, 93–110 (2018).
32. Zhuang, J. *et al.* Degraded and osteogenic properties of coated magnesium alloy AZ31; an experimental study. *J. Orthop. Surg. Res.* **11**, 30 (2016).
33. Zhao, D. *et al.* Current status on clinical applications of magnesium-based orthopaedic implants: A review from clinical translational perspective. *Biomaterials* **112**, 287–302 (2017).
34. Kim, Y.-K. *et al.* Gas formation and biological effects of biodegradable magnesium in a preclinical and clinical observation. *Sci. Technol. Adv. Mater.* **19**, 324–335 (2018).
35. Syntellix. First surgery in Ireland. (2015). Available at: http://www.syntellix.de/en/newspr/aktuelle-news/single-view/?tx_news_pi1%5Bnews%5D=23&cHash=c508574e00c8234c3f17ff8675f65886.
36. Syntellix. First Magnezix® surgery in Iran. (2016). Available at: http://www.syntellix.de/en/newspr/latest-news/single-view/?tx_news_pi1%5Bnews%5D=34&cHash=33ce6146dee249f62675bf26b6d746da.
37. Biber, R., Pauser, J., Brem, M. & Bail, H. J. Bioabsorbable metal screws in traumatology: A promising innovation. *Trauma Case Reports* **8**, 11–15 (2017).
38. Kose, O., Turan, A., Unal, M., Acar, B. & Guler, F. Fixation of medial malleolar fractures with magnesium bioabsorbable headless compression screws: Short-term clinical and radiological outcomes in eleven patients. *Arch. Orthop. Trauma Surg.* **138**, 1069–1075 (2018).
39. Zhao, D. *et al.* Vascularized bone grafting fixed by biodegradable magnesium screw for treating osteonecrosis of the femoral head. *Biomaterials* **81**, 84–92 (2016).
40. Lee, J.-W. *et al.* Long-term clinical study and multiscale analysis of in vivo biodegradation mechanism of Mg alloy. *Proc. Natl. Acad. Sci.* **113**, 716–721 (2016).
41. Lee, J.-H., Han, H.-S., Kim, Y.-C., Lee, J.-Y. & Lee, B.-K. Stability of biodegradable metal (Mg–

- Ca–Zn alloy) screws compared with absorbable polymer and titanium screws for sagittal split ramus osteotomy of the mandible using the finite element analysis model. *J. Cranio-Maxillofacial Surg.* **45**, 1639–1646 (2017).
42. Rapetto, C. & Leoncini, M. Magmaris: A new generation metallic sirolimus-eluting fully bioresorbable scaffold: Present status and future perspectives. *J. Thorac. Dis.* S903–S913 (2017).
 43. Mao, L. *et al.* A promising biodegradable magnesium alloy suitable for clinical vascular stent application. *Sci. Rep.* **7**, 46343 (2017).
 44. Moravej, M. & Mantovani, D. Biodegradable metals for cardiovascular stent application: Interests and new opportunities. *Int. J. Mol. Sci.* **12**, 4250–4270 (2011).
 45. Erne, P., Schier, M. & Resink, T. J. The road to bioabsorbable stents: Reaching clinical reality? *Cardiovasc. Intervent. Radiol.* **29**, 11–16 (2006).
 46. O'Brien, B. & Carroll, W. The evolution of cardiovascular stent materials and surfaces in response to clinical drivers: A review. *Acta Biomater.* **5**, 945–958 (2009).
 47. Ge, Q., Dellasega, D., Demir, A. G. & Vedani, M. The processing of ultrafine-grained Mg tubes for biodegradable stents. *Acta Biomater.* **9**, 8604–8610 (2013).
 48. Esmaily, M. *et al.* Fundamentals and advances in magnesium alloy corrosion. *Prog. Mater. Sci.* **89**, 92–193 (2017).
 49. Gu, X. N., Zheng, Y. F. & Chen, L. J. Influence of artificial biological fluid composition on the biocorrosion of potential orthopedic Mg–Ca, AZ31, AZ91 alloys. *Biomed. Mater.* **4**, 65011 (2009).
 50. Johnson, I., Jiang, W. & Liu, H. The effects of serum proteins on magnesium alloy degradation in vitro. *Sci. Rep.* **7**, 14335 (2017).
 51. Ning, C. *et al.* Influence of surrounding cations on the surface degradation of magnesium alloy implants under a compressive pressure. *Langmuir* **31**, 13561–13570 (2015).
 52. Saris, N.-E. L., Mervaala, E., Karppanen, H., Khawaja, J. A. & Lewenstam, A. Magnesium: An update on physiological, clinical and analytical aspects. *Clin. Chim. Acta* **294**, 1–26 (2000).
 53. Zhang, E., Xu, L., Yu, G., Pan, F. & Yang, K. In vivo evaluation of biodegradable magnesium alloy bone implant in the first 6 months implantation. *J. Biomed. Mater. Res. Part A* **90**, 882–893 (2009).
 54. Zhang, F. *et al.* Quantitative analysis of near-implant magnesium accumulation for a Si-containing coated AZ31 cage from a goat cervical spine fusion model. *BMC Musculoskelet. Disord.* **19**, 105 (2018).
 55. Gu, X., Zheng, Y., Cheng, Y., Zhong, S. & Xi, T. In vitro corrosion and biocompatibility of binary magnesium alloys. *Biomaterials* **30**, 484–498 (2009).
 56. Witte, F., Ulrich, H., Rudert, M. & Willbold, E. Biodegradable magnesium scaffolds: Part 1: Appropriate inflammatory response. *J. Biomed. Mater. Res. Part A* **81A**, 748–756 (2007).
 57. Zhao, M. & Li, L. Dissecting the bone marrow HSC niches. *Cell Res.* **26**, 975–976 (2016).
 58. Morrison, S. J. & Scadden, D. T. The bone marrow niche for haematopoietic stem cells. *Nature* **505**, 327–334 (2014).
 59. Scadden, D. T. The stem-cell niche as an entity of action. *Nature* **441**, 1075 (2006).
 60. Ehninger, A. & Trumpp, A. The bone marrow stem cell niche grows up: Mesenchymal stem cells and macrophages move in. *J. Exp. Med.* **208**, 421–428 (2011).
 61. Kfoury, Y. & Scadden, D. T. Mesenchymal cell contributions to the stem cell niche. *Cell Stem Cell* **16**, 239–253 (2015).

62. da Silva Meirelles, L., Sand, T. T., Harman, R. J., Lennon, D. P. & Caplan, A. I. MSC frequency correlates with blood vessel density in equine adipose tissue. *Tissue Eng. Part A* **15**, 221–229 (2008).
63. Diaz-Tocados, J. M. *et al.* Magnesium chloride promotes osteogenesis through notch signaling activation and expansion of mesenchymal stem cells. *Sci. Rep.* **7**, 7839 (2017).
64. Kikuchi, M., Itoh, S., Ichinose, S., Shinomiya, K. & Tanaka, J. Self-organization mechanism in a bone-like hydroxyapatite/collagen nanocomposite synthesized in vitro and its biological reaction in vivo. *Biomaterials* **22**, 1705–1711 (2001).
65. Bassi, A., Gough, J., Zakikhani, M. & Downes, S. 5 - Bone tissue regeneration BT - electrospinning for tissue regeneration. in *Woodhead Publishing Series in Biomaterials* 93–110 (Woodhead Publishing, 2011).
66. Dimitriou, R., Jones, E., McGonagle, D. & Giannoudis, P. V. Bone regeneration: Current concepts and future directions. *BMC Med.* **9**, 66 (2011).
67. Jeffcoat, M. K. & Chesnut, C. H. 3rd. Systemic osteoporosis and oral bone loss: Evidence shows increased risk factors. *J. Am. Dent. Assoc.* **124**, 49–56 (1993).
68. Wu, L., Feyerabend, F., Schilling, A. F., Willumeit-Römer, R. & Luthringer, B. J. C. Effects of extracellular magnesium extract on the proliferation and differentiation of human osteoblasts and osteoclasts in coculture. *Acta Biomater.* 294–304 (2015).
69. Silva, E. L., Lamaka, S. V., Mei, D. & Zheludkevich, M. L. The reduction of dissolved oxygen during magnesium corrosion. *ChemistryOpen* **7**, 664–668 (2018).
70. Maier, J. A. M., Malpuech-Brugère, C., Zimowska, W., Rayssiguier, Y. & Mazur, A. Low magnesium promotes endothelial cell dysfunction: Implications for atherosclerosis, inflammation and thrombosis. *Biochim. Biophys. Acta* **1689**, 13–21 (2004).
71. Zhao, N. & Zhu, D. Endothelial responses of magnesium and other alloying elements in magnesium-based stent materials. *Metallomics* **7**, 118–128 (2015).
72. Reinhart-King, C. A. Chapter 3 Endothelial cell adhesion and migration. in *Methods in Enzymology* **443**, 45–64 (Elsevier, 2008).
73. Giancotti, F. G. & Ruoslahti, E. Integrin signaling. *Science* **285**, 1028–1033 (1999).
74. Jeong, S. Y. *et al.* Regulation of magnesium-inhibited cation current by actin cytoskeleton rearrangement. *Biochem. Biophys. Res. Commun.* **339**, 810–815 (2006).
75. Wang, X. *et al.* Role of mesenchymal stem cells in bone regeneration and fracture repair: A review. *Int. Orthop.* **37**, 2491–2498 (2013).
76. Ullah, I., Subbarao, R. B. & Rho, G. J. Human mesenchymal stem cells-current trends and future prospective. *Biosci. Rep.* **35**, e00191 (2015).
77. Blázquez-Prunera, A., Díez, J. M., Gajardo, R. & Grancha, S. Human mesenchymal stem cells maintain their phenotype, multipotentiality, and genetic stability when cultured using a defined xeno-free human plasma fraction. *Stem Cell Res. Ther.* **8**, 103 (2017).
78. Lin, W. *et al.* Mesenchymal stem cells homing to improve bone healing. *J. Orthop. Transl.* **9**, 19–27 (2017).
79. Kurth, T. B. *et al.* Functional mesenchymal stem cell niches in adult mouse knee joint synovium in vivo. *Arthritis Rheumatol.* **63**, 1289–1300 (2011).
80. Karp, J. M. & Leng Teo, G. S. Mesenchymal stem cell homing: The devil is in the details. *Cell Stem Cell* **4**, 206–216 (2009).
81. Ankrum, J. & Karp, J. M. Mesenchymal stem cell therapy: Two steps forward, one step back. *Trends Mol. Med.* **16**, 203–9 (2010).

82. Fakhry, M., Hamade, E., Badran, B., Buchet, R. & Magne, D. Molecular mechanisms of mesenchymal stem cell differentiation towards osteoblasts. *World J. Stem Cells* **5**, 136 (2013).
83. Zachar, L., Bačenková, D. & Rosocha, J. Activation, homing, and role of the mesenchymal stem cells in the inflammatory environment. *J. Inflamm. Res.* **9**, 231–240 (2016).
84. Sargenti, A. *et al.* Magnesium deprivation potentiates human mesenchymal stem cell transcriptional remodeling. *Int. J. Mol. Sci.* **19**, 1410 (2018).
85. Hu, T., Xu, H., Wang, C., Qin, H. & An, Z. Magnesium enhances the chondrogenic differentiation of mesenchymal stem cells by inhibiting activated macrophage-induced inflammation. *Sci. Rep.* **8**, 3406 (2018).
86. Birmingham, E., Niebur, G. L. & McHugh, P. E. Osteogenic differentiation of mesenchymal stem cells is regulated by osteocyte and osteoblast cells in a simplified bone niche. *Eur. Cell. Mater.* **12**, 13–27 (2012).
87. Hass, R., Kasper, C., Böhm, S. & Jacobs, R. Different populations and sources of human mesenchymal stem cells (MSC): A comparison of adult and neonatal tissue-derived MSC. *Cell Commun. Signal.* **9**, 12 (2011).
88. Casiraghi, F., Noris, M. & Remuzzi, G. Immunomodulatory effects of mesenchymal stromal cells in solid organ transplantation. *Curr. Opin. Organ Transplant.* **15**, 731–7 (2010).
89. Pers, Y.-M., Ruiz, M., Noël, D. & Jorgensen, C. Mesenchymal stem cells for the management of inflammation in osteoarthritis: State of the art and perspectives. *Osteoarthr. Cartil.* **23**, 2027–2035 (2015).
90. Nagamura-Inoue, T. & He, H. Umbilical cord-derived mesenchymal stem cells: Their advantages and potential clinical utility. *World J. Stem Cells* **6**, 195–202 (2014).
91. Sarugaser, R., Lickorish, D., Baksh, D., Hosseini, M. M. & Davies, J. E. Human umbilical cord perivascular (HUCPV) cells: A source of mesenchymal progenitors. *Stem Cells* **23**, 220–229 (2005).
92. Broxmeyer, H. E. *et al.* Cord blood stem and progenitor cells. in *Methods in enzymology* **419**, 439–473 (Elsevier, 2006).
93. Montesinos, J. J. *et al.* Human mesenchymal stromal cells from adult and neonatal sources: Comparative analysis of their morphology, immunophenotype, differentiation patterns and neural protein expression. *Cytotherapy* **11**, 163–176 (2009).
94. Schugar, R. C. *et al.* High harvest yield, high expansion, and phenotype stability of CD146 mesenchymal stromal cells from whole primitive human umbilical cord tissue. *Biomed Res. Int.* **2009**, 789526 (2009).
95. Rajatileka, S. *et al.* Isolation of human genomic DNA for genetic analysis from premature neonates: A comparison between newborn dried blood spots, whole blood and umbilical cord tissue. *BMC Genet.* **14**, 105 (2013).
96. Corselli, M., Chen, C.-W., Crisan, M., Lazzari, L. & Péault, B. Perivascular ancestors of adult multipotent stem cells. *Arterioscler. Thromb. Vasc. Biol.* **30**, 1104–1109 (2010).
97. Davies, J. E., Walker, J. T. & Keating, A. Concise review: Wharton's jelly: The rich, but enigmatic, source of mesenchymal stromal cells. *Stem Cells Transl. Med.* **6**, 1620–1630 (2017).
98. Baudin, B., Bruneel, A., Bosselut, N. & Vaubourdolle, M. A protocol for isolation and culture of human umbilical vein endothelial cells. *Nat. Protoc.* **2**, 481–5 (2007).
99. Janeway Jr, C. A., Travers, P., Walport, M. & Shlomchik, M. J. The structure of a typical antibody molecule. in *Immunobiology: The Immune System in Health and Disease* (Garland

- Science, 2001).
100. Keeney, M., Gratama, J. W., Chin-Yee, I. H. & Sutherland, D. R. Isotype controls in the analysis of lymphocytes and CD34+ stem and progenitor cells by flow cytometry--time to let go! *Cytom. Part A* **34**, 280–283 (1998).
 101. Maecker, H. T. & Trotter, J. Flow cytometry controls, instrument setup, and the determination of positivity. *Cytom. Part A* **69A**, 1037–1042 (2006).
 102. Jiang, G. *et al.* Expression levels of microRNA-199 and hypoxia-inducible factor-1 alpha in brain tissue of patients with intractable epilepsy. *Int. J. Neurosci.* **126**, 326–334 (2016).
 103. Peng, Z.-R., Yang, A.-L. & Yang, Q.-D. The effect of hyperbaric oxygen on intracerebral angiogenesis in rats with intracerebral hemorrhage. *J. Neurol. Sci.* **342**, 114–123 (2014).
 104. Paunescu, V. *et al.* Endothelial cells from hematopoietic stem cells are functionally different from those of human umbilical vein. *J. Cell. Mol. Med.* **7**, 455–460 (2003).
 105. Balaiya, S., Murthy, R. K. & Chalam, K. V. Resveratrol inhibits proliferation of hypoxic choroidal vascular endothelial cells. *Mol. Vis.* **19**, 2385–2392 (2013).
 106. Merry, H. E., Phelan, P., Doaks, M., Zhao, M. & Mulligan, M. S. Functional roles of tumor necrosis factor-alpha and interleukin 1-Beta in hypoxia and reoxygenation. *Ann. Thorac. Surg.* **99**, 1200–1205 (2015).
 107. Jiang, F. *et al.* Amniotic mesenchymal stem cells can enhance angiogenic capacity via MMPs in vitro and in vivo. *Biomed Res. Int.* **2015**, 324014 (2015).
 108. Policastro, L. L., Ibanez, I. L., Notcovich, C., Duran, H. A. & Podhajcer, O. L. The tumor microenvironment: Characterization, redox considerations, and novel approaches for reactive oxygen species-targeted gene therapy. *Antioxid. Redox Signal.* **19**, 854–895 (2013).
 109. Shapiro, H. M. *Practical flow cytometry*. (John Wiley & Sons, 2005).
 110. Kato, H. *et al.* Promoting effect of 1, 25 (OH) 2 vitamin D3 in osteogenic differentiation from induced pluripotent stem cells to osteocyte-like cells. *Open Biol.* **5**, 140201 (2015).
 111. Donovan, D., Brown, N. J., Bishop, E. T. & Lewis, C. E. Comparison of three in vitro human 'angiogenesis' assays with capillaries formed in vivo. *Angiogenesis* **4**, 113–121 (2001).
 112. Davis, G. E. & Senger, D. R. Endothelial extracellular matrix: Biosynthesis, remodeling, and functions during vascular morphogenesis and neovessel stabilization. *Circ. Res.* **97**, 1093–1107 (2005).
 113. Zwietering, M. H., Jongenburger, I., Rombouts, F. M. & Van't Riet, K. Modeling of the bacterial growth curve. *Appl. Environ. Microbiol.* **56**, 1875–1881 (1990).
 114. Faulkner, A. *et al.* A thin layer angiogenesis assay: A modified basement matrix assay for assessment of endothelial cell differentiation. *BMC Cell Biol.* **15**, 41 (2014).
 115. Chance, B. & Williams, G. R. The respiratory chain and oxidative phosphorylation. *Adv. Enzymol. Relat. Areas Mol. Biol.* **17**, 65–134 (1956).
 116. Johnson, L. V, Walsh, M. L., Bockus, B. J. & Chen, L. B. Monitoring of relative mitochondrial membrane potential in living cells by fluorescence microscopy. *J. Cell Biol.* **88**, 526–535 (1981).
 117. Han, Y. H., Kim, S. H., Kim, S. Z. & Park, W. H. Antimycin A as a mitochondrial electron transport inhibitor prevents the growth of human lung cancer A549 cells. *Oncol. Rep.* **20**, 689–693 (2008).
 118. Li, N. *et al.* A systematic assessment of mitochondrial function identified novel signatures for drug-induced mitochondrial disruption in cells. *Toxicol. Sci.* **142**, 261–73 (2014).
 119. Kalbacova, M., Vrbacky, M., Drahota, Z. & Melkova, Z. Comparison of the effect of

- mitochondrial inhibitors on mitochondrial membrane potential in two different cell lines using flow cytometry and spectrofluorometry. *Cytom. A* **52**, 110–116 (2003).
120. Geelen, M. J. H. The use of digitonin-permeabilized mammalian cells for measuring enzyme activities in the course of studies on lipid metabolism. *Anal. Biochem.* **347**, 1–9 (2005).
 121. Fiskum, G. Intracellular levels and distribution of Ca²⁺ in digitonin-permeabilized cells. *Cell Calcium* **6**, 25–37 (1985).
 122. Floryk, D. & Houštěk, J. Tetramethyl rhodamine methyl ester (TMRM) is suitable for cytofluorometric measurements of mitochondrial membrane potential in cells treated with digitonin. *Biosci. Rep.* **19**, 27–34 (1999).
 123. Kumar, V. B. S., Viji, R. I., Kiran, M. S. & Sudhakaran, P. R. Angiogenic response of endothelial cells to fibronectin. in *Biochemical Roles of Eukaryotic Cell Surface Macromolecules* (eds. Sudhakaran, P. R. & Surolia, A.) 131–151 (Springer, 2012).
 124. Puchtler, H., Meloan, S. N. & Terry, M. S. On the history and mechanism of alizarin and alizarin red S stains for calcium. *J. Histochem. Cytochem.* **17**, 110–124 (1969).
 125. Kinoshita, S. *et al.* Mitomycin derivatives. 1. Preparation of mitosane and mitosene compounds and their biological activities. *J. Med. Chem.* **14**, 103–109 (1971).
 126. Cohen, M. M. & Shaw, M. W. Effects of mitomycin C on human chromosomes. *J. Cell Biol.* **23**, 386–395 (1964).
 127. Luisa, I. M. & Helene, S. E. Endothelial cells exhibiting angiogenesis in vitro proliferate in response to TGF- β 1. *J. Cell. Biochem.* **52**, 414–430 (2018).
 128. Olesen, S.-P., Clapham, D. & Davies, P. Haemodynamic shear stress activates a K⁺ current in vascular endothelial cells. *Nature* **331**, 168–170 (1988).
 129. Majack, R. A. Beta-type transforming growth factor specifies organizational behavior in vascular smooth muscle cell cultures. *J. Cell Biol.* **105**, 465–471 (1987).
 130. Manwaring, M. E., Walsh, J. F. & Tresco, P. A. Contact guidance induced organization of extracellular matrix. *Biomaterials* **25**, 3631–3638 (2004).
 131. Chen, L. B. Mitochondrial membrane potential in living cells. *Annu. Rev. Cell Biol.* **4**, 155–181 (1988).
 132. Baracca, A., Sgarbi, G., Solaini, G. & Lenaz, G. Rhodamine 123 as a probe of mitochondrial membrane potential: Evaluation of proton flux through F₀ during ATP synthesis. *Biochim. Biophys. Acta* **1606**, 137–146 (2003).
 133. Emaus, R. K., Grunwald, R. & Lemasters, J. J. Rhodamine 123 as a probe of transmembrane potential in isolated rat-liver mitochondria: Spectral and metabolic properties. *Biochim. Biophys. Acta* **850**, 436–448 (1986).
 134. Lu, C. *et al.* The role of oxygen during fracture healing. *Bone* **52**, 220–229 (2013).
 135. Carlier, A., Geris, L., Gastel, N. Van, Carmeliet, G. & Oosterwyck, H. Van. Oxygen as a critical determinant of bone fracture healing — A multiscale model. *J. Theor. Biol.* **365**, 247–264 (2015).
 136. Ciapetti, G. *et al.* Effects of hypoxia on osteogenic differentiation of mesenchymal stromal cells used as a cell therapy for avascular necrosis of the femoral head. *Cytotherapy* **18**, 1087–1099 (2016).
 137. Rankin, E. B., Giaccia, A. J. & Schipani, E. A central role for hypoxic signaling in cartilage, bone, and hematopoiesis. *Curr. Osteoporos. Rep.* **9**, 46–52 (2011).
 138. Banai, S., Haggroth, L., Epstein, S. E. & Casscells, W. Influence of extracellular magnesium on capillary endothelial cell proliferation and migration. *Circ. Res.* **67**, 645–650 (1990).

139. Sgambato, A. *et al.* Isolation of normal epithelial cells adapted to grow at nonphysiological concentration of magnesium. *Biochem. Biophys. Res. Commun.* **286**, 752–757 (2001).
140. Cines, D. B. *et al.* Endothelial cells in physiology and in the pathophysiology of vascular disorders. *Blood* **91**, 3527–3561 (1998).
141. Boutilier, R. G. Mechanisms of cell survival in hypoxia and hypothermia. *J. Exp. Biol.* **204**, 3171–3181 (2001).
142. Steiner, D., Lampert, F., Stark, G. B. & Finkenzeller, G. Effects of endothelial cells on proliferation and survival of human mesenchymal stem cells and primary osteoblasts. *J. Orthop. Res.* **30**, 1682–1689 (2012).
143. Schmitt, C. J. *et al.* Homo- and heterotypic cell contacts in malignant melanoma cells and desmoglein 2 as a novel solitary surface glycoprotein. *J. Invest. Dermatol.* **127**, 2191–2206 (2007).
144. Labernadie, A. *et al.* A mechanically active heterotypic E-cadherin/N-cadherin adhesion enables fibroblasts to drive cancer cell invasion. *Nat. Cell Biol.* **19**, 224 (2017).
145. Kolesky, D. B. *et al.* 3D bioprinting of vascularized, heterogeneous cell-laden tissue constructs. *Adv. Mater.* **26**, 3124–3130 (2014).
146. Adair, T. H. & Montani, J.-P. *Angiogenesis*. *Angiogenesis* (Morgan & Claypool Life Sciences, 2010).
147. Maier, J. A. M., Bernardini, D., Rayssiguier, Y. & Mazur, A. High concentrations of magnesium modulate vascular endothelial cell behaviour in vitro. *Biochim. Biophys. Acta* **1689**, 6–12 (2004).
148. German, A. E., Mammoto, T., Jiang, E., Ingber, D. E. & Mammoto, A. Paxillin controls endothelial cell migration and tumor angiogenesis by altering neuropilin 2 expression. *J. Cell Sci.* **127**, 1672–1683 (2014).
149. Luthringer, B. J. C. & Willumeit-Römer, R. Effects of magnesium degradation products on mesenchymal stem cell fate and osteoblastogenesis. *Gene* **575**, 9–20 (2016).
150. Burmester, A., Luthringer, B., Willumeit, R. & Feyerabend, F. Comparison of the reaction of bone-derived cells to enhanced MgCl₂-salt concentrations. *Biomatter* **4**, e967616 (2014).
151. Sissi, C. & Palumbo, M. Effects of magnesium and related divalent metal ions in topoisomerase structure and function. *Nucleic Acids Res.* **37**, 702–711 (2009).
152. Bock, C. W., Katz, A. K., Markham, G. D. & Glusker, J. P. Manganese as a replacement for magnesium and zinc: Functional comparison of the divalent ions. *J. Am. Chem. Soc.* **121**, 7360–7372 (1999).
153. Sissi, C. *et al.* DNA gyrase requires DNA for effective two-site coordination of divalent metal ions: Further insight into the mechanism of enzyme action. *Biochemistry* **47**, 8538–8545 (2008).
154. Deweese, J. E., Burgin, A. B. & Osheroff, N. Human topoisomerase II α uses a two-metal-ion mechanism for DNA cleavage. *Nucleic Acids Res.* **36**, 4883–4893 (2008).
155. Drynda, A., Deinet, N., Braun, N. & Peuster, M. Rare earth metals used in biodegradable magnesium-based stents do not interfere with proliferation of smooth muscle cells but do induce the upregulation of inflammatory genes. *J. Biomed. Mater. Res. Part A* **91**, 360–369 (2009).
156. West, K. L. *et al.* Mutagenesis of E477 or K505 in the B' domain of human topoisomerase II beta increases the requirement for magnesium ions during strand passage. *Biochemistry* **39**, 1223–1233 (2000).

157. Riss, T. *et al.* *Cell Viability Assays*. (Eli Lilly & Company and the National Center for Advancing Translational Sciences, 2004).
158. Bernas, T. & Dobrucki, J. Mitochondrial and nonmitochondrial reduction of MTT: Interaction of MTT with TMRE, JC-1, and NAO mitochondrial fluorescent probes. *Cytometry* **47**, 236–242 (2002).
159. Kell, D. B. & John, P. Continuous monitoring of the electrical potential across energy-transducing membranes using ion-selective electrodes application to submitochondrial particles and chromatophores. *FEBS Lett.* **86**, 294–298 (1978).
160. Kell, D. B., John, P. & Ferguson, S. J. On the current voltage relationships of energy-transducing membranes: Phosphorylating membrane vesicles from *Paracoccus denitrificans*. *Biochem. Soc. Trans* **6**, 1292–1295 (1978).
161. Anwikar, S. R., Bandekar, M. S., Patel, T. K., Patel, P. B. & Kshirsagar, N. A. Tetany: Possible adverse effect of bevacizumab. *Indian J. Cancer* **48**, 31–33 (2011).
162. Schempp, C. M. *et al.* Magnesium ions inhibit the antigen-presenting function of human epidermal Langerhans cells in vivo and in vitro. Involvement of ATPase, HLA-DR, B7 molecules, and cytokines. *J. Invest. Dermatol.* **115**, 680–686 (2000).
163. Denton, R. M. Regulation of mitochondrial dehydrogenases by calcium ions. *Biochim. Biophys. Acta* **1787**, 1309–1316 (2009).
164. Vygodina, T., Kirichenko, A. & Konstantinov, A. A. Direct regulation of cytochrome c oxidase by calcium ions. *PLoS One* **8**, e74436 (2013).
165. Belyaeva, E. A., Sokolova, T. V., Emelyanova, L. V & Zakharova, I. O. Mitochondrial electron transport chain in heavy metal-induced neurotoxicity: Effects of cadmium, mercury, and copper. *Sci. World J.* **2012**, 136063 (2012).
166. Krock, B. L., Skuli, N. & Simon, M. C. Hypoxia-induced angiogenesis: Good and evil. *Genes Cancer* **2**, 1117–1133 (2011).
167. Shibuya, M. Vascular endothelial growth factor (VEGF) and its receptor (VEGFR) signaling in angiogenesis: A crucial target for anti-and pro-angiogenic therapies. *Genes Cancer* **2**, 1097–1105 (2011).
168. Pugh, C. W. & Ratcliffe, P. J. Regulation of angiogenesis by hypoxia: Role of the HIF system. *Nat. Med.* **9**, 677 (2003).
169. Scheurer, S. B., Raybak, J. N., Rösli, C., Neri, D. & Elia, G. Modulation of gene expression by hypoxia in human umbilical cord vein endothelial cells: A transcriptomic and proteomic study. *Proteomics* **4**, 1737–60 (2004).
170. Gerber, H.-P., Condorelli, F., Park, J. & Ferrara, N. Differential transcriptional regulation of the two vascular endothelial growth factor receptor genes Flt-1, but not Flk-1/KDR, is up-regulated by hypoxia. *J. Biol. Chem.* **272**, 23659–23667 (1997).
171. Brogi, E. *et al.* Hypoxia-induced paracrine regulation of vascular endothelial growth factor receptor expression. *J. Clin. Invest.* **97**, 469–476 (1996).
172. Ulyatt, C., Walker, J. & Ponnambalam, S. Hypoxia differentially regulates VEGFR1 and VEGFR2 levels and alters intracellular signaling and cell migration in endothelial cells. *Biochem. Biophys. Res. Commun.* **404**, 774–779 (2011).
173. Olszewska-Pazdrak, B., Hein, T. W., Olszewska, P. & Carney, D. H. Chronic hypoxia attenuates VEGF signaling and angiogenic responses by downregulation of KDR in human endothelial cells. *Am. J. Physiol. Cell Physiol.* **296**, C1162–C1170 (2009).
174. Waltenberger, J., Mayr, U., Pentz, S. & Hombach, V. Functional upregulation of the vascular

- endothelial growth factor receptor KDR by hypoxia. *Circulation* **94**, 1647–1654 (1996).
175. Tuder, R. M., Flook, B. E. & Voelkel, N. F. Increased gene expression for VEGF and the VEGF receptors KDR/Flk and Flt in lungs exposed to acute or to chronic hypoxia. Modulation of gene expression by nitric oxide. *J. Clin. Invest.* **95**, 1798–1807 (1995).
 176. Marti, H. H. & Risau, W. Systemic hypoxia changes the organ-specific distribution of vascular endothelial growth factor and its receptors. *Proc. Natl. Acad. Sci.* **95**, 15809–15814 (1998).
 177. Kumazaki, K., Nakayama, M., Suehara, N. & Wada, Y. Expression of vascular endothelial growth factor, placental growth factor, and their receptors Flt-1 and KDR in human placenta under pathologic conditions. *Hum. Pathol.* **33**, 1069–1077 (2002).
 178. Sandner, P., Wolf, K., Bergmaier, U., Gess, B. & Kurtz, A. Hypoxia and cobalt stimulate vascular endothelial growth factor receptor gene expression in rats. *Pflügers Arch.* **433**, 803–808 (1997).
 179. Schwartz, M. A. & Horwitz, A. R. Integrating adhesion, protrusion, and contraction during cell migration. *Cell* **125**, 1223–1225 (2006).
 180. Chen, Y. *et al.* Combined integrin phosphoproteomic analyses and small interfering RNA–based functional screening identify key regulators for cancer cell adhesion and migration. *Cancer Res.* **69**, 3713–3720 (2009).
 181. Hynes, R. O. Integrins: Bidirectional, allosteric signaling machines. *Cell* **110**, 673–687 (2002).
 182. Humphries, J. D., Byron, A. & Humphries, M. J. Integrin ligands at a glance. *J. Cell Sci.* **119**, 3901–3903 (2006).
 183. Humphries, M. J. Cell adhesion assays. in *Methods in Molecular Biology* (eds. Even-Ram, S. & Artym, V.) 203–210 (Springer, 2009).
 184. Cook, H., Stephens, P., Davies, K. J., Thomas, D. W. & Harding, K. G. Defective extracellular matrix reorganization by chronic wound fibroblasts is associated with alterations in TIMP-1, TIMP-2, and MMP-2 activity. *J. Invest. Dermatol.* **115**, 225–233 (2000).
 185. A., J. J. *et al.* Matrix metalloproteinases and their inhibitors in the foreign body reaction on biomaterials. *J. Biomed. Mater. Res. Part A* **84A**, 158–166 (2007).
 186. Matusiewicz, M. Extracellular matrix remodeling. in *Encyclopedia of Cancer* (ed. Schwab, M.) 1362–1365 (Springer Berlin-Heidelberg, 2011).
 187. Lu, J. *et al.* Preparation and preliminary cytocompatibility of magnesium doped apatite cement with degradability for bone regeneration. *J. Mater. Sci. Mater. Med.* **22**, 607–615 (2011).
 188. Pickup, M. W., Mouw, J. K. & Weaver, V. M. The extracellular matrix modulates the hallmarks of cancer. *EMBO Rep.* **15**, 1243–53 (2014).
 189. Ding-Yu, L. *et al.* Integrin-mediated expression of bone formation-related genes in osteoblast-like cells in response to fluid shear stress: Roles of extracellular matrix, Shc, and mitogen-activated protein kinase. *J. Bone Miner. Res.* **23**, 1140–1149 (2009).
 190. Allori, A. C., Sillon, A. M. & Warren, S. M. Biological basis of bone formation, remodeling, and repair-part II: Extracellular matrix. *Tissue Eng. Part B Rev.* **14**, 275–283 (2008).
 191. H., C. E. *et al.* Biomimetic artificial ECMs stimulate bone regeneration. *J. Biomed. Mater. Res. Part A* **79A**, 815–826 (2006).
 192. Noda, M. & Camilliere, J. In vivo stimulation of bone formation by transforming growth factor-beta. *Endocrinology* **124**, 2991–2994 (1989).
 193. Soncin, F. Angiogenin supports endothelial and fibroblast cell adhesion. *Proc. Natl. Acad. Sci. U. S. A.* **89**, 2232–2236 (1992).
 194. Kim, H.-M., Kang, D.-K., Kim, H. Y., Kang, S. S. & Chang, S.-I. Angiogenin-induced protein

- kinase B/Akt activation is necessary for angiogenesis but is independent of nuclear translocation of angiogenin in HUVE cells. *Biochem. Biophys. Res. Commun.* **352**, 509–513 (2007).
195. Xiangwei, G. & Zhengping, X. Mechanisms of action of angiogenin. *Acta Biochim. Biophys. Sin. (Shanghai)*. **40**, 619–624 (2008).
 196. Davies, K. J. The complex interaction of matrix metalloproteinases in the migration of cancer cells through breast tissue stroma. *Int. J. Breast Cancer* **2014**, 839094 (2014).
 197. Seiki, M. The cell surface: The stage for matrix metalloproteinase regulation of migration. *Curr. Opin. Cell Biol.* **14**, 624–632 (2002).
 198. Kessenbrock, K., Plaks, V. & Werb, Z. Matrix metalloproteinases: Regulators of the tumor microenvironment. *Cell* **141**, 52–67 (2010).
 199. Jabłońska-Trypuć, A., Matejczyk, M. & Rosochacki, S. Matrix metalloproteinases (MMPs), the main extracellular matrix (ECM) enzymes in collagen degradation, as a target for anticancer drugs. *J. Enzyme Inhib. Med. Chem.* **31**, 177–183 (2016).
 200. Hoeben, A. N. N. *et al.* Vascular endothelial growth factor and angiogenesis. *Pharmacol. Rev.* **56**, 549–580 (2004).
 201. Spencer, H., Norris, C. & Williams, D. Inhibitory effects of zinc on magnesium balance and magnesium absorption in man. *J. Am. Coll. Nutr.* **13**, 479–484 (1994).
 202. Ravanti, L. & Kähäri, V.-M. Matrix metalloproteinases in wound repair. *Int. J. Mol. Med.* **6**, 391–798 (2000).
 203. Iacono, J. A. *et al.* Interleukin-8 levels and activity in delayed-healing human thermal wounds. *Wound Repair Regen.* **8**, 216–225 (2000).
 204. Pulikkotil, S. J. & Nath, S. Effect on interleukin-1 β and interleukin-8 levels following use of fibrin sealant for periodontal surgery. *Aust. Dent. J.* **59**, 156–164 (2014).
 205. Lai, Y. *et al.* Interleukin-8 induces the endothelial cell migration through the activation of phosphoinositide 3-kinase-Rac1/RhoA pathway. *Int. J. Biol. Sci.* **7**, 782–791 (2011).
 206. Ma, J. *et al.* Mitochondrial dysfunction promotes breast cancer cell migration and invasion through HIF1 α accumulation via increased production of reactive oxygen species. *PLoS One* **8**, e69485 (2013).
 207. Zhao, J. *et al.* Mitochondrial dynamics regulates migration and invasion of breast cancer cells. *Oncogene* **32**, 4814–24 (2013).
 208. Gusarova, G. A. *et al.* Hypoxia leads to Na, K-ATPase down-regulation via Ca²⁺ release-activated Ca²⁺ (CRAC) channels and AMPK activation. *Mol. Cell. Biol.* **31**, 3546–3556 (2011).
 209. Castiglioni, S. *et al.* Magnesium homeostasis in colon carcinoma LoVo cells sensitive or resistant to doxorubicin. *Sci. Rep.* **5**, 16538 (2015).
 210. Hou, J. & Goodenough, D. A. Claudin-16 and claudin-19 function in the thick ascending limb. *Curr. Opin. Nephrol. Hypertens.* **19**, 483–488 (2010).
 211. Hou, J. *et al.* Claudin-16 and claudin-19 interaction is required for their assembly into tight junctions and for renal reabsorption of magnesium. *Proc. Natl. Acad. Sci.* **106**, 15350–15355 (2009).
 212. Tizioto, P. C. *et al.* Calcium and potassium content in beef: Influences on tenderness and associations with molecular markers in Nellore cattle. *Meat Sci.* **96**, 436–440 (2014).
 213. Castiglioni, S. & Maier, J. A. M. The tyrosine phosphatase HD-PTP (PTPN23) is degraded by calpains in a calcium-dependent manner. *Biochem. Biophys. Res. Commun.* **421**, 380–383 (2012).

214. Martin, T. A., Harrison, G. M., Watkins, G. & Jiang, W. G. Claudin-16 reduces the aggressive behavior of human breast cancer cells. *J. Cell. Biochem.* **105**, 41–52 (2008).
215. Arnaoutova, I. & Kleinman, H. K. In vitro angiogenesis: Endothelial cell tube formation on gelled basement membrane extract. *Nat. Protoc.* **5**, 628–635 (2010).
216. Zhao, L. *et al.* Knockdown of ezrin suppresses the migration and angiogenesis of human umbilical vein endothelial cells in vitro. *J. Huazhong Univ. Sci. Technol. Med. Sci.* **36**, 243–248 (2016).
217. Kishore, R. *et al.* The cytoskeletal protein ezrin regulates EC proliferation and angiogenesis via TNF- α -induced transcriptional repression of cyclin A. *J. Clin. Invest.* **115**, 1785–1796 (2005).
218. Ziesenis, A. Hypoxia and the modulation of the actin cytoskeleton—emerging interrelations. *Hypoxia* **2**, 11–21 (2014).
219. Li, T.-S. *et al.* Cellular expression of integrin- β 1 is of critical importance for inducing therapeutic angiogenesis by cell implantation. *Cardiovasc. Res.* **65**, 64–72 (2005).
220. Friedrich, E. B. *et al.* Integrin-linked kinase regulates endothelial cell survival and vascular development. *Mol. Cell. Biol.* **24**, 8134–8144 (2004).
221. Eliceiri, B. P. & Cheresh, D. A. Adhesion events in angiogenesis. *Curr. Opin. Cell Biol.* **13**, 563–568 (2001).
222. Soldi, R. *et al.* Role of α v β 3 integrin in the activation of vascular endothelial growth factor receptor-2. *EMBO J.* **18**, 882–892 (1999).
223. Somanath, P. R., Malinin, N. L. & Byzova, T. V. Cooperation between integrin α v β 3 and VEGFR2 in angiogenesis. *Angiogenesis* **12**, 177–185 (2009).
224. Borges, E., Jan, Y. & Ruoslahti, E. Platelet-derived growth factor receptor beta and vascular endothelial growth factor receptor 2 bind to the beta 3 integrin through its extracellular domain. *J. Biol. Chem.* **275**, 39867–39873 (2000).
225. Byzova, T. V. *et al.* A mechanism for modulation of cellular responses to VEGF: Activation of the integrins. *Mol. Cell* **6**, 851–860 (2000).
226. Friedlander, M. *et al.* Definition of two angiogenic pathways by distinct alpha v integrins. *Science* **270**, 1500–1502 (1995).
227. Schneller, M., Vuori, K. & Ruoslahti, E. α v β 3 integrin associates with activated insulin and PDGF β receptors and potentiates the biological activity of PDGF. *EMBO J.* **16**, 5600–5607 (1997).
228. Senger, D. R. *et al.* Angiogenesis promoted by vascular endothelial growth factor: Regulation through α 1 β 1 and α 2 β 1 integrins. *Proc. Natl. Acad. Sci.* **94**, 13612–13617 (1997).
229. Ravelli, C., Mitola, S., Corsini, M. & Presta, M. Involvement of α v β 3 integrin in gremlin-induced angiogenesis. *Angiogenesis* **16**, 235–243 (2013).
230. Wolf, F. I., Cittadini, A. R. M. & Maier, J. A. M. Magnesium and tumors: Ally or foe? *Cancer Treat. Rev.* **35**, 378–382 (2009).
231. German, A. E., Mammoto, T., Jiang, E., Ingber, D. E. & Mammoto, A. Paxillin controls endothelial cell migration and tumor angiogenesis by altering neuropilin 2 expression. *J. Cell Sci.* **127**, 1672–1683 (2014).
232. Prockop, D. J., Kota, D. J., Bazhanov, N. & Reger, R. L. Evolving paradigms for repair of tissues by adult stem/progenitor cells (MSCs). *J. Cell. Mol. Med.* **14**, 2190–2199 (2010).
233. Granero-Moltó, F. *et al.* Regenerative effects of transplanted mesenchymal stem cells in fracture healing. *Stem Cells* **27**, 1887–1898 (2009).
234. Hofer, H. R. & Tuan, R. S. Secreted trophic factors of mesenchymal stem cells support

- neurovascular and musculoskeletal therapies. *Stem Cell Res. Ther.* **7**, 131–145 (2016).
235. Kim, K.-J. *et al.* Magnesium ions enhance infiltration of osteoblasts in scaffolds via increasing cell motility. *J. Mater. Sci. Mater. Med.* **28**, 96 (2017).
236. Brown, A., Zaky, S., Ray, H. & Sfeir, C. Porous magnesium/PLGA composite scaffolds for enhanced bone regeneration following tooth extraction. *Acta Biomater.* **11**, 543–553 (2015).
237. Liu, C. *et al.* Biodegradable Mg-Cu alloys with enhanced osteogenesis, angiogenesis, and long-lasting antibacterial effects. *Sci. Rep.* **6**, 27374 (2016).
238. Zhou, X. *et al.* Human umbilical cord-derived mesenchymal stem cells improve learning and memory function in hypoxic-ischemic brain-damaged rats via an IL-8-mediated secretion mechanism rather than differentiation pattern induction. *Cell. Physiol. Biochem.* **35**, 2383–2401 (2015).
239. Yoshizawa, S., Brown, A., Barchowsky, A. & Sfeir, C. Role of magnesium ions on osteogenic response in bone marrow stromal cells. *Connect. Tissue Res.* **55 Suppl 1**, 155–159 (2014).
240. Schipani, E., Maes, C., Carmeliet, G. & Semenza, G. L. Regulation of osteogenesis-angiogenesis coupling by HIFs and VEGF. *J. Bone Miner. Res.* **24**, 1347–1353 (2009).
241. Hou, Y. *et al.* IL-8 enhances the angiogenic potential of human bone marrow mesenchymal stem cells by increasing vascular endothelial growth factor. *Cell Biol. Int.* **38**, 1050–1059 (2014).
242. Feng, N. *et al.* HIF-1alpha and HIF-2alpha induced angiogenesis in gastrointestinal vascular malformation and reversed by thalidomide. *Sci. Rep.* **6**, 27280 (2016).
243. Lee, Y.-H. *et al.* Gain of HIF-1alpha under normoxia in cancer mediates immune adaptation through the AKT/ERK and VEGFA axes. *Clin. Cancer Res.* **21**, 1438–1446 (2015).
244. Pizurki, L., Zhou, Z., Glynos, K., Roussos, C. & Papapetropoulos, A. Angiopoietin-1 inhibits endothelial permeability, neutrophil adherence and IL-8 production. *Br. J. Pharmacol.* **139**, 329–336 (2003).
245. Ng, F. *et al.* PDGF, TGF-beta, and FGF signaling is important for differentiation and growth of mesenchymal stem cells (MSCs): Transcriptional profiling can identify markers and signaling pathways important in differentiation of MSCs into adipogenic, chondrogenic, and osteogenic lineages. *Blood* **112**, 295–307 (2008).
246. García-Cardena, G., Oh, P., Liu, J., Schnitzer, J. E. & Sessa, W. C. Targeting of nitric oxide synthase to endothelial cell caveolae via palmitoylation: Implications for nitric oxide signaling. *Proc. Natl. Acad. Sci.* **93**, 6448–6453 (1996).
247. Tsutsumi, S. *et al.* Retention of multilineage differentiation potential of mesenchymal cells during proliferation in response to FGF. *Biochem. Biophys. Res. Commun.* **288**, 413–419 (2001).
248. S., H. *et al.* FGF-2 addition during expansion of human bone marrow-derived stromal cells alters MSC surface marker distribution and chondrogenic differentiation potential. *Cell Prolif.* **46**, 396–407 (2013).
249. Lokesh, B. V. *et al.* Human placenta and bone marrow derived MSC cultured in serum-free, b-FGF-containing medium express cell surface frizzled-9 and SSEA-4 and give rise to multilineage differentiation. *Differentiation* **75**, 279–291 (2006).
250. Tasso, R. *et al.* The role of bFGF on the ability of MSC to activate endogenous regenerative mechanisms in an ectopic bone formation model. *Biomaterials* **33**, 2086–2096 (2012).
251. Song, H. *et al.* Transfection of mesenchymal stem cells with the FGF-2 gene improves their survival under hypoxic conditions. *Mol. Cells* **19**, 402–407 (2005).

252. Lieu, C., Heymach, J., Overman, M., Tran, H. & Kopetz, S. Beyond VEGF: Inhibition of the fibroblast growth factor pathway and antiangiogenesis. *Clin. Cancer Res.* **17**, 6130–6139 (2011).
253. Murakami, M. & Simons, M. Fibroblast growth factor regulation of neovascularization. *Curr. Opin. Hematol.* **15**, 215–220 (2008).
254. Che, N. *et al.* Impaired B cell inhibition by lupus bone marrow mesenchymal stem cells is caused by reduced CCL2 expression. *J. Immunol.* **193**, 5306–5314 (2014).
255. Cui, R. *et al.* Human mesenchymal stromal/stem cells acquire immunostimulatory capacity upon cross-talk with natural killer cells and might improve the NK cell function of immunocompromised patients. *Stem Cell Res. Ther.* **7**, 88–101 (2016).
256. Cunningham, L. D., Brecher, P. & Cohen, R. A. Platelet-derived growth factor receptors on macrovascular endothelial cells mediate relaxation via nitric oxide in rat aorta. *J. Clin. Invest.* **89**, 878–882 (1992).
257. López-Rivera, E. *et al.* Matrix metalloproteinase 13 mediates nitric oxide activation of endothelial cell migration. *Proc. Natl. Acad. Sci. U. S. A.* **102**, 3685–3690 (2005).
258. Bourboulia, D. & Stetler-Stevenson, W. G. Matrix metalloproteinases (MMPs) and tissue inhibitors of metalloproteinases (TIMPs): Positive and negative regulators in tumor cell adhesion. *Semin. Cancer Biol.* **20**, 161–168 (2010).
259. Kudo, Y. *et al.* Matrix metalloproteinase-13 (MMP-13) directly and indirectly promotes tumor angiogenesis. *J. Biol. Chem.* **287**, 38716–28 (2012).
260. Li, A., Dubey, S., Varney, M. L., Dave, B. J. & Singh, R. K. IL-8 directly enhanced endothelial cell survival, proliferation, and matrix metalloproteinases production and regulated angiogenesis. *J. Immunol.* **170**, 3369–3376 (2003).
261. Nauck, M. *et al.* Induction of vascular endothelial growth factor by platelet-activating factor and platelet-derived growth factor is downregulated by corticosteroids. *Am. J. Respir. Cell Mol. Biol.* **16**, 398–406 (1997).
262. Risau, W. *et al.* Platelet-derived growth factor is angiogenic in vivo. *Growth factors* **7**, 261–266 (1992).
263. Pierce, G. F. *et al.* Detection of platelet-derived growth factor (PDGF)-AA in actively healing human wounds treated with recombinant PDGF-BB and absence of PDGF in chronic nonhealing wounds. *J. Clin. Invest.* **96**, 1336–1350 (1995).
264. Demaria, M. *et al.* An essential role for senescent cells in optimal wound healing through secretion of PDGF-AA. *Dev. Cell* **31**, 722–733 (2014).
265. Marx, M., Perlmutter, R. A. & Madri, J. A. Modulation of platelet-derived growth factor receptor expression in microvascular endothelial cells during in vitro angiogenesis. *J. Clin. Invest.* **93**, 131–139 (1994).
266. Nicosia, R. F., Nicosia, S. V & Smith, M. Vascular endothelial growth factor, platelet-derived growth factor, and insulin-like growth factor-1 promote rat aortic angiogenesis in vitro. *Am. J. Pathol.* **145**, 1023–1029 (1994).
267. Wang, J. *et al.* Bone marrow-derived mesenchymal stem cell-secreted IL-8 promotes the angiogenesis and growth of colorectal cancer. *Oncotarget* **6**, 42825–42837 (2015).
268. Dyer, L. A., Pi, X. & Patterson, C. The role of BMPs in endothelial cell function and dysfunction. *Trends Endocrinol. Metab.* **25**, 472–480 (2014).
269. Neve, A., Cantatore, F. P., Maruotti, N., Corrado, A. & Ribatti, D. Extracellular matrix modulates angiogenesis in physiological and pathological conditions. *Biomed Res. Int.* **2014**, 756078

- (2014).
270. Deshmane, S. L., Kremlev, S., Amini, S. & Sawaya, B. E. Monocyte chemoattractant protein-1 (MCP-1): An overview. *J. Interf. Cytokine Res.* **29**, 313–326 (2009).
 271. Kyriakides, T. R. *et al.* The CC chemokine ligand, CCL2/MCP1, participates in macrophage fusion and foreign body giant cell formation. *Am. J. Pathol.* **165**, 2157–2166 (2004).
 272. Petzelbauer, P., Watson, C. A., Pfau, S. E. & Pober, J. S. IL-8 and angiogenesis: Evidence that human endothelial cells lack receptors and do not respond to IL-8 in vitro. *Cytokine* **7**, 267–272 (1995).
 273. Hirschi, K. K., Rohovsky, S. A. & D'Amore, P. A. PDGF, TGF- β , and heterotypic cell–cell interactions mediate endothelial cell–induced recruitment of 10T1/2 cells and their differentiation to a smooth muscle fate. *J. Cell Biol.* **141**, 805–814 (1998).
 274. Takehara, K., LeRoy, E. C. & Grotendorst, G. R. TGF-beta inhibition of endothelial cell proliferation: Alteration of EGF binding and EGF-induced growth-regulatory (competence) gene expression. *Cell* **49**, 415–422 (1987).
 275. van Meeteren, L. A. & ten Dijke, P. Regulation of endothelial cell plasticity by TGF- β . *Cell Tissue Res.* **347**, 177–186 (2012).
 276. Roberts, A. B. & Sporn, M. B. Regulation of endothelial cell growth, architecture, and matrix synthesis by TGF- β . *Am. Rev. Respir. Dis.* **140**, 1126–1128 (1989).
 277. Behzadian, M. A., Wang, X.-L., Windsor, L. J., Ghaly, N. & Caldwell, R. B. TGF- β increases retinal endothelial cell permeability by increasing MMP-9: Possible role of glial cells in endothelial barrier function. *Invest. Ophthalmol. Vis. Sci.* **42**, 853–859 (2001).
 278. Huang, B. *et al.* CCL2/CCR2 pathway mediates recruitment of myeloid suppressor cells to cancers. *Cancer Lett.* **252**, 86–92 (2007).
 279. Lecomte, J. *et al.* Bone marrow-derived mesenchymal cells and MMP13 contribute to experimental choroidal neovascularization. *Cell. Mol. Life Sci.* **68**, 677–686 (2011).
 280. Almalki, S. G. & Agrawal, D. K. Effects of matrix metalloproteinases on the fate of mesenchymal stem cells. *Stem Cell Res. Ther.* **7**, 129–141 (2016).
 281. Warstat, K., Felka, T. & Mittag, F. The TGF- β 1-induced expression of matrix metalloproteinases in mesenchymal stromal cells is influenced by type of substrate. *J. Tissue Sci. Eng.* **02**, 1–7 (2011).
 282. Lozito, T. P., Jackson, W. M., Nesti, L. J. & Tuan, R. S. Human mesenchymal stem cells generate a distinct pericellular zone of MMP activities via binding of MMPs and secretion of high levels of TIMPs. *Matrix Biol.* **34**, 132–143 (2014).
 283. Charles, N. *et al.* Perivascular nitric oxide activates notch signaling and promotes stem-like character in PDGF-induced glioma cells. *Cell Stem Cell* **6**, 141–152 (2010).
 284. Bidarra, S. J. *et al.* Phenotypic and proliferative modulation of human mesenchymal stem cells via crosstalk with endothelial cells. *Stem Cell Res.* **7**, 186–197 (2011).
 285. Gershovich, J. G., Dahlin, R. L., Kasper, F. K. & Mikos, A. G. Enhanced osteogenesis in cocultures with human mesenchymal stem cells and endothelial cells on polymeric microfiber scaffolds. *Tissue Eng. Part A* **19**, 2565–2576 (2013).
 286. Lee, H. K. *et al.* CCL2 deficient mesenchymal stem cells fail to establish long-lasting contact with T cells and no longer ameliorate lupus symptoms. *Sci. Rep.* **7**, 41258 (2017).
 287. Deem, T. L. & Cook-Mills, J. M. Vascular cell adhesion molecule 1 (VCAM-1) activation of endothelial cell matrix metalloproteinases: Role of reactive oxygen species. *Blood* **104**, 2385–2393 (2004).

288. Haas, T. L. & Madri, J. A. Extracellular matrix-driven matrix metalloproteinase production in endothelial cells: Implications for angiogenesis. *Trends Cardiovasc. Med.* **9**, 70–77 (1999).
289. Cross, M. J. & Claesson-Welsh, L. FGF and VEGF function in angiogenesis: signalling pathways, biological responses and therapeutic inhibition. *Trends Pharmacol. Sci.* **22**, 201–207 (2001).
290. Liu, Z.-J. *et al.* Regulation of notch1 and Dll4 by vascular endothelial growth factor in arterial endothelial cells: implications for modulating arteriogenesis and angiogenesis. *Mol. Cell. Biol.* **23**, 14–25 (2003).
291. Nobta, M. *et al.* Critical regulation of bone morphogenetic protein-induced osteoblastic differentiation by delta1/jagged1-activated notch1 signaling. *J. Biol. Chem.* **280**, 15842–15848 (2005).
292. Qi, X. *et al.* Exosomes secreted by human-induced pluripotent stem cell-derived mesenchymal stem cells repair critical-sized bone defects through enhanced angiogenesis and osteogenesis in osteoporotic rats. *Int. J. Biol. Sci.* **12**, 836–849 (2016).
293. Skliar, M. *et al.* Membrane proteins significantly restrict exosome mobility. *Biochem. Biophys. Res. Commun.* **501**, 1055–1059 (2018).
294. Medici, D. Endothelial-mesenchymal transition in regenerative medicine. *Stem Cells Int.* **2016**, 6962801 (2016).
295. Shi, Y. & Massague, J. Mechanisms of TGF-beta signaling from cell membrane to the nucleus. *Cell* **113**, 685–700 (2003).

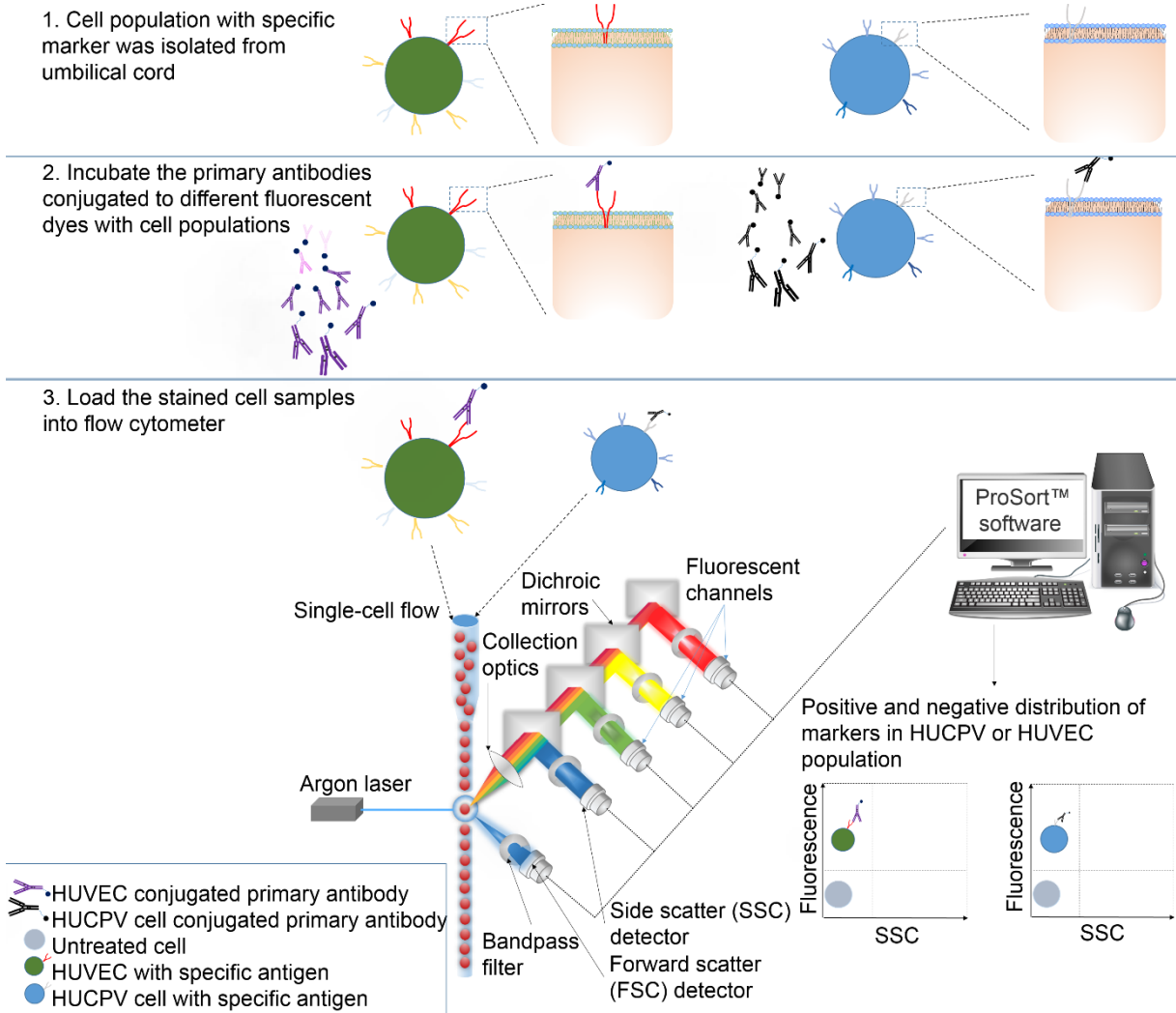
Acknowledgements

I would like to express my sincere appreciation to Prof. Dr. Regine Willumeit-Römer for the opportunity to work with a great research team. I sincerely thank Dr. Bérengère J.C. Luthringer-Feyerabend for sharing knowledge not limited to experimental ideas, writing and management experience. Additionally, the instruction from Prof. Willumeit-Römer and Dr. Luthringer-Feyerabend also expanded my horizons for a further research career. Special thanks to Prof. Maier Jeanette Anne Marie, my mentor during the PhD research. Thanks to all the members in our wonderful and warm group for their work support and daily communication. Thanks to Dr. Heike Helmholtz for writing suggestions and AAS support. I will be forever thankful to all my colleagues in Helmholtz Zentrum Geesthacht for their thoughtful work support. Thanks for the umbilical cord donation from Asklepios Klinik Altona supported by Prof. Dr. Volker Ragoesch. Special thanks to Ms. Qian Wang and my family. I appreciate the China Scholarship Council (CSC) for sponsoring my research in Germany.

Appendix

Supplementary figures

Fig. S1 Procedures of immunophenotyping in flow cytometry.



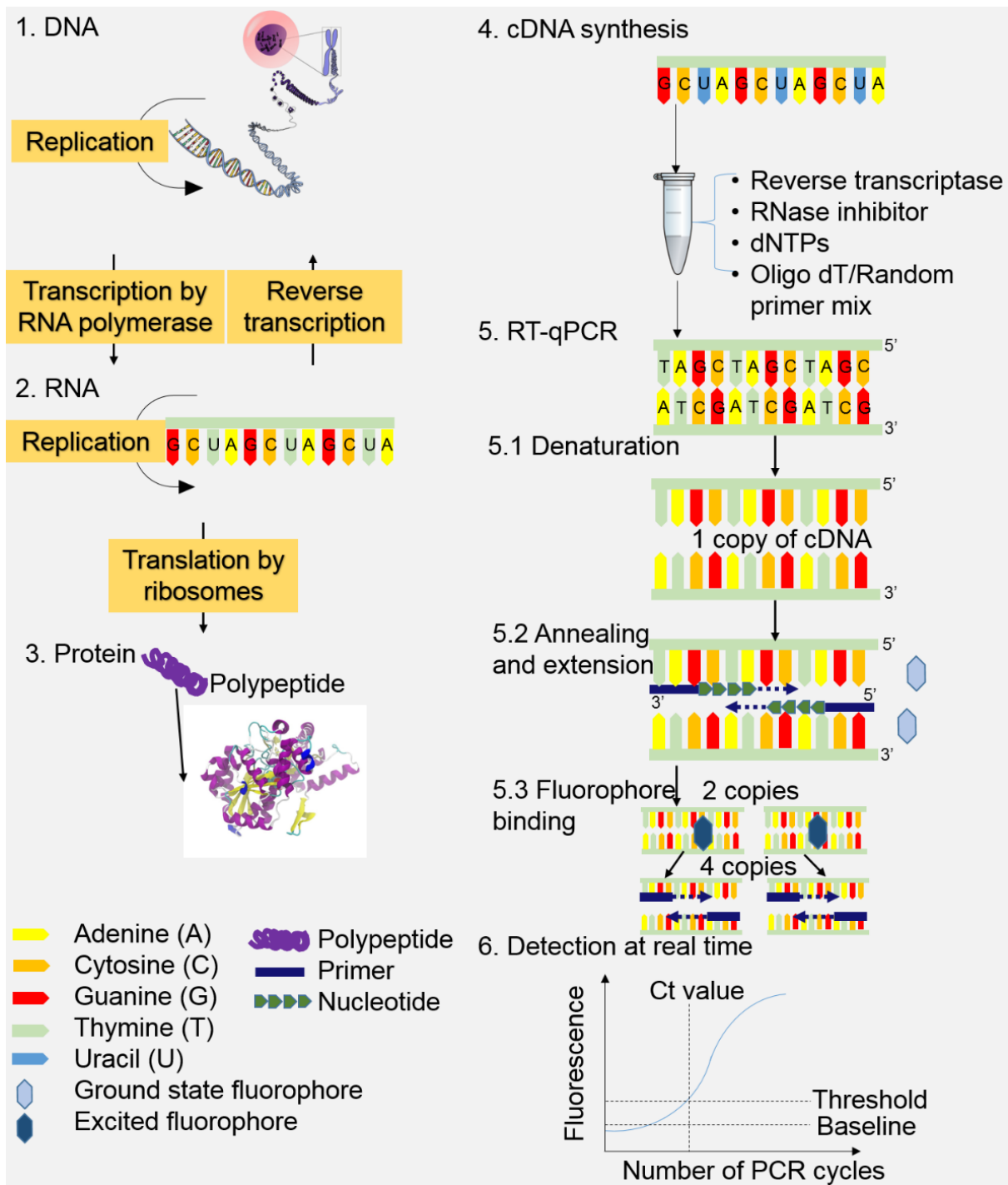


Fig. S2 Principles of real-time qPCR.

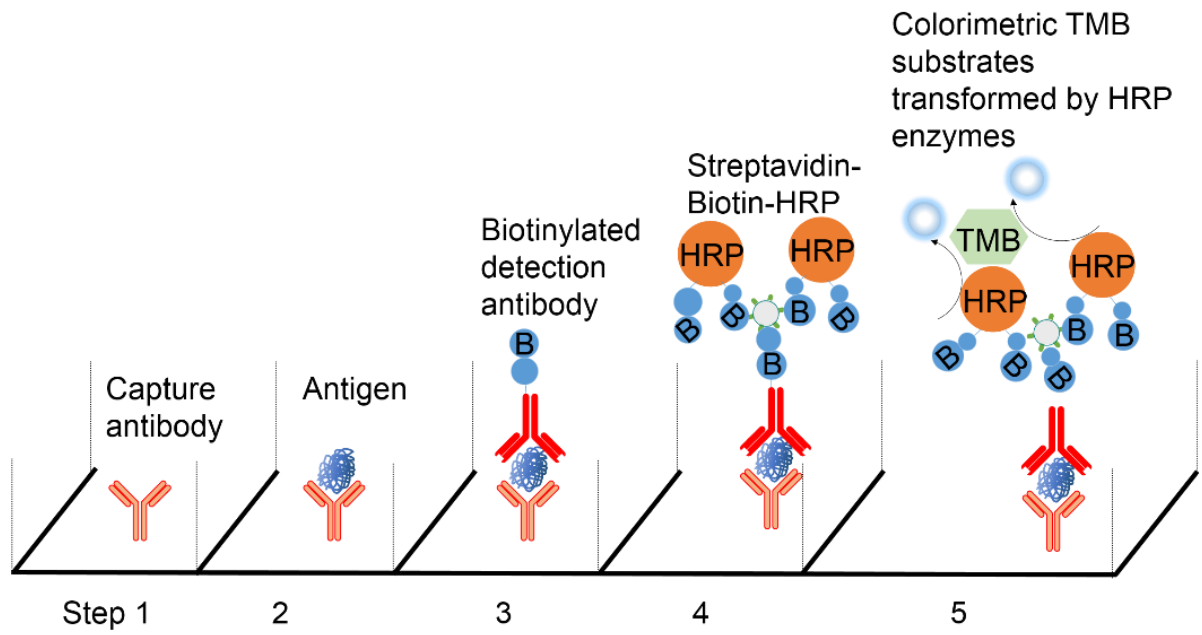


Fig. S3 Schematic of sandwich ELISA.

Symbols and abbreviations

Acronym	Definition
AAS	Atomic absorption spectroscopy
ALP	Alkaline phosphatase
AMPK	AMP-activated protein kinase
ANG	Angiogenin
ANOVA	Analysis of variance
ARS	Alizarin Red S
ATP	Adenosine triphosphate
BMD	Bone mineral density
BMP	Bone morphogenetic protein
BSA	Bovine serum albumin
CRAC	Ca ²⁺ release-activated Ca ²⁺ channels
CRP	C-reactive protein
CSF	Colony-stimulating factor
DNA	Deoxyribonucleic acid
ECAP	Equal-channel angular pressing
ECGM	Endothelial cell growth medium
ECGS	Endothelial cell growth supplement
ECM	Extracellular matrix
EDTA	Ethylenediaminetetraacetic acid
EGF	Epidermal growth factor
ELISA	Enzyme-linked immunosorbent assay
EPAS	Endothelial PAS domain-containing protein
EZR	Ezrin
FBS	Foetal bovine serum
FGF	Fibroblast growth factor
FITC	Fluorescein isothiocyanate
FSC	Forward scatter
GAPDH	Glyceraldehyde 3-phosphate dehydrogenase
GSH	Glutathione
HEPES	4-(2-hydroxyethyl)-1-piperazineethanesulfonic acid
HIF	Hypoxia-inducible factor
HUCPV	Human umbilical cord perivascular
HUVEC	Human umbilical vein endothelial cell
ICAM	Intercellular adhesion molecule
ICP-MS	Inductively coupled plasma mass spectrometry
ITGAM	Integrin alpha M
JSN	Joint space narrowing
KDR	Kinase insert domain receptor
LDEV	Lactate dehydrogenase elevating virus
MAP	Mitogen-activated protein
MAPK	Mitogen-activated protein kinase

MCP	Monocyte chemoattractant protein
MEM	Minimum essential medium
MMP	Matrix metalloproteinase
MSC	Mesenchymal stem cell
NADH	Nicotinamide adenine dinucleotide (reduced form)
NMDAR	N-methyl-D-aspartate receptor
NOS	Nitric oxide synthases
ONFH	Osteonecrosis of the femoral head
OPG	Osteoprotegerin
PBS	Phosphate-buffered saline
PCR	Polymerase chain reaction
PDGF	Platelet-derived growth factor
PLA	Poly(lactic acid)
PTH	Parathyroid hormone
RNA	Ribonucleic acid
ROS	Reactive oxygen species
SELE	Selectin
SNK	Student-Newman-Keuls
SSC	Side scatter
TBAR	Thiobarbituric acid reactive substances
TBARS	Thiobarbituric acid reactive
TIMP	TIMP metalloproteinase inhibitor
TLA	Thin-layer assay
TMB	Tetramethylbenzidine
TNF	Tumour necrosis factor
UCB	Umbilical cord blood
USA	United States of America
VCAM	Vascular cell adhesion molecule
VEGF	Vascular endothelial growth factor
VEGFR	Vascular endothelial growth factor receptor
WST-1	Water-soluble tetrazolium salt-1

Curriculum Vitae

Lei Xu

xulei667@gmail.com

Nationality: Chinese

Birth: 11. Oct. 1988, China

Education

- Sep 2007 – June 2012

Bachelor of Medicine Department of Public Health, Xi'an Medical University, Shaanxi, China

- Sep 2012 – June 2015

Master of Medicine Chinese Centre for Disease Control and Prevention, Beijing, China

- Sep 2015 – June 2019

Dr.-Ing. Helmholtz-Zentrum Geesthacht (Faculty of Engineering, Christian-Albrecht-University (CAU) Kiel), Germany

Research experience

- Sep 2012 – June 2015 China National Centre for Food Safety Risk Assessment (CFSA)

The study on developmental neurotoxicity mechanism of PBDEs using neurons differentiation model of embryonic stem cell

- Sep 2015 – Feb 2018 Helmholtz-Zentrum Geesthacht (HZG), Germany

Effects of magnesium degradation products and hypoxia on angiogenesis and osteogenesis during fracture healing

List of publications and conferences

Peer-reviewed Journals:

L. Xu, R. Willumeit-Römer, B. Luthringer-Feyerabend. Effect of magnesium-degradation products and hypoxia on the angiogenesis of human umbilical vein endothelial cells. *Acta Biomaterialia*, 2019 <https://doi.org/10.1016/j.actbio.2019.02.018>

L. Xu, R. Willumeit-Römer, B. Luthringer-Feyerabend. *Hypoxia influences the effect of magnesium degradation on the coculture of mesenchymal stem cell and endothelial cell. Under review.*

L. Xu, R. Willumeit-Römer, B. Luthringer-Feyerabend. *Oxygen and mesenchymal stem cell regulate endothelial activities in magnesium degradation products. In preparation.*

L. Xu†, S. Behr†, H. Helmholz, R. Willumeit-Römer, B. Luthringer-Feyerabend. *Magnesium and cytokines: relevance for the behaviour of osteoclasts and osteoblasts. In preparation.*

Q. Wang, L. Xu, H. Helmholz, R. Willumeit-Römer, B. Luthringer-Feyerabend. *Crosstalk between mesenchymal stem cell and PBMCs in magnesium degradation products. In preparation.*

Conference contribution:

L. Xu, R. Willumeit-Römer, B. Luthringer-Feyerabend. Effect of magnesium-degradation products on mesenchymal stem cell osteogenesis. *der Deutschen Gesellschaft für Biomaterialien*, Aachen, Germany, 2016 (**Poster**)

L. Xu, R. Willumeit-Römer, B. Luthringer-Feyerabend. Effect of magnesium-degradation products and hypoxia on the angiogenesis of human umbilical cord vein-derived endothelial cells. *9th Symposium on Biodegradable Metals*, Bertinoro, Italy, 2017 (**Short oral presentation**)

L. Xu, R. Willumeit-Römer, B. Luthringer-Feyerabend. Effect of magnesium-degradation products and hypoxia on the angiogenesis of human umbilical cord vein-derived endothelial cells. *European Cells and Materials eCM Meeting Abstracts*, 2017, Collection 4, (Page 74) ISSN 2522-235X

L. Xu, R. Willumeit-Römer, B. Luthringer-Feyerabend. The effect of magnesium-degradation products can be influenced by hypoxia in the coculture of endothelial and mesenchymal stem cells. *10th Symposium on Biodegradable Metals*, Oxford, UK, 2018 (**Keynote**)